The Dissertation Committee for Prateek Kathel Certifies that this is the approved version of the following dissertation:

Experiments and Modeling of Wettability Alteration in Low Permeability Porous Media

Committee:

Kishore K. Mohanty, Supervisor

Gary A. Pope

David A. DiCarlo

Hugh Daigle

Farzam Javadpour

Experiments and Modeling of Wettability Alteration in Low Permeability Porous Media

by

Prateek Kathel, B.Tech., M.S.E

Dissertation

Presented to the Faculty of the Graduate School of

The University of Texas at Austin

in Partial Fulfillment

of the Requirements

for the Degree of

Doctor of Philosophy

The University of Texas at Austin

December 2015

Dedication

Dedicated to my parents for their eternal love, support and encouragement.

Acknowledgements

I would like to express my deepest gratitude to my supervisor, Dr. Kishore Mohanty for his excellent guidance, support and encouragement throughout this work. Working with him has been a privilege and a great learning experience. I am thankful to Dr. Gary Pope for the wonderful discussions during the research consortium meetings. I would like to thank my dissertation committee members: Dr. David DiCarlo, Dr. Hugh Daigle and Dr. Farzam Javadpour for their valuable time and suggestions.

I would like to acknowledge the efforts of all the professors at the University who have enriched my knowledge and skills through various courses. Every experience was unique in its own way and has contributed towards building a solid foundation for my research. I am grateful to the staff of Petroleum and Geosystems Engineering department for their help in managing the various administrative tasks. Special thanks to Barbara Messmore for always being patient, kind and helpful. I would like to thank Daryl Nygaard at the machine shop for providing assistance with the different experimental requirements and Gary Miscoe for helping me with the coring needs.

I am thankful to Dr. Eric Dao who has been a great resource with his innovative solutions and creative ideas for troubleshooting the experimental setups. I would like to thank all my lab mates over the years for their friendship and cooperation. It was great working with you all. The stay in Austin was made marvelous by the presence of a lot of people. I have made friends for life and together we have cherished many wonderful moments. A big thanks to all of you.

Finally, I would like to acknowledge the love and support of my parents throughout this journey.

Experiments and Modeling of Wettability Alteration in Low Permeability Porous Media

Prateek Kathel, Ph.D.

The University of Texas at Austin, 2015

Supervisor: Kishore K. Mohanty

Naturally fractured reservoirs contain a significant amount of global hydrocarbon reserves. In fractured reservoirs, the efficiency of water flood is governed by spontaneous imbibition of water into oil-containing matrix blocks. When the matrix is oil-wet or mixed-wet, little oil can be recovered by imbibition. Wettability alteration provides a possible solution to enhance oil recovery in oil/mixed-wet fractured formations. Different chemicals such as surfactants, enzymes, selective ions can be used to alter wettability from oil-wet towards more water-wet which can substantially increase the oil recovery. Understanding recovery mechanisms for these processes at different inverse bond numbers (ratio of capillary to buoyancy forces) and developing scaling rules are critical for estimating feasibility at field scale.

Surfactants were identified which altered the wettability of a low permeability (0.03 – 0.23 mD) mixed-wet/oil-wet sandstone reservoir. Static imbibition experiments in the surfactant solution resulted in high oil recovery (42-68% OOIP) compared to 15% OOIP in formation brine. High (>240) inverse bond numbers for these experiments indicate recovery mechanism as counter-current imbibition driven by capillary forces. Numerically simulated saturation and velocity profiles on validated datasets were analyzed to study the

recovery mechanisms. Velocity profiles indicate counter current flows with velocity vectors pointing outwards. Similar visual observations were made during experiments, which were captured through images. The saturation front moves radially inward with symmetric profiles at the top and bottom. An analysis of scaling laws for the capillary driven flow suggests that imbibition recovery curves do not correlate with traditional scaling groups (Mattax and Kyte, 1962; Ma et al. 1997). The scaling equations analyzed are for strongly water-wet porous media and are insufficient to explain the dynamics of changing wettability from oil-wet to water-wet. The recovery data shows that oil recovery varies linearly with square root of time. It was observed that the rate of recovery was higher for the higher IFT cases in experiments performed on cores with almost same initial oil saturation using the same surfactant, but at different salinities. As a result of varying the salinity, interfacial tension between oil/water is varied.

To evaluate the application of wettability altering processes at larger scales experiments were performed on outcrop cores of different dimensions and at dynamic conditions. Surfactant formulation was developed which altered the wettability from oil-wet to water-wet on outcrop rocks Estaillades Limestone and Texas Cream Limestone. Using the surfactant formulation static and dynamic imbibition experiments were performed on cores with different dimensions and boundary conditions. It is observed that dynamic imbibition process recovers oil faster than static imbibition. Imbibition experiments performed on cores with varying height and diameter show that oil recovery decreases with increasing diameter and height. Study of numerically simulated velocity and saturation profile on validated input datasets established the recovery mechanism as gravity dominated flow.

Analytical scaling groups for gravity dominated flow were tested considering pressure drop only in water phase, pressure drop only in oil phase, and pressure drop across

both water and oil phases. The model with pressure drop in both phases captures the decrease in recovery with increase in diameter and height of the core. Sensitivity to change in oil recovery with change in height is fairly accurate whereas the model over-predicts oil recovery with change in diameter. A new space-time scaling function (t/DH) is proposed for surfactant aided gravity dominated processes. Data with same boundary conditions, rock, fluids and varying dimensions can be correlated with the scaling function at early times with no fitting parameters involved. A good correlation is obtained with the data from different studies indicating the effectiveness of the scaling function. The scaling is applicable to both static as well as dynamic imbibition cases.

Corefloods were performed on cores from different reservoirs to study the effect of wettability altering surfactant flood in a viscous pressure gradient driven process (as opposed to capillary or buoyancy driven imbibition process). Incremental oil recoveries over waterflood were analyzed for different injection schemes. Incremental recoveries over waterflood of 16% and 11% were obtained for secondary surfactant flood and slug process (surfactant slug injection after short initial waterflood) respectively for carbonate reservoir 1. Similarly, incremental recoveries over waterflood of 11% and 7% were obtained for secondary surfactant flood and slug process respectively for carbonate reservoir 2. The incremental oil recovery due to surfactant injection is attributed to the favorable increase in the relative permeability values of oil as the wettability is changed from oil-wet to water-wet. Experiments indicate that surfactant performance at the reservoir conditions (temperature, salinity, heterogeneity) is a key variable in these processes. Despite the differences in these conditions, for both the reservoirs oil recovery is more in the secondary surfactant injection mode compared to the slug process.

Table of Contents

List of Tables

List of Figures

Chapter 1: Introduction

1.1 Motivation and Objectives

There are vast amounts of oil deposits in fractured reservoirs. In low permeability fractured formations, primary and secondary recovery remains as low as 15-25% of original oil in place (Manrique et al. 2010) which presents a great opportunity for developing tertiary recovery processes. The oil recovery in fractured reservoirs depends critically on the wetting properties of the rock matrix, fracture density and fracture orientation. Waterflooding is not effective in fractured, oil-wet reservoirs because the injected water moves through the fractures without imbibing into the oil-wet matrix. Hence, recovery in oil-wet fractured sandstone and carbonate reservoirs is a challenge. In these reservoirs, if the wettability is altered to water-wet, large amount of oil can be recovered through spontaneous imbibition.

Wettability alteration from an oil/mixed-wet system towards a more water-wet system provides a possible solution to enhance oil recovery in a fractured formation. Wettability can be altered thermally or chemically using surfactants, enzymes or selective ions. Oil can also be recovered by lowering the oil/water interfacial tension without wettability alteration. In this work wettability alteration is investigated using surfactants. The agents for wettability alteration differ for each reservoir and depend on the given rock, oil and brine system. Brine salinity, hardness and reservoir temperature are key factors governing the surfactant selection process. Finding the wettability altering surfactant for a given reservoir is a challenge especially at harsh reservoir conditions (high hardness, high temperature). In this study, a systematic methodology is adopted to screen the surfactants which can alter wettability at dilute concentrations (0.1 - 0.25 wt%).

Performance of a wettability altering surfactant can be evaluated through spontaneous imbibition in a static as well as a dynamic setup. From a reservoir frame of reference, the fluid surrounding the core in a static imbibition cell represents the fluid in the fracture and the core represents the matrix. Static imbibition experiments are characterized by no fluid injection in the fracture whereas in dynamic imbibition experiments there is injection of fluid in the fractures. Static imbibition has been the experiment of choice for researchers for many decades spanning numerous studies (Austad et al. 1997, Standnes et al. 2000, Xie et al. 2005, Zhang and Hirasaki 2004, Seethepalli et al. 2004, Adibhatla et al. 2008, Zhang et al. 2009, Gupta et al. 2010, Halvorsen 2010, Nasiri et al., 2011, Sharma et al. 2013). However, for understanding application of these processes in a reservoir where the fluid in the fracture will be mobile, it is imperative that imbibition recovery through wettability alteration is investigated in a dynamic setup. Dynamic imbibition experimental studies in literature (Putra et al. 1999, Wang et al. 2009) have focused on waterflooding in a fractured water-wet media, but wettability alteration has never been studied dynamically.

Oil recovery in a spontaneous imbibition process depends on capillary and buoyancy forces. Variables like surfactant phase behavior and its wettability altering capabilities result in different combination of these forces. If capillary forces are dominant then counter-current imbibition is the recovery mechanism whereas dominant buoyancy forces lead to co-current imbibition. An in-depth understanding of these recovery mechanisms is essential for developing more robust numerical models and optimizing the imbibition processes at different reservoir conditions.

Scaling rules facilitate studying of imbibition processes with increased understanding of the physics and the first order mechanisms dictating the process. They can serve as an effective tool to determine the sensitivity with different parameters like

absolute and relative permeability, porosity, viscosity etc. They are also an important means to predict recovery in larger dimension matrix blocks in a matrix-fracture system. Using the scaling relationships, recovery behavior for a large reservoir matrix block can be estimated from an imbibition test on a small core sample. Several researchers (Mattax and Kyte 1962, Hagoort et al. 1980, Schechter et al. 1994, Ma et al. 1997, Li and Horne 2002 & 2006) have developed scaling groups for imbibition processes but these do not apply for the surfactant aided wettability alteration processes and hence cannot be used for predicting recovery at larger scales. Therefore, new scaling rules are required for understanding the behavior of these processes.

To evaluate feasibility of imbibition processes at larger scales there is a need to perform experiments on cores with different dimensions at both static and dynamic conditions. This data is critical for understanding the effect of increase in rock dimensions on oil recovery as well as for developing and validating new scaling rules.

Wettability alteration corefloods (Mohan et al. 2011, Sharma et al. 2013) in porous media have shown potential to recover oil in a viscous pressure gradient driven process as opposed to capillary or buoyancy driven spontaneous imbibition process. The incremental oil recovery due to surfactant injection is attributed to the favorable increase in the relative permeability values of oil as the wettability is changed from oil-wet to water-wet. Results from past studies show that incremental recovery over waterflood in an oil-wet reservoir can be achieved if wettability altering surfactant flood is started straight after primary production however effect of incremental recovery over waterflood needs to be investigated in a process where surfactant slug is injected post waterflood.

1.2 DESCRIPTION OF CHAPTERS

Wettability alteration is an attractive recovery method in fractured oil-wet reservoirs as changing the wettability to water-wet favors oil recovery through spontaneous imbibition. In this study different aspects of this process are analyzed such as: 1) determining wettability altering surfactants in different rock/oil/brine systems through a systematic methodology; 2) evaluating performance of these surfactants at different experimental conditions through static imbibition, dynamic imbibition and corefloods; 3) establishing imbibition recovery mechanisms and applicability of scaling rules. This dissertation is divided in 7 chapters. An overview of the contents is provided in the following paragraphs.

Chapter 2 describes the literature review covering EOR processes in general, EOR in fractured reservoirs, fundamentals of wettability and its impact on petrophysical parameters, the mechanisms of wettability alteration, scaling groups for capillary and gravity dominated processes and numerical simulation models for wettability alteration. Chapter 3 presents the materials and methodology used in the experimental studies.

Details of the experiments conducted in this study are provided in Chapter 4. It is divided into three main sections. The first section deals with capillary dominated flow in a sandstone reservoir. In these experiments a dilute (0.1 wt%) surfactant solution alters the wettability from mixed-wet/oil-wet to water-wet without significant reduction in IFT. The experiments are performed on tight reservoir rocks (0.03 – 0.23 mD) leading to high positive capillary forces after wettability alteration. In the second section results for gravity dominated flow are discussed. These include imbibition recovery curves under static and dynamic imbibition conditions as a function of core dimensions. The last section presents the work on wettability altering corefloods and

comparison of different injection schemes including secondary surfactant flood as well as a tertiary surfactant flood after short (0.5 PV) waterflood to mimic the conditions of the reservoirs already undergoing waterflood.

Chapter 5 focusses on the recovery mechanisms for capillary and gravity dominated imbibition flow. Input parameters are validated by comparing simulated oil recovery with the experimental recovery data. Velocity and saturation profiles generated through validated parameters are analyzed to understand and contrast the behavior of the two (capillary and gravity dominated) processes.

Chapter 6 analyzes the scaling rules for gravity dominated imbibition processes. Assumptions, key steps in derivation, applicability under different conditions as well as advantages and limitations are discussed for the analytical scaling groups. A new scaling function is proposed and validated by experimental data from different studies.

Chapter 7 describes the conclusions of this study and presents the recommendations for future work.

Chapter 2: Literature Review

2.1 INTRODUCTION

Oil recovery processes can be classified into three phases: primary, secondary and tertiary, which is also known as Enhanced Oil Recovery (EOR). Primary recovery results from the use of natural energy present in the reservoir. These processes include solution gas drive, gas cap drive, natural water drive, fluid and rock expansion and gravity drainage. The natural forces present in a given reservoir depend on rock and fluid properties, geologic structure and geometry of the reservoir. Secondary recovery results from the augmentation on natural energy through injection of water or gas to displace oil towards producing wells. At the end of secondary recovery, a significant amount of oil (40-60% OOIP) is still left behind in the reservoir due to many factors including unfavorable wettability, heterogeneity of reservoir rocks (naturally and induced fractures, coexistence of impermeable or high permeable zones) and capillary trapped hydrocarbon. The way to further increase oil production is through a tertiary recovery method or an EOR process. Although more expensive to employ on a field, EOR can produce a large volume of the remaining oil in the reservoir.

Oil production from existing oil fields is consistently declining (Figure 2-1); to maintain supply for the current oil demand, some form of an EOR process is necessary. EOR processes involve the injection of a fluid or a combination of fluids into a reservoir. The injected fluids and injection processes not only supplement the natural energy present in the reservoir to displace oil, but also interact with the reservoir to create conditions favorable for oil recovery. These interactions might result in lowering of IFT, oil swelling, oil viscosity reduction, wettability modification, increase of the water viscosity (polymer injection), and improved mobility control. The ultimate goal of EOR processes is to increase the overall oil displacement efficiency, which is a function of microscopic and

macroscopic displacement efficiency. Microscopic displacement refers to the displacement or mobilization of oil at the pore scale (Green and Willhite, 1998) whereas macroscopic displacement efficiency relates to the effectiveness of displacing fluid in sweeping the reservoir volume both areally and vertically (also known as sweep efficiency).

EOR processes can be divided broadly into four categories: thermal, chemical, gas and other methods. The selection of these methods depend on the characteristics of the reservoir and availability of injection fluid. Thermal methods particularly steam drive and miscible gas (CO_2, hydrocarbon gases) injection account for largest share of EOR projects. Economics plays a major role in considering the applicability of EOR processes as they are more expensive than both secondary and primary methods of oil recovery. EOR projects have been strongly influenced by crude oil prices. Over the past few years high crude oil prices have seen a lot of investment and planning for initiating new EOR projects but with the current downturn in prices many of these projects have been shelved as the price per incremental barrel of oil produced is not profitable.

Chemical methods have been used both to increase the macroscopic sweep efficiency and microscopic displacement efficiency. In these processes oil trapped in pores due to capillary pressure or capillary forces (residual oil saturation) is mobilized by reducing the interfacial tension (IFT) between the oil and water by about 10,000. Figure 2-2 shows the effect of IFT on recovery in a displacement process where wetting or non-wetting phase residual saturation is correlated as a function of capillary number. Examples of the chemical processes are alkali surfactant polymer flooding (ASP) (Clark et al. 1993), polymer-gel to shut-off the high-permeability areas of the reservoirs (Seright and Liang, 1994) and polymer flooding to increase the viscosity of the injected water to increase the sweep in the reservoir (Chauveteau and Sorbie, 1991; Yang et al., 2006).

It is also possible to enhance the oil production through wettability alteration of the reservoir. Wettability alteration is an attractive recovery method in fractured oil-wet reservoirs as changing the wettability to water-wet favors oil recovery through spontaneous imbibition (Austad et al. 1997, Adibhatla et al 2005, Gupta et al 2008. Kathel et al. 2013, Chen et al.2013). Several experiments at lab scale have shown great potential for this process and its effectiveness under different scenarios is further investigated in this work.

2.2 EOR IN FRACTURED RESERVOIRS

Naturally fractured reservoirs contain a significant amount of global hydrocarbon reserves. In North America alone, there are greater than 30 billion barrels of oil reserves in fractured formations (Forrest et al. 2011). These reservoirs are characterized by a system of fractures existing within a background rock matrix (Figure 2-3). Nelson (2001) identified four types of naturally fractured reservoirs. In Type-I reservoirs, fractures provide the essential reservoir storage capacity (porosity) and permeability. In Type-II systems, fractures provide the essential permeability, but the matrix provides the essential porosity. In Type-III reservoirs, the matrix permeability is relatively high, with the fractures acting to further increase flow capacity. In Type-IV fractured reservoirs, the fractures are filled with minerals and provide no additional porosity or permeability. In this case the fractures create significant reservoir anisotropy and tend to form barriers to fluid flow and partition formations into relatively small blocks. Type II and Type III reservoirs are of interest for this study.

Oil recovery in oil-wet fractured sandstone and carbonate reservoirs is a challenge. In low permeability fractured formations, primary recovery remains as low as 10-15 % of original oil in place, even after long horizontal wells have been drilled and massively fractured (Manrique et al. 2010). The recovery efficiency by waterflooding is very low if

the formation is oil-wet and fractured (poor sweep) as no oil can be recovered through spontaneous imbibition and the rock matrix remains saturated with oil (Figure 2-4 and Figure 2-5)

Oil recovery in fractured reservoirs depends critically on the wetting properties of the rock matrix. Large remaining oil after primary production in such reservoirs is a strong motivation to develop new oil recovery methods. Many researchers have investigated recovering oil by fracturing tight formations (Miller et al., 2008, Buffington et al., 2010). There have been studies focused on CO_2 injection in tight oil reservoirs (Arshad et al. 2009, Ren et al. 2011), but existence of fractures in the formation is detrimental to CO_2 flooding leading to poor sweep (Arshad et al. 2009) and early gas breakthrough.

Wettability alteration provides a possible solution to enhance oil recovery in oil/mixed wet fractured formations. Different chemicals such as surfactants, enzymes, selective ions can be used to alter wettability. The agents for wettability alteration differ for each reservoir and depend on the given rock, oil and brine system. High oil recovery in spontaneous imbibition experiments using these surfactant formulations have confirmed their efficacy as agents for altering wettability.

2.3 WETTABILITY ALTERATION IN FRACTURED RESERVOIRS

2.3.1 Introduction

Wettability is defined as the tendency of one fluid to spread onto or adhere to a solid surface in the presence of a second immiscible fluid (Anderson, 1986a). Wettability can be quantified by the contact angle between the phases as shown in Figure 2-6. Wettability can be classified in three categories based on contact angle measurement. Figure 2-7 shows the schematic of the position of oil drop in water-wet, oil-wet and

intermediate wet systems, respectively. The force balance in a water/oil/solid system is given by young's equation:

$$\gamma_{ow}\cos\theta = \gamma_{os} - \gamma_{ws} \quad (2\text{-}1)$$

where γ_{os} is IFT between oil-solid, γ_{ws} is IFT between water-solid, and γ_{ow} is IFT between water-oil.

Treiber and Owens (1972) used the water advancing contact angle to examine the wettability of 55 oil reservoirs with contact angle as criterion of wettability. Contact angles (measured through the water phase) from 0 to 75° were categorized as water-wet, from 75° to 105° were intermediate wet, and from 105° to 180° were oil-wet. As summarized in Table 2-1, 37 (67 %) of the reservoirs tested were classified as oil-wet, 3 were of intermediate wettability, and 15 were water-wet. Most of the oil-wet reservoirs were mildly oil-wet, with a contact angle between 120° and 140°. Of the carbonate reservoirs concerned, 8% were water-wet, 8% were intermediate, and 84% were oil-wet. Most of the carbonate reservoirs were from the west Texas area, so there is a geographical bias in the data. Chilingar and Yen (1983) reported similar results for carbonate formations: 80% oil-wet, 12% intermediate-wet, and 8% water-wet. A reason for this can be attributed to the fact that carbonate surfaces are usually positively charged in neutral pH brine (Hirasaki and Zhang, 2004). This attracts negatively charged compounds in crude oils, such as carboxylic acids. Therefore carbonate formations are usually intermediate-wet to oil-wet.

2.3.2 Impact of Wettability on Rock-Fluid Interactions

Wettability is an important petrophysical property which impacts the distribution of fluid phases (Figure 2-8) which has a significant impact on capillary pressure (Figure 2-9), relative permeability (Figure 2-11) and residual saturations. These changes in properties

of porous media can in turn have a significant impact on the rate of oil recovery and ultimate oil recoveries through various flooding or imbibition processes (Figure 2-12).

Wettability is considered to be one of the most important parameters influencing distribution and flow of fluids in porous media. The wetting fluid occupies the small pores, forms a thin film around the solid grains and occupies the corners of the grain contacts. The non-wetting phase occupies the large pores and are located at the center of the pores. These pore scale fluid distributions are shown schematically in Figure 2-8 for water-wet, mixed-wet and oil-wet porous media.

When two immiscible fluids are in contact, there is a pressure discontinuity between the two fluids which depends on the curvature of the interface separating the two fluids. This pressure difference or excess pressure is known as the capillary pressure. Capillary pressure is dependent on wettability. It is positive ($P_C = P_{Oil} - P_{Water}$) for water-wet media (red curve in Figure 2-9), for mixed-wet media part of the curve is positive and partly negative at high water saturation values, for oil-wet media capillary pressure is negative. Figure 2-10 shows the change in the capillary force vectors as the wettability is changed from oil-wet to water-wet. Initially the capillary forces are opposing the buoyancy forces as the core is oil-wet. If this core is surrounded by brine solution no imbibition will take place. On the other hand if the wettability of the core is altered to water-wet by placing it in a wettability altering surfactant solution then the capillary forces change direction and align with gravitational forces (Figure 2-10) resulting in spontaneous imbibition of surfactant solution in the core (hence displacement of oil out of the core).

Relative permeability undergoes significant changes with change in wettability. Figure 2-11 shows the relative permeability curves for different wetting states: blue curve is for water-wet media, water has low relative permeability here since it is lining the grains which reduces its mobility. Oil has high relative permeability since it's occupying the

porous media as connected globules surrounded by water which renders less resistance to its flow. On similar arguments, as the wetting state transitions towards neutral-wet and finally oil-wet, water becomes more mobile hence its relative permeability increases. Oil on the other hand becomes less mobile and its relative permeability decreases.

2.3.3 Wettability Measurement

Many methods have been proposed for measurement of wettability of a rock/oil/brine system. They include quantitative methods like contact angle measurement, imbibition and forced displacement (Amott test) and USBM wettability method. Table 2-2 lists the characterization of wettability based on range of values obtained from these methods.

In contact angle measurement, the mineral surface is typically immersed in brine and then a drop of oil is placed on the rock surface. The angle, which is measured through the more dense fluid (water) is known as contact angle. Figure 2-13 shows contact angle measurement by a goniometer on a polished calcite plate placed in a surfactant solution. For these measurements to be accurate the rock surface has to be smooth, for this purpose the mineral surfaces are polished first to remove any microscopic unevenness which can result in erroneous contact angle values. The measured contact angle is close to 0° for strongly water-wet surfaces and around 180° for strongly oil-wet surfaces.

Wettability can also be estimated qualitatively based on spontaneous imbibition experiments. Amount of oil recovered from an oil saturated core immersed in brine is a good indicator of the wetting state of the core. The core is strongly water-wet if large volumes of brine are rapidly imbibed, while lower rates and smaller volumes imply a more weakly water-wet core. If no water is imbibed, the core is either oil-wet or neutrally wet. Gravity and capillary forces play a key role in determining recovery and rate of recovery

through these processes. The relative strength of these forces determine the flow modes and type of imbibition process: counter-current or co-current. In counter-current imbibition the aqueous and oleic phases flow in opposite direction whereas in co-current imbibition aqueous and oleic phases flow in the same direction. If capillary forces are stronger than gravity forces and in the favorable wetting region then counter-current imbibition is observed. If capillary forces are negligible (interfacial tension reduced to ultra-low values), then even in an oil-wet state gravity forces can overcome them which leads to oil recovery through co-current flows.

2.3.5 Wettability Altering Agents

In fractured reservoirs, if the wettability is altered to water-wet, large amount of oil can be recovered through spontaneous imbibition. Wettability of a rock can be altered thermally (Macaulay, 1995; Al-Hadhrami et al. 2001), chemically using surfactants, low salinity brine (Nasralla et al. 2013, Mahani et al. 2015) as well as through selective ions (Tweheyo et al 2006, Zhang et al. 2006, RezaeiDoust et al. 2009, Gupta et al. 2011).

The thermal process needs a very high temperature (~200 °C); even the low salinity brine process needs a high temperature (RezaeiDoust et al. 2010). Past studies have identified cationic (Austad et al. 1997, Standnes et al. 2000, Sharma et al. 2013, Xie et al. 2005), anionic (Seethepalli et al. 2004, Adibhatla et al. 2008, Gupta et al. 2010) and non-ionic surfactants (Standnes et al. 2002, Xie et al. 2005, Gupta et al. 2010, Sharma et al. 2013) as wettability altering agents. Some studies have also investigated the role of enzymes (Nasiri et al., 2011, Halvorsen 2010) as wettability altering agents.

The Austad research group at University of Stavanger have conducted a series of studies on oil recovery from oil-wet chalk cores by use of surfactant solutions. They have shown that cationic surfactants, such as Dodecyl Trimethyl Ammonium Bromide (DTAB),

are quite effective in imbibing water into originally oil-wet cores at concentrations higher than their CMC (~1 wt.%). Xie et al. (2005) applied a combination of cationic surfactant and a nonionic surfactant to study imbibition oil recovery in dolomite cores. They found that recovery rate with the nonionic surfactant was faster than that with the cationic surfactant because the former had higher interfacial tension. Tweheyo et al., (2006) conducted imbibition experiments and found that wettability of chalks can be altered at high temperatures by divalent ions like SO_4^{2-} and Ca^{2+}. They showed that three divalent ions Ca^{2+}, Mg^{2+} and SO_4^{2-}, which are naturally present in seawater, are important in changing the surface charge of chalk and are more effective when they are all present in solution in favorable ratios.

Anionic surfactants make a good choice for use as wettability alteration agents for sandstones because they have a negative charge like the sandstone surface which results in low adsorption. Carbonates have positively charged surface, in such a scenario anionic surfactant can be used with an alkali like sodium carbonate which increases pH above the pH corresponding to the point of zero charge. This causes the surface to acquire negative charge and repel the like charged anionic polar head group of the surfactant thereby reducing adsorption (Seethepalli et al. 2004, Ahmadall et al. 1993).

2.3.4 Static and Dynamic Imbibition Experiments

Spontaneous imbibition can be evaluated in a static as well as a dynamic setup (Figure 2-15). In a static imbibition test, an oil saturated rock sample is immersed in brine or surfactant solution and the production of oil (collected at the top in the cell) is measured as a function of time. Figure 2-14 shows an imbibition cell with a core inside it. The oil recovery is governed by imbibition of the water surrounding the core into the oil saturated core. From a reservoir frame of reference, the fluid surrounding the core represents the

fluid in fracture and the core represents the matrix. Water imbibes spontaneously into the matrix blocks if the matrix is water-wet however when the matrix is oil-wet or mixed-wet, little oil can be recovered by imbibition. Static imbibition has been the experiment of choice for researchers for many decades spanning numerous studies. However, for understanding application of these processes in a reservoir where the fluid in the fracture will be mobile, it is imperative that recovery through imbibition process is investigated in a dynamic setup.

In a dynamic imbibition experiment there is fluid flow through the fracture. A schematic setup is shown in Figure 2-15 where a fracture is created axially in a cylindrical core, fluid (brine or surfactant solution) injection takes place at the bottom and produced fluids are collected at the top. Depending on the objectives of study the top and/or bottom of the core could be open or sealed through epoxy. Dynamic imbibition experimental studies have been performed on water-wet media (Putra et al. 1999, Jialu et al. 2009) but they have not been investigated in a wettability altering setup. Putra et al. concluded that optimization of injection rate in the fractures is important prior to conducting waterflooding in naturally fractured reservoirs. According to them, as the flow rate increases, contact time between matrix and fluid in fracture decreases, thereby reducing the effectiveness of capillary imbibition. Wang et al., 2009 observed that recovery was highest for cores with the maximum water-wetness. Abbasi-Asl et al., 2010 performed numerical simulation studies of surfactant flood in a grid block model having multiple fractures, they concluded that a transverse pressure gradient is able to push the surfactant into the matrix which is possible due to the formation of high viscosity microemulsion phase in the fracture.

Mirzaei (2013) performed dynamic imbibition experiments in oil saturated Estaillades Limestone cores with no initial water saturation. The cores were cut into two halves axially and were put together using tape and epoxy glue. The reformed core was

epoxy molded and placed in a CT setup for the experiment to obtain fluid distribution in core with time during experiment. An ultra-low IFT Surfactant formulation was injected into the fracture at the bottom of the core and oil recovery was observed with time. They found that gravity is the main driving force for imbibition and oil recovery decreased with increasing length and diameter of the core.

2.4 MECHANISMS OF WETTABILITY ALTERATION

Wettability depends on the brine, oil and mineral compositions as well as temperature (Anderson et al. 1986, Buckley, 2001, Gupta 2010). Most of the reservoir minerals are originally strongly water-wet. The surface active agents present in crude oil (polar compounds containing oxygen, nitrogen, sulphur) are responsible to alter the wettability of these minerals to oil-wet. These compounds contain polar end which sticks to the rock surface as well as hydrocarbon end which interacts with bulk oil making the mineral oil-wet. These compounds are acidic in nature and are more prevalent in heavier fractions of crude oil such as resins and asphaltenes. There are other factors which influence the original reservoir wettability. When the oil invades the rock, the thin water films separate rock surface from the oil. If the oil contains surface active agents which can easily diffuse through the water film, it is easy to render the surface oil-wet. Natural surfactants in crude are often sufficiently soluble in water to adsorb onto rock surface after passing through a thin layer of water (Anderson 1986).

Wang and Gupta (1995) studied the influence of temperature and pressure on wettability of reservoir rocks. Pressure did not have a significant effect on contact angle; in contrast, temperature showed a significant effect on the wettability of crude-oil/brine/quartz systems. Buckley et al (1998) investigated the mechanisms of wettability alteration by crude oils and identified four main categories of crude oil/brine/rock

interactions which are illustrated in Figure 2-16. These include: 1) Polar interactions, which can only occur when there is no water present in the system and is likely to happen between polar surface and polar components; 2) Precipitation of asphaltenes onto the surface when the oil is a poor solvent for the heavy fraction; 3) Acid/base interactions, which take place between sites of opposite electrical charge; 4) Ion binding, which divalent or multivalent ions in the brine can bridge the mineral surface to oil/brine interface.

Different mechanisms for wettability alteration by surfactants have been postulated in the literature. Standnes and Austad stated that wettability alteration takes place by ion pair formation between the cationic surfactant and adsorbed negatively charged carboxylates from oil on chalk surfaces. For anionic surfactants, Austad (1998) claimed that the surfactant molecules could form a monolayer on the rock surface through hydrophobic interactions with the adsorbed crude oil components.

Using atomic force microscopy (AFM), Kumar et al. (2008) proposed micellar solubilization of adsorbed organic components by anionic surfactants. They showed that wettability of a rock is controlled by adsorption of asphaltenic components on the mineral surface. In their study saturates, aromatics, resins, and asphaltene fractions of an oil sample were extracted and silica and mica surfaces were aged with these fractions. The adsorption of these different fractions on the rock surfaces was then evaluated using AFM.

Al-Hadhrami and Blunt (2001) performed experiments on core from fields in Oman and found that the rock surface transitioned from oil-wet to water-wet as the temperature is increased. The temperature could be increased in a reservoir setting through steam or hot water injection. A proposed mechanism for wettability alteration at elevated temperatures is based on the assumption that adsorption of polar components on carbonate rock surface is an exothermic reaction (Madsen and Lind, 1998), increased temperature or addition of heat will therefore lead to desorption of polar components from the rock surface.

Tweheyo *et al.* (2006) conducted imbibition experiments and found that wettability of chalks can be altered at high temperatures by divalent ions like SO_4^{2-} and Ca^{2+} without any surfactant. It was documented by zeta potential measurements that Ca^{2+}, Mg^{2+} and SO_4^{2-} acted as potential determining ions towards the rock surface (Chalk), i.e., they were able to adsorb onto the chalk surface and modify the surface charge. Some studies havc also attributed wettability alteration to mineral dissolution. Chen and Mohanty (2013) used a sequestering agent ethylene diamine tetra-acetic acid (EDTA) along with an anionic surfactant in a hard brine. They proposed that EDTA aided in dissolution of dolomite which altered the wettability. Zhou et al. (2000) conducted a study of the chemical interactions between brine solutions and dolomite. They found that although the pH of injection brine (KCl solution) varied from 4 to 10, the pH values of effluent samples were consistently around 10 due to dissolution of dolomite mineral. They observed that absence of cationic ions Mg^{2+}, Ca^{2+} in the injection brine promotes the dissolution of the dolomite.

2.5 SCALING OF SPONTANEOUS IMBIBITION PROCESSES

Scaling rules facilitates studying of imbibition processes and are beneficial for a variety of reasons:

- To understand the physics and the first order mechanisms governing the process.
- To predict recovery in larger dimension matrix blocks with an aim to understand the feasibility of the process at larger scales.
- To determine the sensitivity with different parameters like absolute and relative permeability, porosity, viscosity etc.

Oil recovery through imbibition processes is slow and it has been of particular interest among researchers to study scaling of these processes with regard to feasibility of oil recovery rate at larger scales as well as for optimization of these processes. Using these

relationships, recovery behavior for a large reservoir matrix block can be estimated and influence of key parameters like permeability, viscosity etc. can be predicted from an imbibition test on a small core sample. Many researcher's (Mattax and Kyte 1962, Hagoort et al. 1980, Schechter et al. 1994, Li and Horne 2002 & 2006, Schmidt et al. 2012) have proposed dimensionless time for scaling of experimental data. Figure 2-17 shows a plot where the data from different experiment sets collapses to a single curve indicating a good correlation with the dimensionless time.

Imbibition and drainage of wetting and non-wetting phases from the matrix blocks of fractured reservoirs are driven by a combination of capillary, gravity and viscous forces. The ratio of capillary to gravitational forces is termed as macroscopic bond number and is defined as (Schechter et al. 1994):

$$N_B^{-1} = C\frac{\sigma\sqrt{\frac{\phi}{k}}}{\Delta\rho g H} \tag{2-2}$$

where C=0.4 for capillary tube model, σ is the interfacial tension, ϕ is porosity, k is the absolute permeability, Δρ is the density difference, and H is the height of the core. At high values of inverse bond number (typically N_B^{-1} >5) or high ratio of capillary to gravity forces the flow is capillary dominated and countercurrent. At low (N_B^{-1} <<1), gravity forces dominate the flow. For intermediate values of N_B^{-1} both capillarity and gravity contribute to flow. For $N_B^{-1} < 0.1$, the process is gravity driven.

Mattax and Kyte (1962) were the first to propose a scaling group for capillarity-controlled imbibition where effect of gravity was not considered. Their scaling group is given by:

$$t_D = t\sqrt{\frac{k}{\varphi}}\frac{\sigma}{\mu_w}\frac{1}{L^2} \tag{2-3}$$

Ma et al. 1997 modified the scaling group to include viscosity of the displaced phase as well as a characteristic length. The scaling group by Ma et al is given by:

$$t_D = t\sqrt{\frac{k}{\phi}}\frac{\sigma}{\sqrt{\mu_o\mu_w}}\frac{1}{L_c^2} \qquad L_c = \frac{Ld}{2\sqrt{d^2+2L^2}} \tag{2-4}$$

The scaling group is applicable to strongly water-wet cases where effect of gravity is negligible. The scaling group was validated with experimental data (Figure 2-17) from Mattax and Kyte (1962), Hamon and Vidal (1986) and Zhang et al. (1996). However for processes wettability is altered this scaling group fails to correlate the data (Figure 2-18).

Li and Horne (2002) developed a scaling group for oil-water-rock systems which can incorporate different initial wetting state based on relative permeability and capillary pressure (gravity not considered). The model predicts a linear correlation between the oil recovery by spontaneous water imbibition and the square root of dimensionless time. It is given by:

$$R_{OOIP} = \frac{c}{V_p(1-S_{wi})}t^{1/2} \tag{2-5}$$

$$c = A\sqrt{2P_C^*M_e^*\phi(S_{wf}-S_{wi})} \tag{2-6}$$

$$t_D = \frac{M_e^*P_c^*}{\phi}\frac{S_{wf}-S_{wi}}{L_a^2}t \tag{2-7}$$

$$M_e^* = \frac{k_e^*}{\mu_e} = \frac{M_w^*M_o^*}{M_w^*+M_o^*} = k\frac{\frac{k_{rw}^*}{\mu_w}\frac{k_{ro}^*}{\mu_o}}{\frac{k_{rw}^*}{\mu_w}+\frac{k_{ro}^*}{\mu_o}} \tag{2-8}$$

$$\frac{\partial P_C}{\partial x} = \frac{P_C}{x} \tag{2-9}$$

here * indicates values at S_{wf} which is the average water saturation behind the imbibition front, k_{rw} is the water relative permeability and k_{ro} is the oil relative permeability, t_D is

dimensionless time, μ_o , μ_w are water and oil viscosities respectively, A is the area open to flow, L_a is the characteristic length evaluated in the same manner as Morrow et al. (1997). A critical assumption in their derivation is given by equation 2-9 which is valid for piston like displacement which is not the case in porous media. Another limitation in their analysis is that the value c (constant value) is determined by matching each experiment data set which is not an accurate measure of accounting for capillary pressure and mobility effect on oil recovery. Later (2006) they proposed a modified model to include the effect of gravity. The modified equations are:

$$t_D = c^2 \frac{M_e^* P_c^*}{\phi} \frac{S_{wf} - S_{wi}}{L_a^2} t \tag{2-10}$$

$$c = \frac{b_0}{a_0}, a_0 = \frac{A M_e^* \mathrm{P}_c^* (S_{wf} - S_{wi})}{L} \quad b_0 = A M_e^* \Delta\rho g \tag{2-11}$$

$$q_w = a_0 \frac{1}{R} - b_0 \tag{2-12}$$

$$(1 - R^*) R^* = e^{-t_D} \tag{2-13}$$

In addition to the limitations mentioned above another limitation of this analysis is that it can either consider co-current flow or counter-current flow but not a combination of both. Such an assumption is not valid when gravity and capillarity both have effect on oil recovery.

Hagoort (1980) analyzed one dimensional gravity drainage by a gas and proposed the following dimensionless time. Since the gravity drainage scaling term was developed for gas-oil system it does not take into account varying wettability and IFT. It also does not include displacing fluid viscosity because it was developed for an inviscid displacing fluid.

$$t_{Dg} = \frac{k k_{ro} \Delta\rho g}{(S_{oi} - S_{or}) \phi \mu_o H} t \tag{2-14}$$

Schechter et al. 1994 proposed the following dimensionless number for gravity dominated imbibition process which is given by:

$$t_D = \frac{\lambda^* \Delta\rho g}{H\phi} t \tag{2-15}$$

where λ^* is the reference mobility for co-current gravity dominated flow.

The above two models for gravity dominated flow assume that only bottom of the core is exposed to the fluid for co-current imbibition hence there is no effect of the radial or lateral dimension of the core.

Mirzaei et al. (2013) modified the scaling group proposed by Schechter et al. (1994) to include the effect of imbibition from the side of the core. The new scaling group for gravity dominated imbibition which predicts scaling with both horizontal and vertical fracture spacing is given by:

$$t_D = \frac{\lambda^* \Delta\rho g}{\phi}\left(\frac{1}{H} + \frac{8\gamma}{\pi D}\right)t \tag{2-16}$$

where $\lambda^* = k\frac{k_r^*}{\mu^*}$ is the reference mobility for co-current gravity dominated flow, $\gamma = \frac{q_{side}}{q_{bottom}}$ is the ratio between flux from the side and flux from the bottom of the core which was determined from the experimental data. As per their findings the scaling group was able to scale the experimental results with varying height but for cores with different diameters it wasn't able to scale the results as shown in Figure 2-19.

2.6 Numerical Modeling of Wettability Alteration

Reservoir simulation is an essential tool for mechanistic understanding of a process, performance prediction at larger scales and reservoir management. Numerical simulators (John et al. 2005, Shutang et al. 1996) have been developed in the past for chemical

flooding in which the IFT changes along the reservoir with time. John et al. (2005) incorporated oil/surfactant/brine-phase behavior using Hand's rule and trapping number model for relative permeability in their simulator. Most simulation studies are focused on the study of chemical EOR in non-fractured reservoirs without wettability alteration.

In order to better understand the process of oil recovery from an initially oil-wet matrix block using surfactant-aided wettability alteration, a numerical model of the system was developed by Adibhatla et al. (2008). The simulator uses a 3D finite volume, two-phase, four-component implicit numerical scheme that accounts for surfactant convection/diffusion, consequent IFT and contact angle changes. The injected surfactant moves into the matrix because of flow caused by wettability alteration and IFT reduction. The capillary pressure between the oil and brine phase, the relative permeabilities and the residual saturations of both phases were considered as functions of wettability and IFT. Capillary pressure is assumed to depend on saturation through a power-law model.

$$P_C(S_{DW}) = P_{CA} + P_{CB}(S_{DW})^{n_c} \tag{2-17}$$

In equation 2-17, P_{CA} and P_{CB} determine the endpoints of the capillary pressure curve, n_c is the exponential parameter and S_{DW} is the dimensionless water saturation defined by

$$S_{Dj} = \frac{S_j - S_{jr}}{1 - S_{wr} - S_{or}} \tag{2-18}$$

According to the Leverett J-function, the effects of interfacial tension σ contact angle θ on capillary pressure are described with the following equation:

$$P_C = P_{C0}(S_{DW}) \frac{\sigma \cos\theta}{\sigma_0 \cos\theta_0} \tag{2-19}$$

The subscript '0' on capillary pressure, interfacial tension and contact angle indicates values for an initial oil-wet system. Relative permeability curves are described by a modified Brooks-Corey model, i.e.,

$$k_{rj} = k_{rj}^0 (S_{Dj})^{n_j} \tag{2-20}$$

where k_{rj}^0 is the end is point relative permeability of phase j and n_j is the relative permeability exponent of phase j. The end point relative permeability and exponent vary with contact angle as presented below:

$$k_{rj}^0 = k_{r,wet}^0 + \frac{\cos\theta_j - \cos\theta_0}{\cos(\pi - \theta_0) - \cos\theta_0}(k_{r,nw}^0 - k_{r,wet}^0) \tag{2-21}$$

$$n_j = n_{wet} + \frac{\cos\theta_j - \cos\theta_0}{\cos(\pi - \theta_0) - \cos\theta_0}(n_{nw} - n_{wet}) \tag{2-22}$$

θ_j is the contact angle measured through phase j, $k_{r,wet}^0$ corresponds to the wetting phase endpoint relative permeability and $k_{r,nw}^0$ corresponds to the non-wetting phase endpoint relative permeability. For considering the effect of IFT on change in residual saturations and consequent change in relative permeability parameters, the above equations can be modified with the trapping number. Interfacial tension and contact angle variation with surfactant concentration is modeled as polynomial and linear functions, respectively, with endpoint parameters obtained from experimental data.

UTCHEM, the University of Texas in-house compositional chemical simulator has the capability to model the effect of wettability on relative permeability, capillary pressure and residual oil saturation. In the wettability alteration model of UTCHEM, two extremes wetting states of strongly water-wet and strongly oil-wet are defined for the relative

permeability and capillary pressure. As the surfactant enters a grid block, it reduces the IFT, and as a result, the trapping number increases. The IFT reduction and oil-mobilization effect of surfactants affects the residual-phase saturations, endpoint relative permeabilities and exponents. The mobilization effect on residual-phase saturations is modeled (Delshad et al. 1986) as:

$$S_{lr} = \min\left[S_l, \left(S_l^{high} + \frac{S_{lr}^{low} - S_{lr}^{high}}{1 + T_l N_{Tl}} \right) \right] \tag{2-23}$$

$$N_{Tl} = \frac{\left| -\bar{\bar{k}}.\nabla\Phi_{l'} - \bar{\bar{k}}.[g(\rho_{l'} - \rho_l).\vec{\nabla}h] \right|}{\sigma_{ll'}} \tag{2-24}$$

where l and l' are the displaced and displacing fluids, respectively; Φ is the flow potential; g is the gravitational acceleration; k is the permeability tensor; h is the height to a reference datum; ρ_l and $\rho_{l'}$ are densities of the displaced and displacing fluids, respectively. The relative permeability in each grid block is calculated using a linear interpolation between relative permeability curves of the initial and final wetting states, provided that the surfactant concentration is higher than Critical Micelle Concentration (C.M.C.), i.e.

$$k_r = \omega k_r^{final} + (1-\omega) k_r^{initial} \tag{2-25}$$

$k_r^{initial}$ and k_r^{final} represent the relative permeabilities and capillary pressure corresponding to the initial and final wettability states respectively and ω is the interpolation scaling factor defined as:

$$\omega = \frac{\hat{C}_{surf}}{\hat{C}_{surf} + C_{surf}} \tag{2-26}$$

where $\hat{C}_{surf}$ and C_{surf} are adsorbed and total surfactant concentration in each grid block respectively. A constant value of scaling factor can also be assigned which bypasses the

above definition of scaling factor. The capillary pressure is also modified in a similar manner to account for change of wettability using the same linear interpolation as relative permeability. Effect of oil/micro-emulsion IFT is also considered for as given in equation 2-27.

$$P_C = \omega P_C^{final} + (1-\omega)\,\mathrm{P}_C^{initial} \tag{2-27}$$

$$P_C = P_{COW}\frac{\sigma_{om}}{\sigma_{ow}} \tag{2-28}$$

Recently, a commercial simulator CMG has added the capability to model wettability alteration. In their model relative permeability and capillary pressure data can be interpolated as functions of surfactant concentration or capillary number to incorporate the effect of changing wettability. The data for capillary pressure and relative permeability has to be entered in tabular format at different values of the interpolation variable considered.

2.6.1 Dual Porosity Simulation in Fractured Reservoirs

Dual porosity systems are characterized by two porosities. A primary porosity which is that of the matrix and a secondary porosity corresponding to fractures in the media. The dual porosity approach was formulated by Barenblatt and Zheltov (1960) for single phase in naturally fractured reservoir composed of two superimposed media, a continuous fracture system and a discontinuous system of matrix blocks.

Warren and Root (1963) presented a practical model for fractured systems (Figure 2-20). They considered an idealized case comprised of a set of identical rectangular parallelepipeds, representing the matrix blocks, which are separated by fractures. Kazemi et al. (1976) presented an extension of the dual-porosity model of Warren and Root (1963) to two-phase flow which could account for relative fluid mobilities, gravitational effects,

imbibition, and variation in formation properties. They derived two flow equations, one for the matrix and another for the fracture which were coupled via a transfer function. Thomas et al. (1983) developed a three-dimensional, three-phase model for simulating the flow of water, oil, and gas in fractured systems. Donato and Blunt (2003) presented a model combining a streamline simulation technique with a dual-porosity model.

Other approaches for simulating fluid flow in fractured reservoirs include discrete fracture network (DFN) modeling (Noorishad and Mehran, 1982) and a less computationally intensive embedded dicrete fracture model (EDFN). The DFN represents each fracture as a geometrically well-defined entity and each fracture is modeled explicitly. It incorporates unstructured grid blocks and a large number of grid blocks located near fractures which makes it computationally intensive. It requires a lot of geological input and hence models heterogeneity well. There is no need of a transfer function in a discrete fracture network model. Compared to the DFN, the EDFN has a structured grid, It also requires accurate geological input and fracture inputs to compute the intersection of fracture and matrix grid block. Fractures are approximated by arbitrary planar rectangles or other arbitrary orientation in horizontal plane. The fracture matrix interaction is given by

$$q = \frac{Ak_m}{\mu}\frac{(P_m - P_f)}{d} \tag{2-29}$$

where A is facture surface area in the gridblock , k_m, harmonic average of matrix and fracture permeabilities and d, distance between the two control volumes. EDFN is faster compared to DFN and can be used for field scale simulations.

Spontaneous imbibition is an important oil recovery mechanism in naturally fractured reservoirs. Behbahani et al. (2006) attempted to find a matrix fracture transfer

function for counter current imbibition in strongly water-wet systems. Their transfer function however requires a functional scaling group to correlate the experimental imbibition data. This leads to a dependence of the transfer function on the scaling group. They used the scaling group proposed by Ma et al. (1997) for generating simulation results based on their transfer function. Also, the transfer function is dependent on time which is a global variable rather than local properties like saturation which can be related at each grid block level. The transfer function proposed by Behbahani et al. (2006) cannot be used as an input to the existing dual porosity simulators as it is not expressed in the form of a coefficient to the pressure difference between fracture and matrix. Gupta and Civan (1994) also attempted to find a transfer function but it was in the form of a scaling group which cannot be incorporated in the existing dual porosity simulators and hence cannot be used for field scale simulation.

Farhadinia et al. (2010) studied wettability alteration and interfacial tension reduction due to surfactants in a dual porosity system using UTCHEM. Relative permeability and capillary pressure was scaled between the initial and final states as mentioned previously (Equation 2-25, 2-27). To match the dual porosity UTCHEM simulation with explicit fracture simulations a numerical constant was multiplied to the transfer function. The values for the numerical constant were 1.15, 0.2 and 0.35 for water, alkali and alkali/surfactant floods, respectively. Values of 0.2 and 0.35 indicate a significant retardation in rate of oil recovery due to surfactant processes as compared to waterflooding in a water-wet media. They also noted that the dual porosity model may not be adequate to model the dynamic changes in capillary pressure and relative permeability due to wettability modification and interfacial tension reduction.

	Contact angle (degrees)	Silicate reservoirs	Carbonate reservoirs	Total reservoirs
Water-wet	0-75	13	2	15
Intermediate wet	75-105	2	1	3
Oil-wet	105-180	5	22	37
Total		30	25	55

Table 2-1: Distribution of reservoir wettabilities based on contact angle (Treiber and Owens, 1972)

	Water-Wet	Neutrally Wet	Oil-Wet
Contact angle			
Minimum	0°	60 to 75°	105 to 120°
Maximum	60 to 75°	105 to 120°	180°
USBM wettability index	*W* near 1	*W* near 0	*W* near −1
Amott wettability index			
Displacement-by-water ratio	Positive	Zero	Zero
Displacement-by-oil ratio	Zero	Zero	Positive
Amott-Harvey wettability index	$0.3 \leq I \leq 1.0$	$-0.3 < I < 0.3$	$-1.0 \leq I \leq -0.3$

Table 2-2: Relationship between wettability, contact angle, Amott and USBM wettability indexes (Anderson, 1986b)

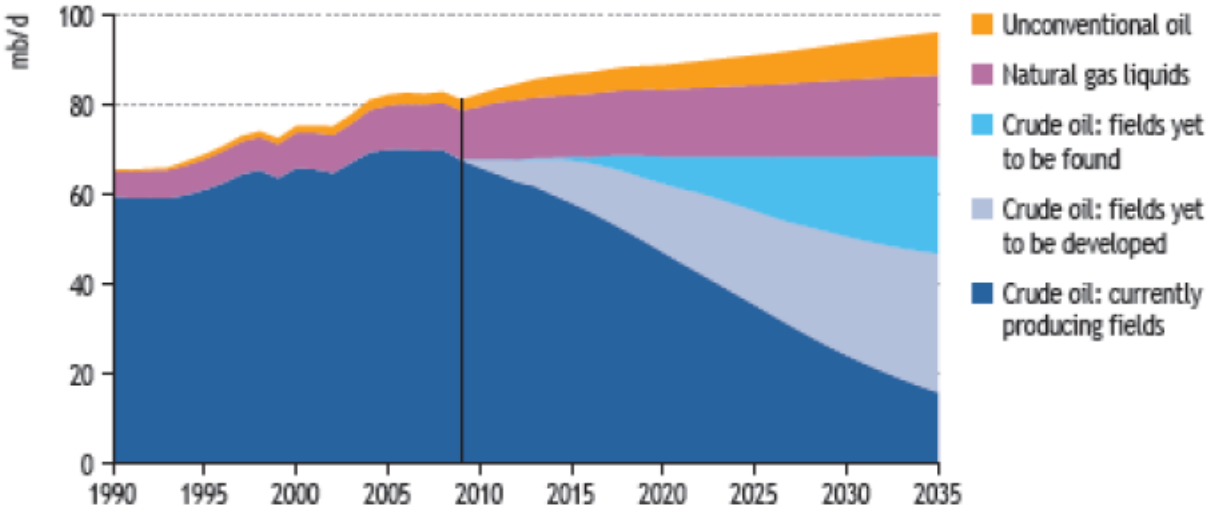

Figure 2-1: World Oil Production (World Energy Outlook, 2010)

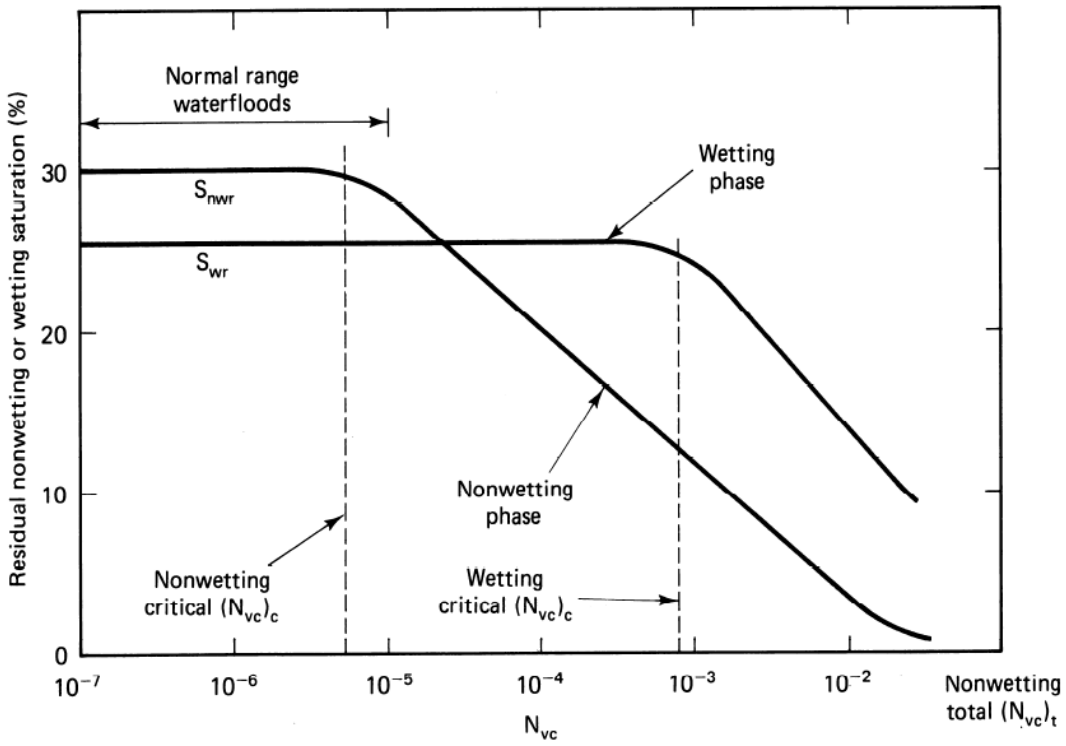

Figure 2-2: Schematic of a capillary desaturation curve (Lake, 1984)

(a)

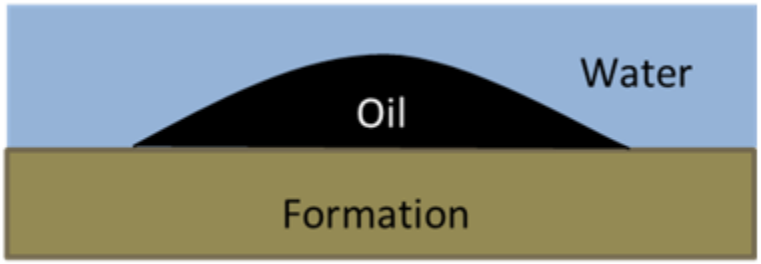

(b)

Figure 2-3: (a) Vertically running natural fractures in an outcrop rock. (b) Schematic representation of oil-wetness.

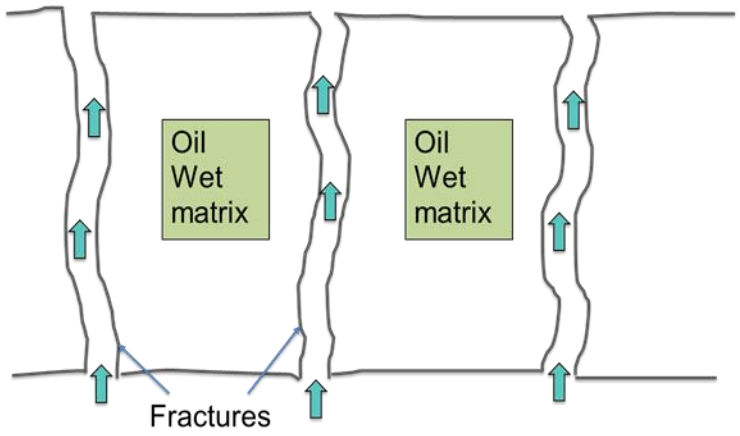

Figure 2-4: Waterflooding results in low oil recovery when matrix is oil-wet

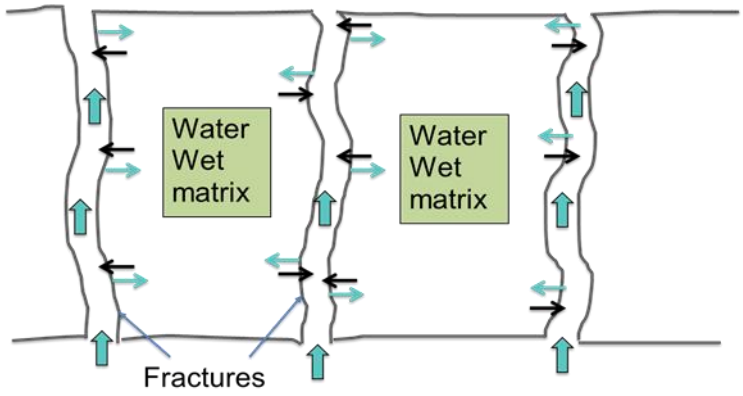

Figure 2-5: Waterflooding results in high oil recovery when matrix is water-wet due to spontaneous imbibition of water into oil containing matrix blocks.

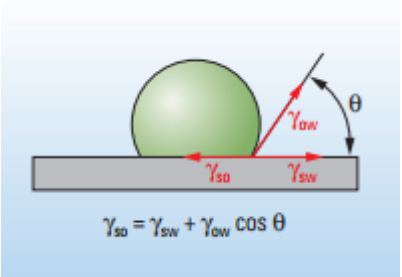

Figure 2-6: Schematic description of force balance for an oil droplet immersed in water. (Fundamentals of Wettability, Schlumberger 2007)

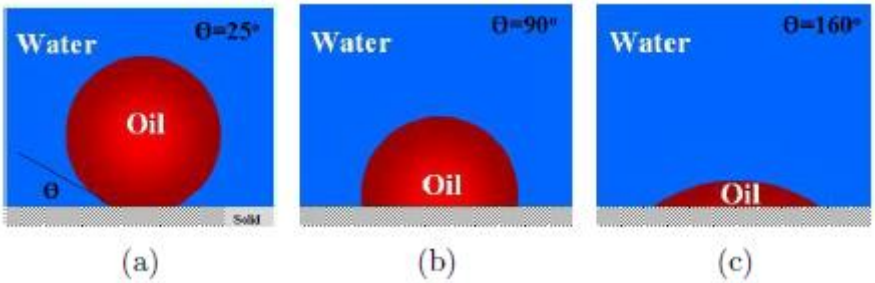

Figure 2-7: Classification of wettability based on contact angles between water and oil. (a) Strongly water-wet, (b) Intermediate wet, (c) Oil-wet. (Morrow, 1990)

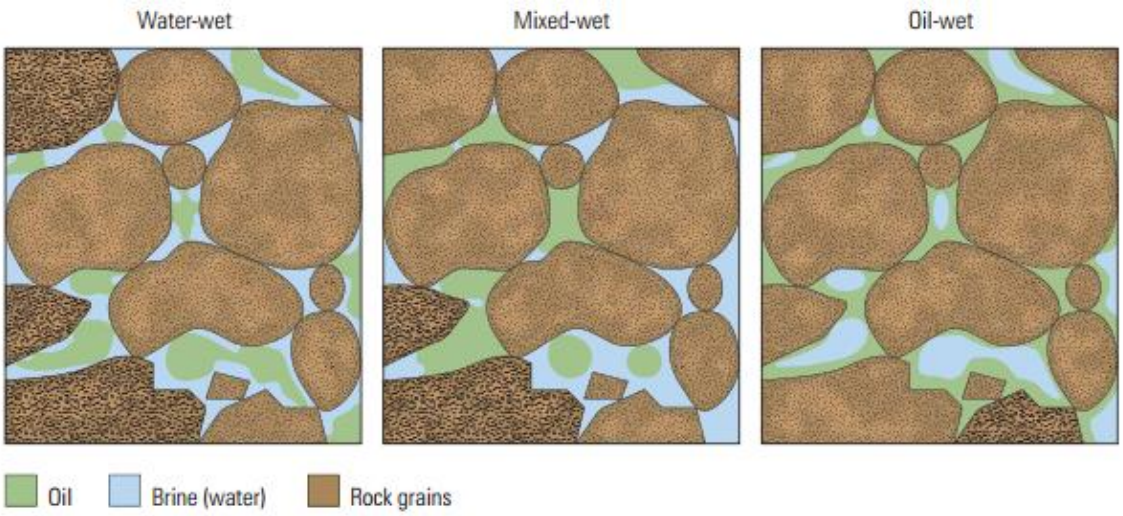

Figure 2-8: Distribution of oil and water under different wettability conditions. (Schlumberger 2007)

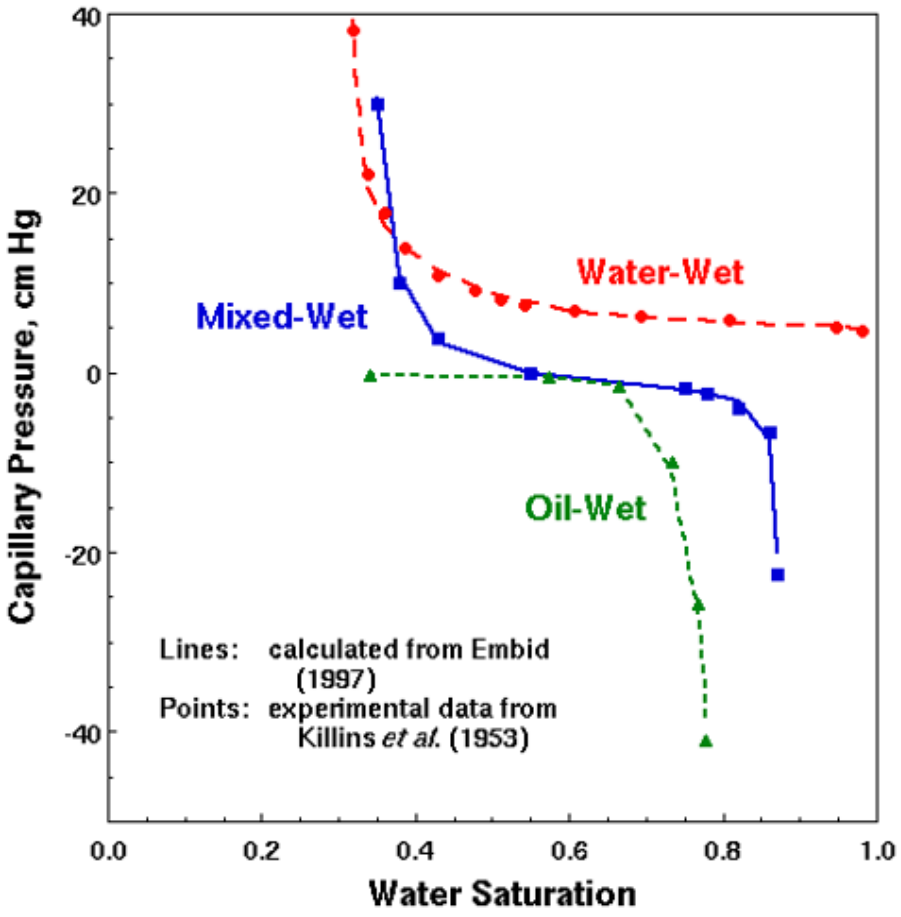

Figure 2-9: Capillary pressure curves for different reservoir wetting states.

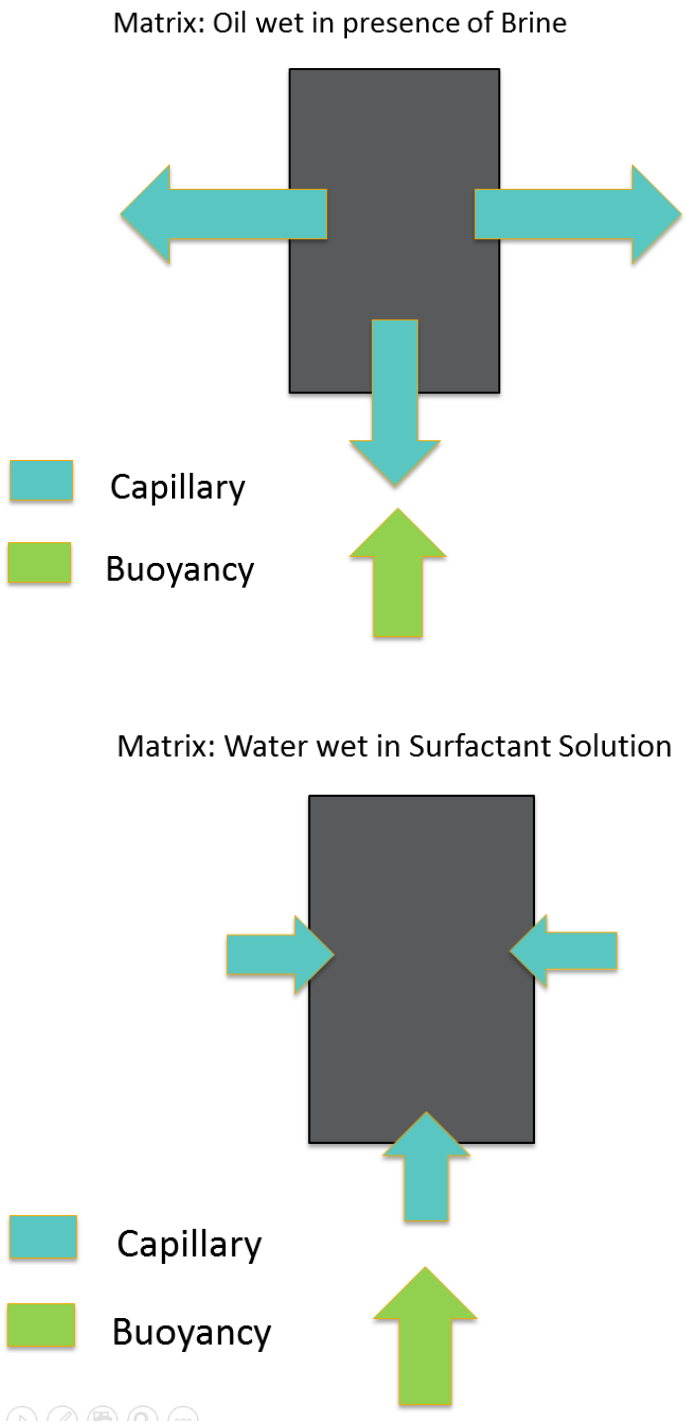

Figure 2-10: Schematic of change in capillary force vectors as the wettability of the core changes from oil-wet to water-wet.

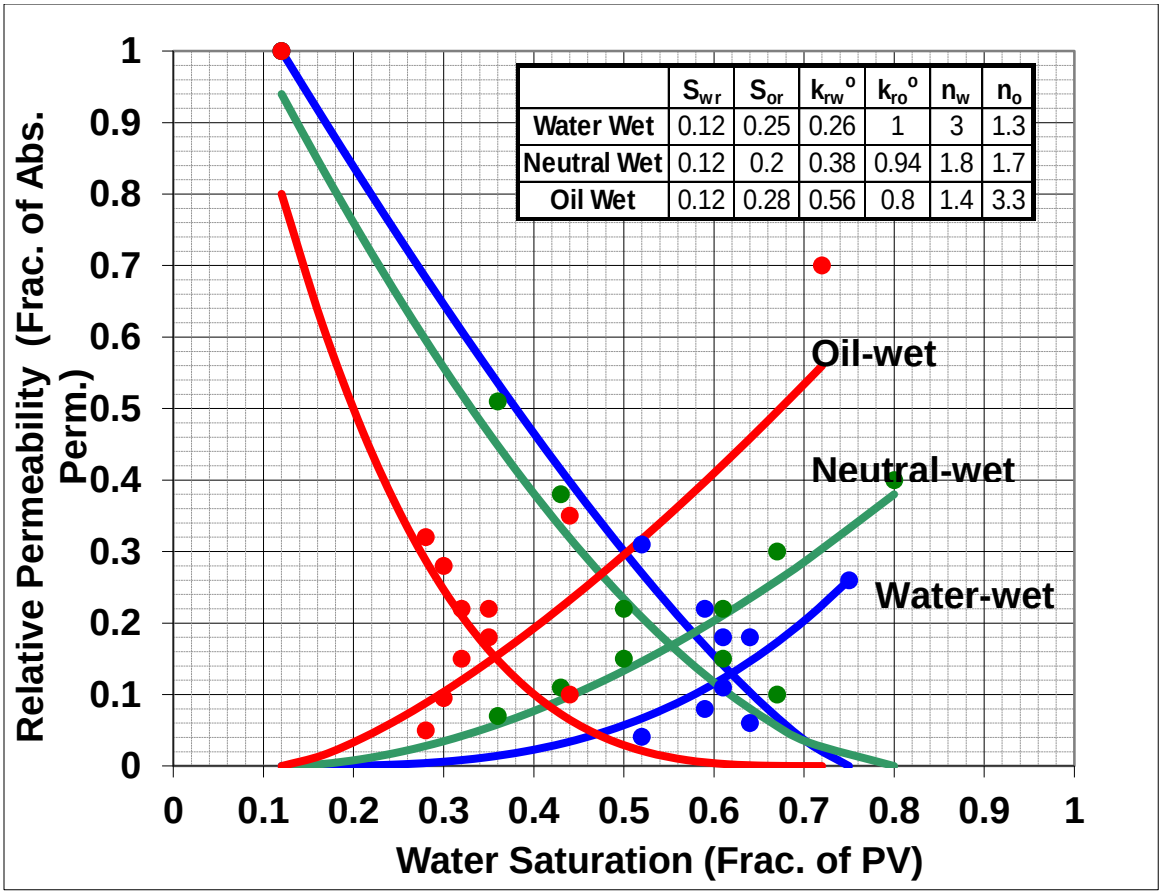

	S_{wr}	S_{or}	k_{rw}^o	k_{ro}^o	n_w	n_o
Water Wet	0.12	0.25	0.26	1	3	1.3
Neutral Wet	0.12	0.2	0.38	0.94	1.8	1.7
Oil Wet	0.12	0.28	0.56	0.8	1.4	3.3

Figure 2-11: Relative permeability curves for different wetting states (Morrow 1973).

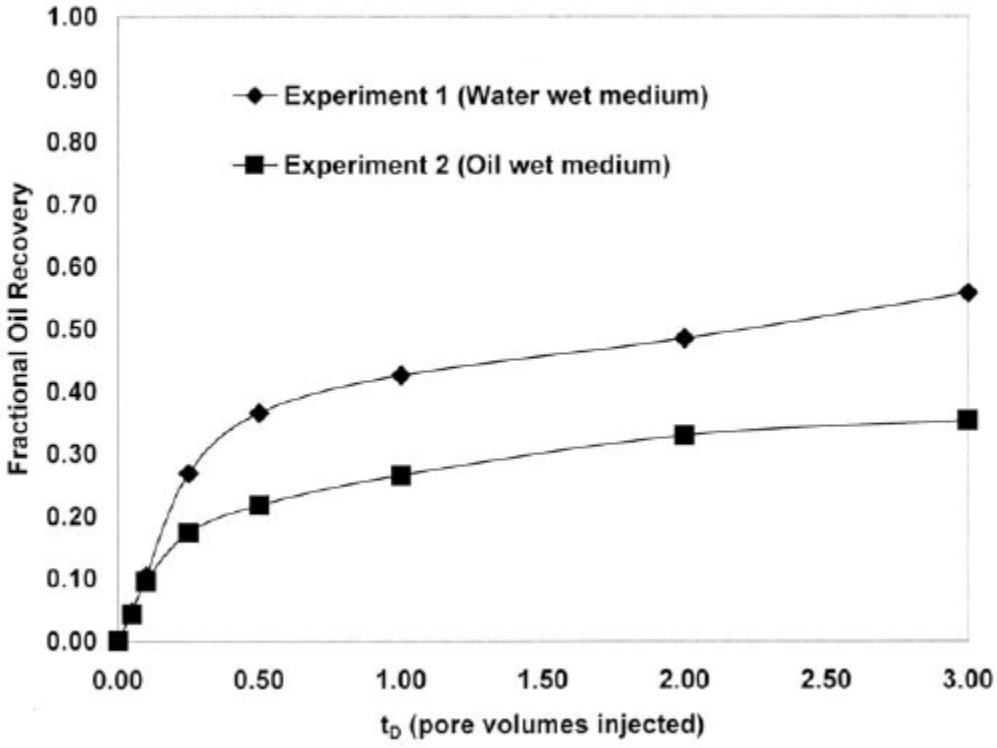

Figure 2-12: Effect of wettability on waterflood performance (Peters, 2009).

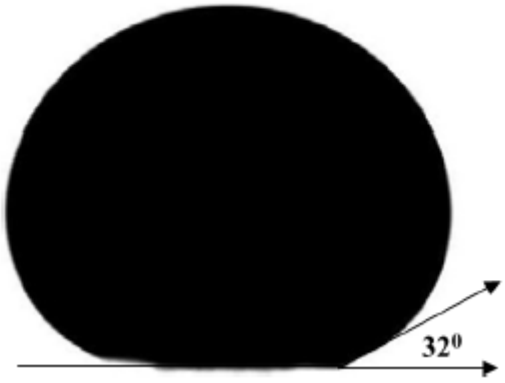

Figure 2-13: Contact angle measurement on a goniometer (Rame Hart Model 500) on a polished calcite plate post wettability alteration by an anionic surfactant (Seethepalli et al. 2004).

Figure 2-14: A core immersed in a surfactant solution in an imbibition cell.

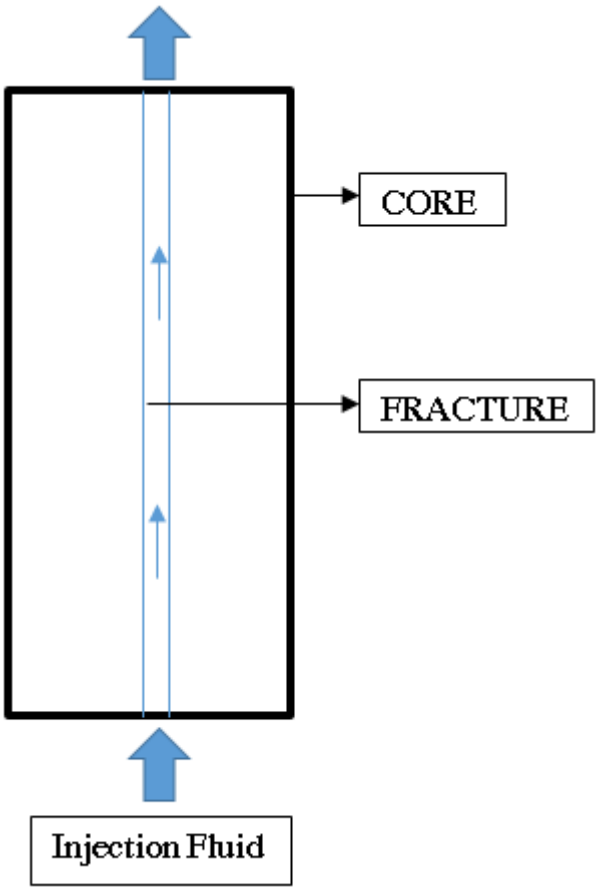

Figure 2-15: Schematic of a dynamic imbibition setup with fluid injection in the fracture.

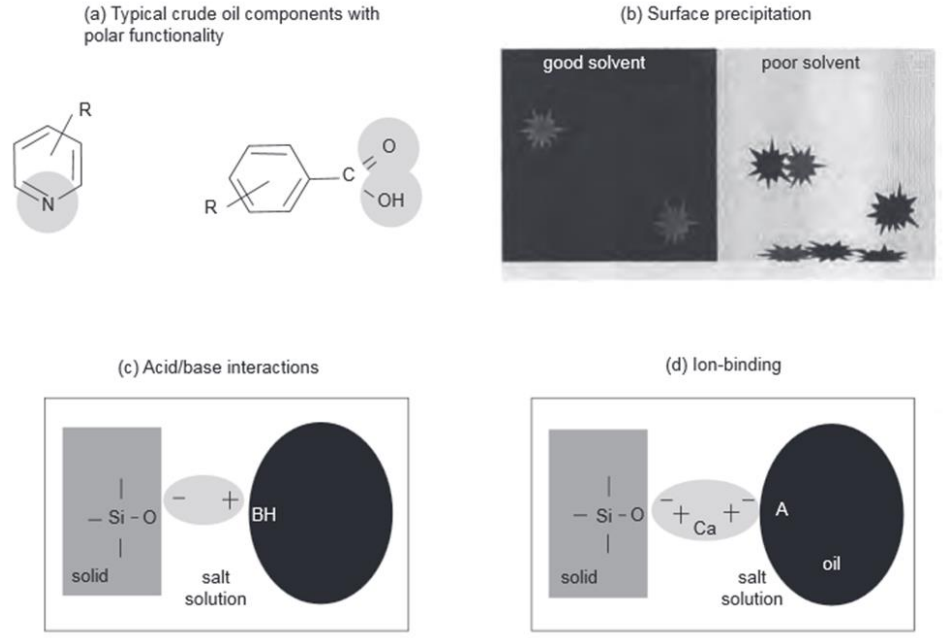

Figure 2-16: Interaction between crude oil and rock components (Buckley et al. 1998)

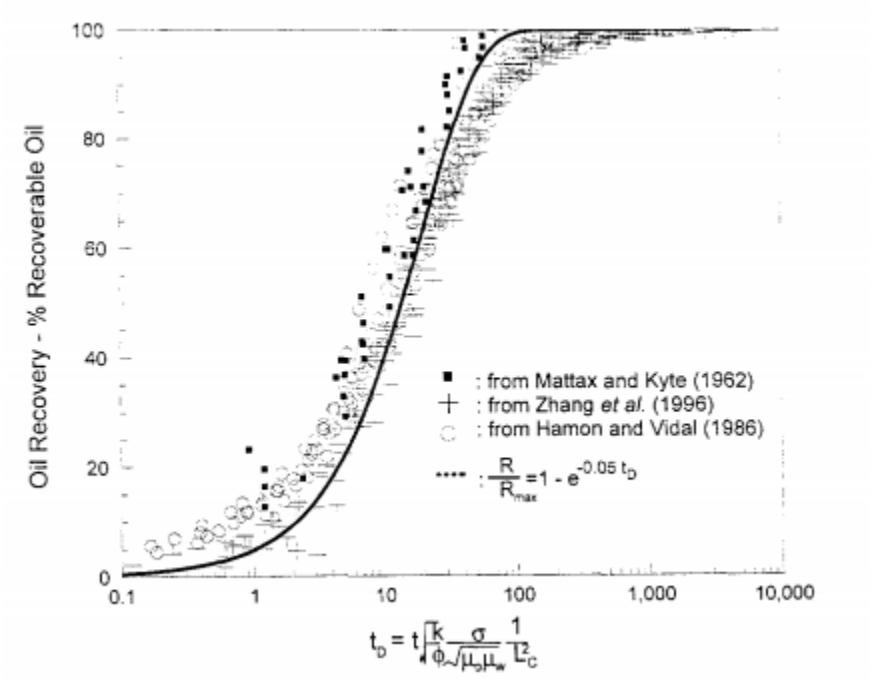

Figure 2-17: Recovery plotted with dimensionless time shows strong correlation (Ma et al. 1997)

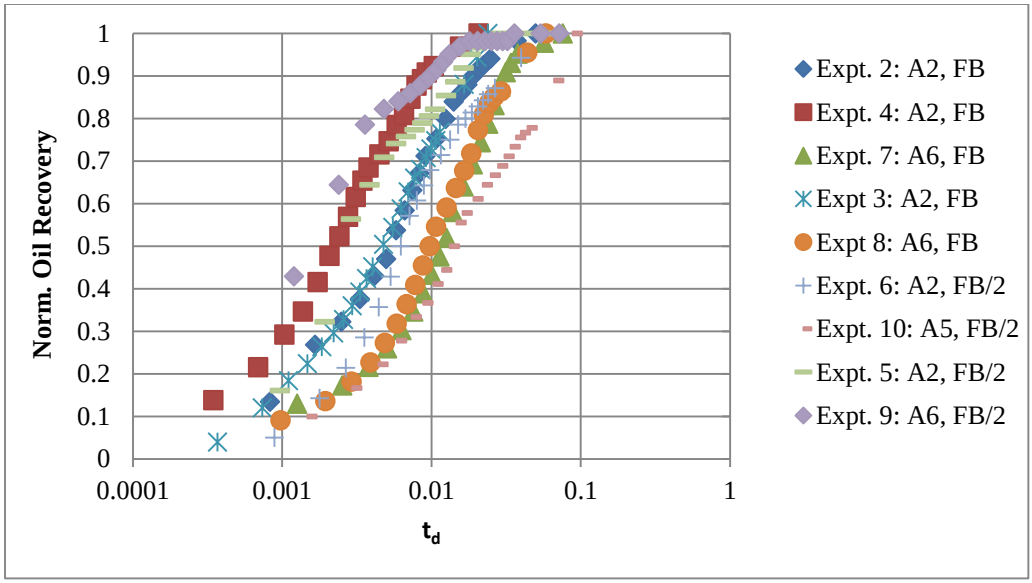

Figure 2-18: Scattering of wettability altering imbibition data when plotted with the Ma and Morrow dimensionless time (Kathel et al. 2013)

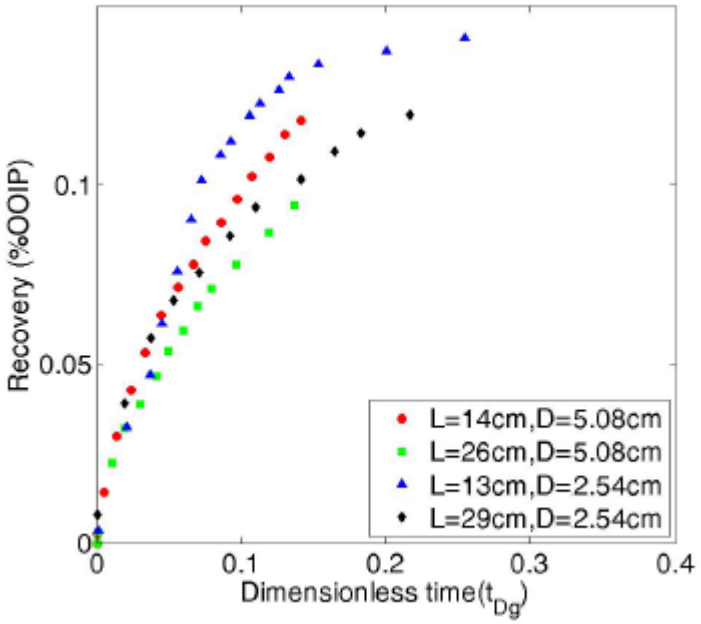

Figure 2-19: Application of the scaling group proposed by Mirzaei et al. 2013 on the recovery curves generated by them on varying length and diameter cores.

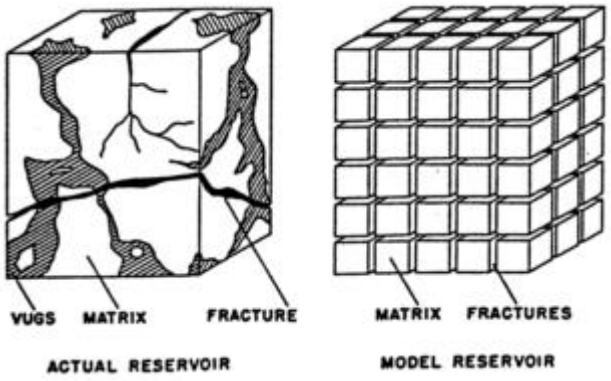

Figure 2-20: Representation of a heterogeneous fractured medium on the left to an idealized dual porosity system on the right. (Warren and Root, 1963)

Chapter 3: Materials and Methodology

In this study, wettability altering static imbibition, dynamic imbibition and coreflood experiments are performed. In all the experiments reservoir crude oil is used. The imbibition experiments are divided into two sets and data related to these will be presented in this section, other data will be presented along with the experimental details as necessary in the appropriate section. The first set (A) of experiments were performed on low permeability (0.03 – 0.23 mD) sandstone reservoir cores. The second set (B) of experiments were performed on outcrop cores (Estaillades Limestone and Texas Cream Limestone). All the materials used are described in the beginning followed by methodology for different experiments performed.

3.1 MATERIALS

3.1.1 Formation and Injection Brine

For study A, the formation brine contains sodium chloride, sodium sulphate, magnesium chloride and calcium chloride adding up to a total salinity of 132606 ppm with hardness of 3636 ppm. The ion composition is described in Table 3-1. The density of the brine is 1.02 g/cc and viscosity 0.82 cp at the experimental temperature (59° C). The injection brine is the same as that of the formation brine in majority of experiments, some experiments were performed with half the salinity of the formation brine by diluting the formation brine. All saturations are performed with the formation brine, injection brine where mentioned refers to the brine surrounding the core in static imbibition tests.

For the second set of experiments (study B), the formation brine contains sodium chloride, sodium sulphate, magnesium chloride and calcium chloride adding up to a total salinity of 8469 ppm with hardness of 305 ppm. The ion composition is described in Table 3-2. Density of brine is 1 g/cc and viscosity 1 cp at the experiment temperature (23° C).

The injection brine is the same as that of formation brine for all the experiments. All the salts were procured from Fischer Scientific.

3.1.2 Surfactants

A surfactant or surface active agent, is any substance that lowers the energy barrier between two immiscible phases. It consists of two parts: a hydrophilic (water-soluble) part and a hydrophobic (oil-soluble) part. Anionic, nonionic and cationic surfactants were used in this study. Anionic surfactants used here belong to the class of EO-PO sulphates (Figure 3-1) and internal olefin sulphonates. Details are mentioned in Table 3-3. In all the experiments surfactant concentrations are less than 0.25 wt%, making these processes less expensive to execute at larger scales. These surfactants are a combination of in-house developed surfactants and commercially available surfactants (Sasol, Dow Chemicals and Sigma Aldrich).

3.1.3 Crude Oil

In all the experiments reservoir crude oils are used to saturate and age the cores. A list of different crude oils used is provided in Table 3-4. Reservoir cores (A) were restored to their native wettability by saturating them and then aging them with crude oil A. Oil wetness was tested after aging the core (Figure 3-2). Oil was checked for contamination by measuring the oil-formation brine IFT which was around 21.8 dyne/cm (Hirasaki and Zhang, 2004). Outcrop cores (B) were saturated and aged with crude oil B from a Middle East carbonate reservoir for 14 days at 80 °C to make them oil-wet.

3.1.4 Rocks

For study A reservoir cores were sent by the company. The core plugs were on an average 1 inch in diameter and 2 inch in length. The contact angle tests were performed on

Cristobalite mineral plates (a mineral with quartz and Kaolinite which was similar to the mineral composition of reservoir cores received). Dimensions of the plates were 1’’x 1’’ x 0.5’’. For study B outcrop core samples of Estaillades Limestone and Texas cream limestone were used. The diameter and height of cores was varied as per the requirement of experiment.

3.2 METHODOLOGY

3.2.1 Aqueous Stability Tests

Aqueous stability of surfactants was tested prior to their evaluation for wettability alteration. Surfactant solution was prepared at the desired surfactant concentration, salinity and ion composition. This solution was monitored for precipitation or phase separation at the experiment temperature. A clear solution implies aqueous stability. Aqueous stable surfactants were selected for further evaluations. In general anionic surfactants were found to be more hardness tolerant and thermally stable.

3.2.2 Contact Angle Measurements

Surfactants which were aqueous stable at the experiment temperature were tested for wettability alteration. Mineral plates having approximate dimensions 1’’x1’’x0.5’’ were polished (Figure 3-3) on a 600 mesh diamond polisher. They were first aged in the formation brine for a day and then aged in oil for around 7 days at 80 °C. The elevated temperature aging is done to compensate for the short aging time (compared with the geological time). After this the plates were immersed in surfactant solution (or brine) and the change in water advancing contact angle was observed for at least 2 days (Figure 3-4 and 3-5).

3.2.3 Phase Behavior Study

Surfactant solutions were prepared with varying concentrations of sodium chloride in 5 ml pipets with equal water oil ratio as shown in Figure 3-6. These solutions were equilibrated at the experiment temperature. The number of phases, change in volume of phases and the color of the phases were observed, which indicated the shift from type I (Winsor, 1954) to type II phase behavior with the increase in salinity of the solution. For the range of salinities at which experiments were performed in this study, all the surfactant solutions are in Type I region.

3.2.4 IFT Measurement

The IFT between the brine and oil phases was measured using a spinning drop tensiometer. Surfactant was mixed with brine at the desired salinity and then equilibrated with oil. IFT measurement was made between the equilibrated aqueous and oleic phases.

3.2.5 Core Preparation and Characterization

The different stages in core preparation involve core characterization (determination of porosity, permeability and saturation), injection of fluids and aging the core. Aging a core is required so that it reaches the appropriate wetting conditions for conducting wettability altering studies. For study A reservoir cores received were brine saturated. Crude oil was injected from the top until the cores reached residual water saturation. Final core saturation was established by mass balance based on volume of effluent brine collected. These core were then aged for about a month at 80 °C. After aging their oil-wetness was checked (Figure 3-8) and static imbibition experiments were performed on them.

For study B, outcrop cylindrical cores were used for static and dynamic imbibition. These cores were first dried for a day at 80 °C to remove any moisture present due to the

coring process. Air porosimetry based on Boyle's law is used to estimate the pore volume of the core. The core is then vacuumed (-14 psi) and saturated with CO_2 and then again vacuumed, this cycle is repeated 2-3 times to displace air present in the core with CO_2 which is easier to displace by brine. After final vacuuming, brine is introduced in the core. Brine is displaced by injecting oil from the top. To maintain the initial water saturation constant in all the experiments, a calculated slug of brine is followed by a slug of oil with the outlet valve closed. In these experiments the initial water saturation is maintained at 0.78. After saturation the core is aged in oil for two weeks at 80 °C.

For dynamic imbibition experiments, a fracture is created axially in the saturated and aged core. Weight of the core before and after fracturing is noted to account for the rock loss during fracturing. Figure 3-9 shows a fractured core. The top surface and outer lateral surface of this core is then epoxy coated to allow for imbibition only through the fracture surface (Figure 3-10). Sand is placed in the fracture to keep it open and the two pieces of the core are wrapped together using a Teflon tape (Figure 3-11).

3.2.6 Static Imbibition

A static imbibition test is characterized by no flow of any fluid into or out of the cell. It serves as a true measure for checking the wettability of the core when immersed in a brine solution and for establishing the performance of surfactant formulations. Experiments were performed on cores of different diameter and height. Imbibition cells used in this study are shown in Figure 3-7. These cells were manufactured in-house with parts sourced from Chemglass. A new cell first needs to be calibrated to ascertain the volume of oil collected at the top of the cell per unit marks. Cores are placed on small Teflon stands (Figure 3-4) inside the imbibition cell to open-up the bottom core face for

imbibition. Brine or surfactant solution is then poured up to the top in the cell. Oil recovery with time is observed for 2-3 months.

3.2.7 Dynamic Imbibition

Dynamic imbibition experiments are characterized by fluid flow in fractures. These experiments were performed in a Hassler Type Coreholder. A schematic of the setup is shown in Figure 3-13. Core preparation for these experiments is described in the previous section. Two pumps are connected to the setup. One pump is for maintaining overburden pressure and the other pump is for injection. An overburden pressure of 400 psi was used in this study. It should be noted that the fracture permeability is a function of the overburden pressure but the pressure required to make any significant/ observable changes in fracture permeability are very high (of the order of 1000 psi). Injection flow rate is kept at 2.4 ft/day based on cross section area of the fracture. Oil recovered is collected at the top of the core in a cell with a volume holdup section at the bottom and a thin stem at the top for accuracy in measurement of oil volume.

3.2.8 Corefloods

Corefloods were performed on cores from different reservoirs to study the effect of wettability altering surfactant flood on incremental oil recovery over waterflood. These cores are not fractured and displacement of oil by brine is due to viscous forces unlike the imbibition experiments where gravity and capillary forces are responsible for oil recovery. In these experiments the surfactant slug is injected after half pore volume brine injection. This was done to mimic to current status of these reservoirs so that performance improvement after a switch to wettability altering surfactant slug injection can be gauged. Both these floods were conducted on carbonate cores at reservoir temperatures of 59°C and 95°C.

A schematic diagram of the setup is shown in Figure 3-14. Core holder was kept inside the oven. Cores were characterized, saturated and aged in the same manner as mentioned in the core preparation section. Oil, brine and surfactant solution were filtered with 0.22 micron filter paper. Oil recovery and pressure drop across the core were measured with time.

During transition from injection of brine (waterflood) to surfactant injection (wettability altering surfactant flood) it was ensured that the system does not undergo any pressure or temperature shock by maintaining pressure and temperature continuity in the system. For this purpose, a cylindrical steel vessel of 150 ml capacity containing surfactant solution is placed inside the oven. Bottom of the vessel is connected to the surfactant injection pump and top is connected to the core holder bottom. This allows sufficient residence time for the surfactant solution to heat up to the experiment temperature before it gets injected into the core. Similarly, a long metal tubing is used to provide sufficient residence time inside the oven for heating up injection brine before it enters the core.

Components	mg/L
Ca^{2+}	2898
Mg^{2+}	738
Na^{+}	47654
SO_4^{2-}	250
Cl^{-}	81066
Total Salinity	132606
Hardness	3636

Table 3-1: Brine composition for first set of experiments.

Components	mg/L
Na+	2940
Ca2+	256
Mg2+	49
Cl-	4859
SO42-	365
Total Salinity	8469
Hardness	305

Table 3-2: Brine composition for second set of experiments.

Anionic Surfactants		Source
S.No.	Surfactant Name	
1	TDA-6-EO-Sulphate	In-house
2	TDA-27-EO-Sulphate	In-house
3	TDA-7PO-Sulphate	In-house
4	C(16-17)-7-PO-Sulphate	In-house
5	C(24)-25PO-46EO-Sulphate	In-house
6	C(20)-7PO-30EO-Sulphate	In-house
7	C12-13-7PO-Sulphate	Sasol
8	15-18 IOS	In-house
9	20-24 IOS	In-house
Non Ionic surfactants		
9	15-S-20	Dow Chemicals
10	15-S-30	Dow Chemicals
11	15-S-40	Dow Chemicals
Cationic Surfactant		
12	DTAB (Dodecyl trimethyl ammonium bromide)	Sigma Aldrich

Table 3-3: Description of surfactants applied in this study

Crude Oil	Density (g/cc)	Viscosity (cp)	Experiment Temperature (° C)
A	0.78	2.3	59
B	0.83	13.5	23

Table 3-4: Properties of crude oils used in this study

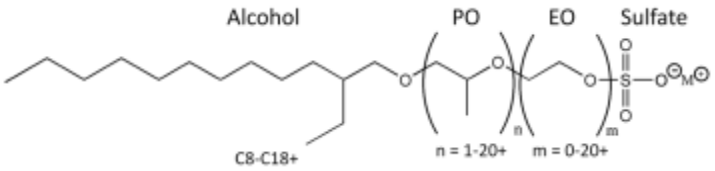

Figure 3-1: General structure of Ethoxy Propoxy Sulphate Surfactants (Source: Sasol)

Figure 3-2: Oil-wet sandstone field core after aging in crude oil for a month days at 80 °C

Figure 3-3: Polished Cristobalite plate for contact angle measurement

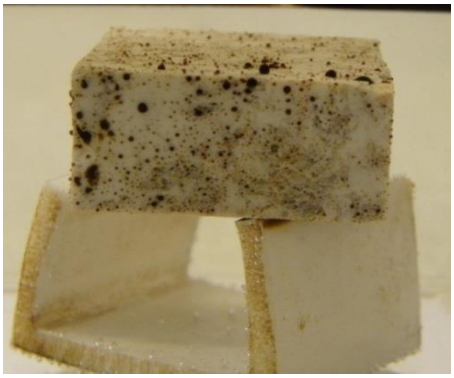

Figure 3-4: Plate with oil drops, inside an optical cell filled with a surfactant

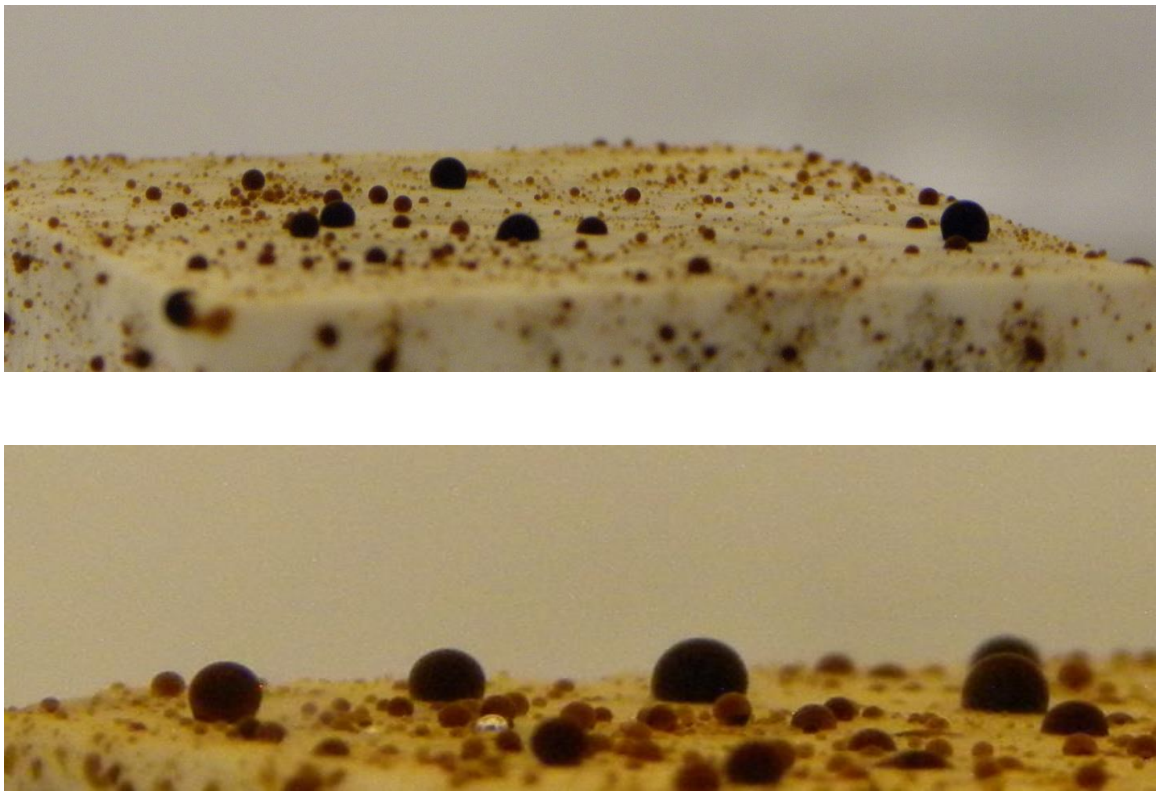

Figure 3-5: High resolution images of the top surface of a polished Cristobalite plate

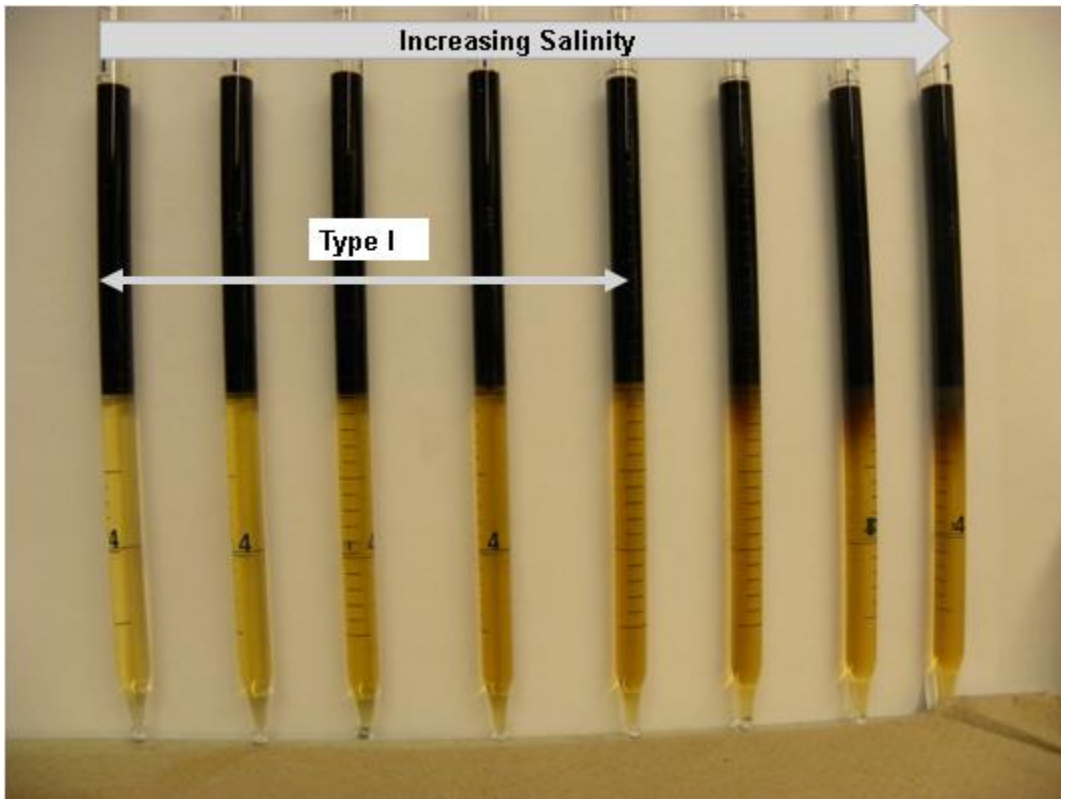

Figure 3-6: Phase behavior pipets with water oil ratio 1:1

Figure 3-7: Different imbibition cells used in experiments. The dimension of the cores in inches are mentioned in the image. Oil recovered can be seen at the top in the stem of the cell.

Figure 3-8: Oil-wet Estaillades Limestone core after aging at 80 °C for two weeks

Figure 3-9: Epoxy coated fractured core for dynamic imbibition study

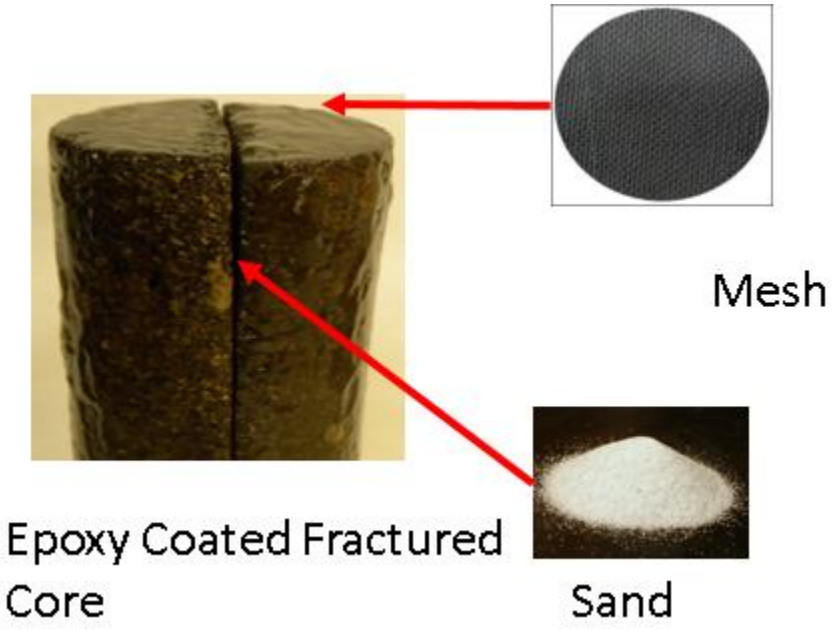

Figure 3-10: Sand placed in fractured core coated with epoxy on lateral and top surface.

Figure 3-11: Lateral surface of a 4 in diameter fractured Estaillades Limestone core with Teflon tape wrapped around it.

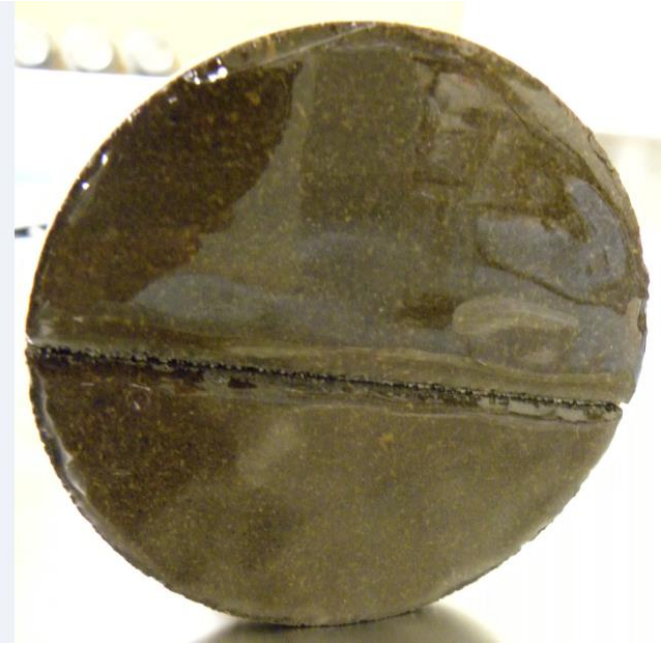

Figure 3-12: Top/bottom face of the cylindrical 4 in diameter Estaillades Limestone core, sand placed in fracture can be seen in the middle of the core cross section.

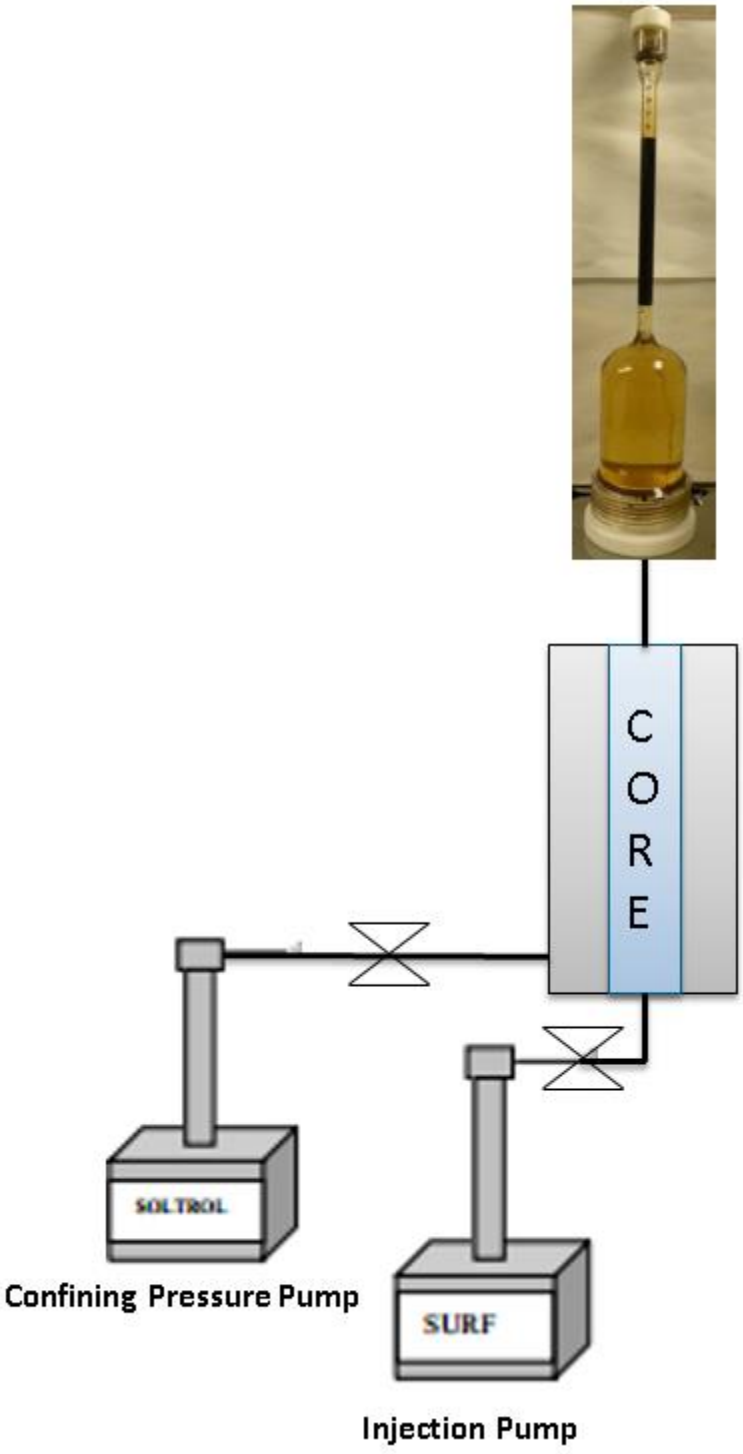

Figure 3-13: Dynamic Imbibition Setup

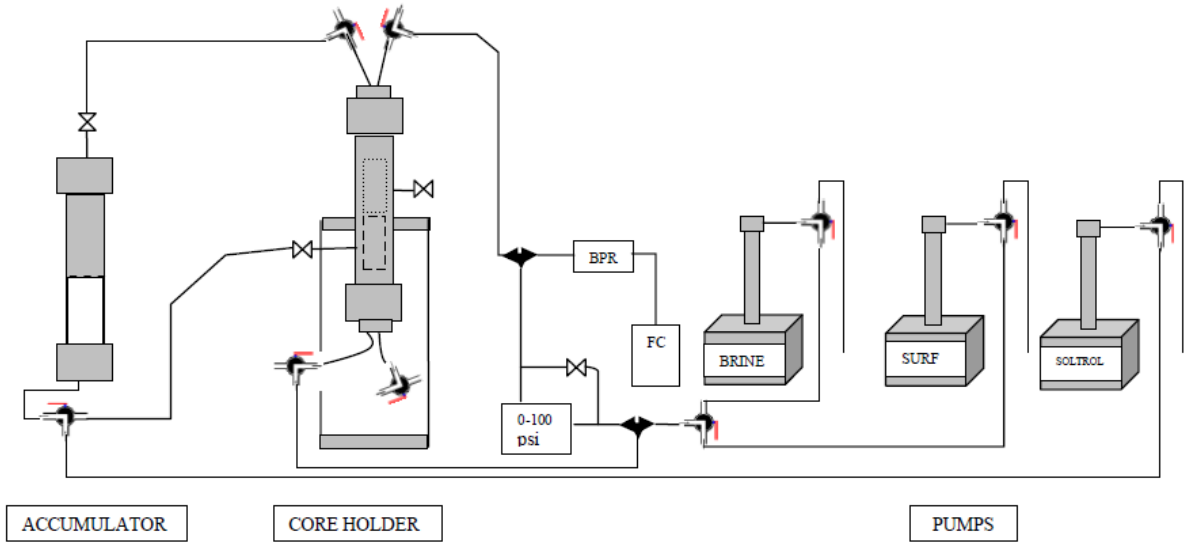

Figure 3-14: A schematic diagram showing the setup for corefloods performed in this study. (Sharma et al. 2013)

Chapter 4: Experimental Results

This chapter presents the results of experiments performed for analyzing the performance of wettability altering surfactants. The first section deals with capillary dominated flow (study A) in a sandstone reservoir. In these experiments a dilute (0.1 wt%) surfactant solution alters the wettability from mixed-wet/oil-wet to water-wet without significant reduction in IFT. The experiments are performed on tight reservoir rocks (0.03 – 0.23 mD) leading to high positive capillary forces after wettability alteration. In the second section (study B) results for gravity dominated flow are discussed. These include imbibition recovery curves under static and dynamic imbibition conditions as a function of core dimensions. Inverse bond numbers for the experiments are in the range of 1-5 implying gravitational forces are comparable to capillary forces. The last section deals with wettability altering corefloods and comparison of different injection schemes including secondary surfactant flood as well as a tertiary surfactant flood after short (0.5 PV) waterflood to mimic the conditions of the reservoirs already undergoing waterflood.

4.1 Capillary Dominated Flow

Oil recovery through spontaneous imbibition can be driven by capillary forces, gravitational forces or a combination of both. When the permeability of formation is very low (of the order of 10 μD), under water-wet conditions the capillary forces are very high and aid in oil recovery. A series of experiments were conducted and surfactants were identified that can alter the wettability of the sandstone formation from mixed-wet to water-wet. These experiments include the aqueous stability tests at the reservoir temperature and salinity, contact angles measurements on a clay-rich sandstone and spontaneous imbibition tests on the reservoir rocks received (Figure 4-8). It was found that a dilute (0.1 wt%) anionic surfactant solution with a large number of ethoxy groups can alter the wettability

from oil-wet towards more water-wet condition on the mineral plates. Incremental oil recovery as high as 68% OOIP is obtained through spontaneous imbibition experiments performed on tight oil-wet/mixed-wet sandstone reservoir cores using the surfactant formulation. Table 4-1 lists the reservoir and core properties for this study. Distribution of absolute permeabilities to brine for the various core plugs received is given in Figure 4-1. The experimental results are discussed in the following sections.

4.1.1 Aqueous Stability Tests

Eight anionic surfactants (A1 to A8: alkyl ether sulphates and internal olefin sulphonates) and three nonionic surfactants (N1, N2 and N3) were tested in this study. Their chemical formula is listed in Table 4-2. No cationic surfactants were used in this study owing to the negative surface charge of sandstone surface. Surfactants A1-A6 were developed in-house. Surfactants A7 and A8 were from Stepan and N1-N3 were from Dow Chemicals.

Figure 4-2 shows the aqueous stability results for anionic surfactants at the reservoir temperature. Ether sulphates (A1, A2, A5, A6) showed better aqueous stability compared to internal olefin sulphonates (A7, A8). Higher salinity diminishes aqueous stability of anionic surfactants. Only two out of the eight surfactants tested were aqueous stable at the formation brine salinity. The number of ethoxy groups in the surfactant plays a major role in aqueous stability at higher salinities. It was observed that more the number of ethoxy groups in the surfactant, the higher was the aqueous stability.

The non-ionic surfactants used in this study are of the form R-EOx where R is a hydrocarbon attached to a chain containing x ethoxy groups. The three surfactants tested contained the same R but different (x) number of ethoxy groups. For all the three

surfactants, the cloud point was higher than the reservoir temperature and they resulted in aqueous stable solutions even at high salinities as shown in Figure 4-3.

4.1.2 Contact Angle and IFT Measurements

Figure 4-5 and 4-6 shows pictures of oil droplets on Cristobalite plates submerged in surfactant/brine solution in an optical cell and Table 4-3 gives the contact angle values. The nonionic surfactants N1, N2 and N3 altered the contact angle, but not to the extent required. Also it was observed that more the number of ethoxy groups (most in N3, least in N1), more was the change in contact angle. But no non-ionic surfactant was able to make the Cristobalite plate water-wet (θ < 80°). Among the six combinations of anionic surfactants which were aqueous stable, five altered the wettability from oil-wet to water-wet. Two surfactants (A2 and A6) altered the wettability at both the salinities that we tested (formation brine and half the formation brine). The average contact angles observed were nearly the same at both the salinities. These surfactants were then studied in detail with regard to their interfacial tension variation with salinity and also reproducibility of spontaneous imbibition experiments. Figure 4-4 shows the IFT between the aqueous and the oleic phases as a function of salinity in the crude oil-brine-surfactant systems. For both of these anionic surfactants IFT decreased with increase in salinity. Increase in salinity leads to more competition between surfactant and salts for solubilization in water, as a result more surfactant monomers tend to move towards the interface. More monomers at the interface result in lowering of the interfacial tension with the increase in salinity.

4.1.3 Spontaneous Imbibition Experiments

Imbibition experiments were performed with the surfactants which altered the wettability of Cristobalite plates. Figure 4-7 shows an oil-wet reservoir core. A water drop placed on top of the aged core does not imbibe, confirming the oil-wetness of the core. Table 4-3 lists

the results of the imbibition experiments. The oil recovery due to spontaneous imbibition is listed for each experiment when an oil-saturated core plug is surrounded by different brines. Experiment 1 is for the formation brine. The oil recovery is 15%, which suggests that the matrix is mixed-wet with a dominant oil-wet fraction. Three imbibition experiments (Experiment 2-4) were performed with surfactant A2 in the formation brine (FB). Experiments 2 and 3 gave similar final oil recovery values (~55%) while Experiment 4 gave a significantly higher value. However, in these three cases with surfactant A2 the recovery was high (54-68%) implying that the surfactant A2 is effective as a wettability altering agent. The difference in final oil recovery can be attributed to heterogeneities in the core since these experiments were performed on different core plugs from the same reservoir. Similarly for Experiments 5 and 6 for surfactant A2 in half the formation brine salinity (FB/2), the oil recovery by spontaneous imbibition is also high (61-67%). Experiments 7 and 8 are for surfactant A6 in formation brine which give oil recoveries of 46-52% OOIP. The lowest recovery (42%) was obtained for surfactant A5 (Experiment 10) in half the formation brine salinity. The oil recovery by spontaneous imbibition is significant (42-68% OOIP) for surfactants A2, A5 and A6.

Ratio of capillary to gravitational forces is termed as macroscopic inverse bond number and is given by equation 4-1:

$$N_B^{-1} = \frac{\sigma\sqrt{\frac{\phi}{k}}}{\Delta\rho g H} \tag{4-1}$$

where σ is the interfacial tension, ϕ is porosity, k is permeability, $\Delta\rho$ is the density difference, and H is the height of the core. It is listed for the imbibition experiments in

Table 4-3. High values of inverse bond numbers (> 248) were obtained for these experiments.

Figure 4-8 shows one of the cores placed in the surfactant solution. Oil droplets come out of the core on all sides as brine imbibes. This suggests that the dominant imbibition mechanism is the counter current imbibition due to the capillary pressure gradient caused by the wettability alteration. Smaller pore throat size (low permeability of porous media) results in high values of capillary forces. High values of inverse bond number imply that capillary forces are far greater compared to buoyancy forces. When the wettability is altered from oil-wet to water-wet, these capillary forces aid in the spontaneous imbibition of brine through the periphery of the core.

Figure 4-9 shows the oil recovery curves as a function of time for the ten spontaneous imbibition experiments performed. The experiment where no surfactant is used shows the lowest recovery (15%). It takes 9 days before any oil is collected at the neck of the imbibition cell. In this period the oil drops appeared on the periphery of the core, but they did not detach and collect in the neck. For the surfactant solutions, 80% of the finally recovered oil is recovered in the first 20 days; the rate of recovery gradually decreases as the saturation of aqueous phase increases in the core. The initial rate of oil recovery varied significantly between the experiments. Our experimental data was plotted using Mattax and Kyte scaling equation (Equation 2-3) as well as the scaling group proposed by Ma et al. (Equation 2-4). Figures 4-10 and 4-11 show that all the data do not fall on one curve, but the correlation was slightly better for Ma et al. (1997) scaling group as compared to Mattax and Kyte (1962). Both the scaling equations are for strongly water-wet porous media and are insufficient to explain the dynamics of changing wettability from oil-wet to water-wet.

Some of the cores had almost the same initial oil saturation and imbibition was performed using the same surfactant, but at different salinities. As a result of varying salinity the interfacial tension between oil/water is varied. Figures 4-12 and 4-13 show the oil recovery curves for imbibition experiments performed with the same surfactant at different salinities. It was observed that the rate of recovery was higher for the higher IFT cases. Also, ultimate oil recovery was higher for the higher IFT case in both the sets.

4.2 GRAVITY DOMINATED FLOW

In this study static and dynamic imbibition experiments were performed on two outcrop rocks: Estaillades Limestone and Texas Cream Limestone. Static imbibition experiments are characterized by no fluid flow surrounding the core whereas in dynamic imbibition experiments there is fluid flow through fractures. The permeability for these cores ranges from 8.4 mD to 150 mD and porosity between 0.26 to 0.28. These outcrop rocks were saturated and aged in a reservoir crude oil from an oil-wet carbonate reservoir. Properties of this oil (B) are mentioned in Table 3-4. Wettability of the cores after the aging process was found to be strongly oil-wet (Figure 4-14). All the experiments were performed at the room temperature.

Capillary forces are primarily determined by the wettability, interfacial tension and permeability of the media whereas for gravitational forces, the density difference between the displaced and displacing fluids is a critical parameter. In a surfactant driven imbibition process if the buoyancy forces exceeds the capillary forces which are altered by the effect of surfactant then the oil recovery is gravity dominated. The ratio of capillary to gravitational forces is termed as the macroscopic inverse bond number (Equation 4-1). For these experiments the inverse bond numbers vary from 1-5 which are in the range of slightly gravity dominated flows (Schechter et al. 1994).

4.2.1 Surfactant Screening

An anionic surfactant (C12-13-7PO-SO4) and cationic surfactant (DTAB) were tested for this study. The anionic surfactant was procured from Sasol and cationic surfactant was procured from Sigma-Aldrich. Both the surfactants were aqueous stable in the formation brine (salinity 8469 ppm, hardness 305 ppm, Table 3-2) at room temperature. Cationic surfactants although expensive are a good option for carbonate reservoirs which have positively charged surface at neutral pH resulting in reduced adsorption of the surfactant. The formulation for anionic surfactant also contained 1.5 wt% EDTA and 2.25 wt% Na_2CO_3. EDTA was added to sequester the hard ions (Ca^{2+} and Mg^{2+}) in the brine to prevent precipitation. Sodium carbonate was added to increase the pH above the point of zero charge for carbonates. This causes the surface to acquire negative charge and repel the like charged anionic polar head group of the surfactant thereby reducing adsorption (Seethepalli et al. 2004, Tabatabal et al. 1993).

4.2.1.1 Contact Angle Studies

Contact angle studies were performed on Estaillades Limestone plates and Texas Cream Limestone plates for the anionic surfactant at 0.25 wt% and at 0.1 wt%, 0.5 wt% for the cationic surfactant. Plates of dimensions 1''x1''x0.5'' were polished on 600 mesh diamond polisher to create a smooth surface for accurate contact angle measurement. Oil-wetness of the plates was first checked by aging them in formation brine for a day at 80 °C followed by aging them in the middle eastern reservoir crude oil (Oil B) for seven days at 80 °C. Figure 4-14 shows films of oil on top of the Estaillades Limestone plate indicating strong oil-wetness. Texas Cream Limestone plate was aged similarly, Figure 4-17 shows mixed-wet/oil-wet nature of the plate. The oil-wet plates were then tested for wettability alteration in the two surfactants. Figure 4-15 shows the change of wettability to water-wet when the plate is placed in the anionic surfactant solution at room temperature. Similar

results were obtained for the Texas Cream Limestone plate in surfactant solution (Figure 4-18). The anionic surfactant formulation was able to alter the wettability to water-wet to a greater extent on the Texas Cream Limestone as compared to the Estaillades Limestone plates. The average contact angle for the oil droplets through the aqueous phase on Texas Cream Limestone and Estaillades Limestone plates was 61° and 75°, respectively.

Wettability change in cationic surfactant was tested at 0.1 wt% and 0.5 wt% on the aged oil-wet Estaillades Limestone plate. Both the solutions reduced the contact angle through the aqueous phase but the plate remained oil-wet. Figure 4-16 shows the oil-wet Estaillades Limestone plate in 0.5 wt% DTAB solution. Wettability altering anionic surfactant formulation was selected for further studies.

4.2.1.2 Phase Behavior Study

Oil-brine phase behavior was studied for the anionic surfactant with varying sodium carbonate salinity (0.5 to 4 wt%) with fixed formation brine salinity, 0.25 wt% surfactant and 1.5 wt% EDTA. Figure 4-19 shows the phase behavior pipettes. A very distinct Winsor Type I region was observed until 2.5 wt% sodium carbonate. All the static and dynamic imbibition experiments were performed at 2.25 wt% sodium carbonate salinity in the Type I region. It is not possible to accurately determine the IFT through phase behavior (miniscule change in volume of phases) in this region for a low surfactant weight percent of 0.25 which is used in this study. IFT value was determined through a spinning drop tensiometer. The IFT between the equilibrated oleic and aqueous phases was found to be 0.6 dyne/cm in the surfactant formulation containing 2.25 wt% sodium carbonate.

4.2.2 Static and Dynamic Imbibition Experiments

Studies have been conducted in the past which showed high incremental recovery in static imbibition experiments performed on oil-wet cores with wettability altering surfactants (Austad et al. 1997, Seethepalli et al. 2004, Adibhatla et al. 2008, Gupta et al. 2010). In addition to altering wettability these surfactants also reduce interfacial tension. The reduction in interfacial tension depends on many factors including the weight percent of surfactant used, salinity, temperature etc. IFT values determine whether capillary forces play a significant role in recovery or not which can be determined by the calculation of inverse bond numbers (Table 4-5). As we study the feasibility of these processes at larger scales it is necessary to study the effect of increase in dimensions and flow in fractures (dynamic versus static conditions) on oil recovery which is addressed in this work.

4.2.2.1 Static Imbibition Results

Experiments were performed two carbonate outcrop rocks (Estaillades Limestone and Texas Cream Limestone) to investigate the effect of core dimensions and dynamic conditions (fluid flow in fracture) keeping the oil- anionic surfactant system same in all the cases. Table 4-4 lists the different experimental parameters for this study along with the macroscopic inverse bond numbers. The inverse bond numbers are in the range of 1-5 which signifies gravity dominated flow. All the cores have same initial oil saturation of 0.78 and were aged for two weeks at 80 °C after saturation. The experiments are performed at the room temperature. Estaillades Limestone is referred to as EL and Texas Cream Limestone is referred to as TC in tables and figure legends.

To check the oil-wetness of the Estaillades Limestone core, an imbibition experiment was performed with just the formation brine as the surrounding fluid. No oil recovery was observed for this case (Figure 4-20) indicating strong oil-wetness of the core. Figure 4-20 also shows the cumulative oil recovery and rate of recovery for a 1.5 in

diameter and 5.75 in height core. High oil recovery (~37 % OOIP) is obtained indicating strong performance of the wettability altering surfactant. Rate of recovery curve in terms of % OOIP/day is also shown in the Figure 4-20 for the same experiment. The initial rate of recovery is the fastest at 3 % OOIP/day which falls to 0.25 % OOIP/day after 1200 hours of starting the experiment. A sharp decline in rate can be observed in the beginning which is followed by a long tail. Cumulative recovery is around 37 % OOIP at the end of 1200 hours, almost half the oil (18 % OOIP) is recovered in the first 240 hours of the experiment. Similar observations were made for the experiments on cores of different dimensions which are described in the next paragraph.

After establishing the strong oil-wetness of the core post aging and the effectiveness of the surfactant formulation, experiments were performed on cores with varying height and diameter. Details are mentioned in Table 4-5 as well as the legend of the plot which lists the diameter first and then the height of the core in inches. Figure 4-21 shows a comparison of oil recovery with height of the core, the diameter being same for both the cores. Increase in the height of the core resulted in decrease in oil recovery. The cumulative recovery after 1160 hours is 37% OOIP and 27% OOIP for the 5.75 inch and 11.5 inch height core, respectively. Increase in height causes an increase in the buoyancy forces, however this does not result in increased recovery since there is increased viscous dissipation in the oil phase. Larger height of the core results in increase in the distance to reach the matrix fracture boundary which results in increased viscous dissipation. Compared to the increase in buoyancy or driving forces due to increased height the viscous dissipation increase is more which causes decrease in oil recovery. This argument is verified mathematically by comparing two models developed by previous researchers (Mirzaei et al. 2013, Chen et al. 2014) and will be discussed further in the scaling analysis section in the next chapter.

Figure 4-22 shows the oil recovery plots for cores with same height (5.75 inch) but with varying diameters (1.5 inch and 4 inch). Imbibition cells used for these experiments are shown in Figure 3-7. Increase in diameter of the core resulted in decrease in recovery. The cumulative recovery after around 1350 hours is 38.9 % and 18.8 % OOIP for the 1.5 inch and 4 inch diameter core respectively. Increase in diameter at lab scale is similar to increase in vertical fracture spacing in a reservoir. As the diameter increases the buoyancy forces remain same (same height of the core) but that driving force is dissipated in a far larger volume compared to the lesser diameter core, hence the oil recovery decreases.

Recovery from all the different dimension cores are plotted together with respect to time in Figure 4-23 and with respect to square root of time in Figure 4-24. It can be seen that the oil recovery varies linearly with square root of time. This is an important observation as it has a significant impact on estimating ultimate recovery at longer times. It is shown later that the same phenomenon is observed for dynamic imbibition experiments as well.

Experiments were performed on Texas Cream Limestone outcrop cores with the same oil and anionic surfactant formulation described in previous sections. Table 4-6 lists the different core and fluid parameters for the experiments. These cores have the same initial oil saturation of 0.78 and all the experiments were performed at room temperature. The only difference from previous experiments is that these experiments were performed on a different outcrop rock of lower permeability and different initial and final wetting states. For establishing the initial wettability of the core, an imbibition experiment with formation brine was performed first. Figure 4-25 shows the recovery curves for the experiments performed on Texas Cream Limestone outcrop cores. Imbibition in formation brine recovered around 2% OOIP oil indicating mixed-wet core with a dominant oil-wet

fraction. Imbibition in surfactant solution resulted in high recoveries indicating good performance of the surfactant even in low permeability cores. Higher recovery was observed (Figure 4-25) for core with diameter 1.5 inch and height 11.5 inch compared to core with 4 inch diameter and 5.75 inch height. Figure 4-26 shows the oil recovery curves plotted with square root of time. These oil recoveries are very similar to the recoveries obtained from the Estaillades Limestone cores with same dimensions even though the permeability for Texas Cream Limestone cores is around one-fourth of the Estaillades Limestone core. If the final wetting state of the cores in the surfactant formulation would have been the same for the two rock-types then the recovery should have been lower for the Texas Cream Limestone cores. However, Texas Cream Limestone turns more water-wet in the surfactant solution compared to Estaillades Limestone as was evident from the contact angle studies performed earlier (Figure 4-15 and 4-18). Also, the Texas Cream Limestone outcrop rock recovers some amount of oil (2% OOIP) during brine imbibition compared to no oil recovery in the case of Estaillades Limestone which suggests that Texas Cream Limestone is initially mixed-wet compared to strongly oil-wet nature of Estaillades Limestone.

4.2.2.2 Dynamic Imbibition Results

Dynamic imbibition experiments are characterized by motion of fluid in contact with the fracture in contrast with static imbibition experiments where the fluid in contact with the fracture is stagnant. The experimental setup is shown in Figure 3-13. These experiments were performed on Estaillades Limestone core plugs. Same anionic surfactant formulation was used in these experiments as in the previous static imbibition experiments. Initial oil saturation in the cores was 0.78, cores were aged for two weeks at 80 °C and all

experiments were performed at room temperature. Table 4-7 lists the values of different parameters for these experiments.

The static and dynamic imbibition experiments were performed on cores with same dimensions and boundary conditions. The only difference between the two experiments was that of flow of fluid surrounding the fracture, all other parameters were same. Only surface open to interaction with the surfactant was the fracture surface, the lateral and top surface of the cylindrical core was sealed using epoxy (Figure 4-27). Fracture width for the dynamic imbibition experiment was around 1 mm and the experiment was performed at a constant flow rate of 0.01 ml/min or a velocity of 2.4 ft/day based on fracture cross section area. The experiment was performed in a core holder with a confining pressure of 400 psi. Fracture permeability was around 80 Darcy. Details regarding core preparation for these experiments can be found in Chapter 2.

Figure 4-28 shows a comparison for the static and dynamic imbibition experiments Dynamic imbibition results in more oil recovery compared to static imbibition experiment having the same boundary conditions. Cumulative oil recovery after 1000 hours is 15% OOIP for the static imbibition experiment and 26.9% OOIP for the dynamic imbibition experiment with an error estimate of 3% as shown through the error bars. The increase in oil recovery for the dynamic imbibition experiments can be attributed to increased capillary pressure gradient. Oil is recovered in the form of small droplets at the matrix fracture boundary. In a dynamic imbibition process these droplets are constantly removed by viscous forces due to flow of injected surfactant. This maintains high water saturation in the fracture resulting in high capillary pressure gradient (Gautam et al. 2003). Higher concentration gradient of the surfactant at the matrix fracture boundary due to constant replenishment of surfactant by injection can also lead to faster rates of diffusion which is considered to be a limiting factor for surfactant aided wettability altering processes (Stoll

et al. 2008). Faster rates of surfactant diffusion can in turn lead to faster oil recovery. These hypothesis need to be verified through numerical analysis.

Figure 4-29 shows a comparison for dynamic imbibition experiments performed on cores having diameter 1.5 inch and 4 inch. The height of cores were same for both the experiments (5.75 inch). Table 4-8 lists the parameters for these experiments. The pressure gradient across the fracture was kept the same for both the cases resulting in injection velocity of 2.4 ft/day. The volumetric flow rate based on the injection velocity was 0.026 ml/min for the 4 inch diameter core and 0.01 ml/min for the 1.5 inch diameter core. All other experimental parameters were kept the same for both the cases. Permeability for the 4 inch core was 40 mD compared to 150 mD for the 1.5 inch diameter core. Reduced permeability and increased diameter retarded the recovery rate for the 4 inch diameter core as seen in Figure 4-29. Figure 4-30 shows linear variation of oil recovery with square root of time, a similar observation was made for the static imbibition experiments (Figures 4-24 and 4-26) as well. A new scaling function proposed in this study (Chapter 5) was able to correlate the recovery curves for different diameter cores. For the dynamic imbibition on 4 inch diameter core a new effluent collection system was introduced which was error free hence no error bars are shown for this experiment.

4.3 WETTABILITY ALTERING COREFLOODS

Corefloods were performed on cores from different reservoirs to study the effect of wettability altering surfactant flood on incremental oil recovery over waterflood. These cores are not fractured and displacement of oil by brine is due to viscous forces unlike the imbibition experiments where gravity and capillary forces are responsible for oil recovery. The incremental oil recovery due to surfactant injection is attributed to the favorable

increase in the relative permeability values of oil as the wettability is changed from oil-wet to water-wet (Figure 2-11).

The corefloods were conducted on carbonate reservoir cores at reservoir temperatures of 52°C and 95°C. In previous work done by other researchers on these reservoirs the secondary surfactant floods were performed to estimate incremental recovery over waterflood. The incremental oil recovery values obtained from these corefloods give a good estimate if after primary recovery methods a direct switch to surfactant flood is made compared to waterflood. However, these reservoirs are already undergoing waterflood. In this study, the injection scheme was altered to take the initial waterflood into account by injecting half pore volume brine and then a switch was made to the surfactant flood. This was done to mimic the current status of these reservoirs so that performance improvement after a switch to wettability altering surfactant slug injection can be gauged. Henceforth the suffix '1' and '2' are used to denote the two carbonate reservoir systems. Tables 4-12 and 4-13 provide a comparison of the different injection schemes for the two reservoirs and are discussed in section 4.3.3.

4.3.1 Carbonate Reservoir 1

Previous extensive studies have shown that surfactant 15-S-20 is a good agent for altering the wettability from oil-wet to water/mixed wet for this rock-oil-brine system. In this flood we used the same surfactant to prepare the surfactant slug (0.2 wt% of surfactant in injection brine). Table 4-9 lists the fluid and core properties along with the experimental parameters for coreflood-1. First 0.5 PV of injection brine (IB) was injected followed by 0.5 PV of surfactant slug (SS) and after that 2 PV of injection brine (IB) was injected. Injection rate for all the fluids was kept constant at 1 ft/day (0.05 ml/min). The pressure drop plot and oil recovery in terms of fraction of original oil in place (OOIP) are shown in

Figure 4-31. Water breakthrough occurs at 0.36 PV; the oil recovery due to waterflood was about 45% OOIP. When the surfactant slug was injected, the oil recovery increased; the total oil recovery after 3 PV of fluid injection is 60% OOIP. Incremental oil recovery over waterflood is about 15% OOIP. In Table 4-11 this coreflood is depicted as coreflood-1.

4.3.2 Carbonate Reservoir 2

Another coreflood with the same objective as mentioned above was performed but on a different carbonate reservoir core at the reservoir temperature of 95°C. Table 4-10 lists the properties of the core used in the flood. The core plug was saturated with field oil till it reached residual water saturation and then aged in oil. After aging the core was flushed with 2 PV of oil. A core composite consisting of 3 cores was formed for performing the flood.

The injection scheme consisted of 0.5 PV of injection brine (IB) followed by 1 PV of surfactant slug (SS) and 2 PV of injection brine (IB). The pressure drop plot and oil recovery in terms of fraction of original oil in place (OOIP) is shown in Figure 4-32. Water breakthrough occurs at 0.34 PV, net oil recovery after 3.5 PV of fluid injection is 54.7% OOIP. Injection rate for all the fluids was kept constant at 1 ft/day (0.05 ml/min). Previous extensive studies have shown that surfactant 0.2% NP-10 + 0.2% DTAB in Injection Brine is a good agent for altering the wettability from oil wet to water/mixed wet for this rock-oil-brine system. In this flood we have used the same surfactant in the surfactant slug. The incremental oil recovery over waterflood is about 7% OOIP. In Table 4-12 this coreflood is depicted as coreflood-2.

4.3.3 Injection Scheme Comparison

Table 4-12 and 4-13 lists the corefloods performed with different injection schemes for carbonate reservoirs 1 and 2 respectively. The permeability and porosity of cores are

similar to the ones mentioned in Table 4-9 and 4-10 leading to nearly same initial oil saturation for cores from the same reservoir. Injection velocity of 1 ft/day is consistent for all the corefloods. For both the reservoirs surfactant injection as a secondary flood or a slug process results in incremental oil recovery. Incremental recoveries over waterflood of 16% and 11% were obtained for secondary surfactant flood and slug process respectively for carbonate reservoir 1. Similarly, incremental recoveries over waterflood of 11% and 7% were obtained for secondary surfactant flood and slug process respectively for carbonate reservoir 2. A key difference between the two reservoir systems is the surfactant slug pore volume. For reservoir 1 only 0.5 PV of surfactant slug leads to higher incremental recoveries compared to around 1 PV of surfactant slug injection for reservoir 2. Surfactant performance at the reservoir conditions (temperature, salinity, heterogeneity) is a key variable in these processes. Despite the differences, for both the reservoirs oil recovery is more in the secondary surfactant injection mode compared to the slug process.

4.4 SUMMARY

Surfactants were identified which altered the wettability of a low permeability (0.03 – 0.23 mD) mixed-wet/oil-wet sandstone reservoir. Static imbibition experiments in the surfactant solution resulted in high oil recovery (42-68% OOIP) compared to 15% OOIP in formation brine. High (>240) inverse bond numbers (ratio of capillary to gravity forces) for these experiments indicate recovery mechanism as counter-current imbibition driven by capillary forces. The recovery data shows that oil recovery varies linearly with square root of time. An analysis of scaling laws for the capillary driven flow suggests that imbibition recovery curves do not correlate with traditional scaling groups (Mattax and Kyte, 1962; Ma et al. 1997). It was observed that the rate of recovery was higher for the higher IFT cases in experiments performed on cores with almost same initial oil saturation

using the same surfactant, but at different salinities. As a result of varying the salinity, interfacial tension between oil/water is varied.

To evaluate the application of wettability altering processes at larger scales experiments were performed on outcrop cores of different dimensions and at dynamic conditions. Surfactant formulation was developed which altered the wettability from oil-wet to water-wet on outcrop rocks Estaillades Limestone and Texas Cream Limestone. Using the surfactant formulation static and dynamic imbibition experiments were performed on aged oil-wet cores with different dimensions and boundary conditions. It was observed that dynamic imbibition process recovers oil faster than static imbibition. Imbibition experiments performed on cores with varying height and diameter show that oil recovery decreases with increasing diameter and height. For both static and dynamic imbibition cases, oil recovery varies linearly with square root of time.

Corefloods were performed on cores from different reservoirs to study the effect of wettability altering surfactant flood in a viscous pressure gradient driven process (as opposed to capillary or buoyancy driven imbibition process). Incremental oil recoveries over waterflood were analyzed for different injection schemes. Incremental recoveries over waterflood of 16% and 11% were obtained for secondary surfactant flood and slug process (surfactant slug injection after short initial waterflood) respectively for carbonate reservoir 1. Similarly, incremental recoveries over waterflood of 11% and 7% were obtained for secondary surfactant flood and slug process respectively for carbonate reservoir 2. The incremental oil recovery due to surfactant injection is attributed to the favorable increase in the relative permeability values of oil as the wettability is changed from oil-wet to water-wet. Experiments indicate that surfactant performance at the reservoir conditions (temperature, salinity, heterogeneity) is a key variable in these processes. Despite the

differences in these conditions, for both the reservoirs oil recovery is more in the secondary surfactant injection mode compared to the slug process.

Property	Value
Average Core Diameter	2.52 cm
Average Core Height	5.56 cm
Average Permeability	50 μD
Average Porosity	10.37%
Formation Brine Salinity	132000 ppm
Hardness	3600 ppm
Reservoir Temperature (RT)	59 °C
Oil Viscosity	2.3 cp @ RT
Oil Density	0.78 g/cc
Connate Water Saturation	0.2 to 0.3

Table 4-1: Reservoir and core properties for study A (capillary dominated flow).

Anionic Surfactants	
Number	Surfactant Name
A1	$C13\text{-}(EO)_{6}$-Sulphate
A2	$C13\text{-}(EO)_{27}$-Sulphate
A3	$C13\text{-}(PO)_{7}$-Sulphate
A4	$C(16\text{-}17)\text{-}(PO)_{7}$-Sulphate
A5	$C24\text{-}(PO)_{25}\text{-}(EO)_{46}$-Sulphate
A6	$C20\text{-}(PO)_{7}\text{-}(EO)_{30}$-Sulphate
A7	15-18 Internal Olefin Sulphonate
A8	20-24 Internal Olefin Sulphonate
Non Ionic surfactants	
N1	15-S-20
N2	15-S-30
N3	15-S-40

Table 4-2: List of anionic and non-ionic surfactants tested for aqueous stability and contact angle studies

Expt No.	Porosity	k (mD)	Length (cm)	Dia. (cm)	Surfactant	Brine	S_{oi}	IFT (dynes/cm)	N_B^{-1}	Oil Recovery (OOIP)
1	0.089	0.03	5.522	2.514	No Surf.	FB	0.51	21.8	3383.2	0.15
2	0.133	0.236	5.584	2.517	A2	FB	0.75	3.73	248.7	0.57
3	0.103	0.035	5.542	2.52	A2	FB	0.79	3.73	573.1	0.54
4	0.101	0.03	5.535	2.522	A2	FB	0.71	3.73	613.8	0.68
5	0.093	0.056	5.536	2.517	A2	FB/2	0.76	7.32	845.9	0.67
6	0.101	0.056	5.645	2.516	A2	FB/2	0.8	7.32	864.5	0.61
7	0.134	0.239	5.573	2.523	A6	FB	0.66	5.64	376.1	0.46
8	0.101	0.103	5.513	2.521	A6	FB	0.72	5.64	502.9	0.52
9	0.131	0.148	5.6	2.518	A6	FB/2	0.72	6.8	567.1	0.6
10	0.096	0.071	5.538	2.521	A5	FB/2	0.79	10.1	1052.7	0.42

Table 4-3: Core properties and spontaneous imbibition results for different experiments

Surfactant	**Brine**	**Wt%**	**Average Contact angle (°)**
-	FB	-	150
A1	FB/2	0.1	130
A2	FB/2	0.1	72
A5	FB/2	0.1	74
A6	FB/2	0.1	70
A2	FB	0.1	74
A6	FB	0.1	74
N1	FB	0.1	145
N2	FB	0.1	110
N3	FB	0.1	90

Table 4-4: Contact angle results for the different aqueous stable surfactants (Capillary dominated flow)

Expt No.	Rock	Type	Dia (in)	Height (in)	k (mD)	Porosity	Fluid	N_B^{-1}
1	EL	Static	1.5	5.75	40	0.26	Brine	2.04
2	EL	Static	1.5	5.75	40	0.26	Surfactant	2.04
3	EL	Static	1.5	11.5	40	0.26	Surfactant	1.02
4	EL	Static	4	5.75	40	0.26	Surfactant	2.04
5	TC	Static	1.5	5.75	8.4	0.26	Brine	4.44
6	TC	Static	1.5	11.5	8.4	0.26	Surfactant	2.22
7	TC	Static	4	5.75	8.4	0.26	Surfactant	4.44
8	EL	Static Fracture	1.5	5.75	150	0.28	Surfactant	1.09
9	EL	Dynamic	1.5	5.75	150	0.28	Surfactant	1.09
10	EL	Dynamic	4	5.75	40	0.26	Surfactant	2.04

Table 4-5: Static and dynamic imbibition experiments performed in this study B.

Core	Estaillades Limestone
Diameter	1.5/4 in
Length	5.75 in / 11.5 in
Porosity	0.26
Permeability	40 mD
Oil	Middle East Crude Oil
Temperature	23 °C
Oil Viscosity	13.5 cp
Surfactant Formulation	0.25 wt% C12-13-7PO-Sulphate, 2.25 wt% Na2CO3, 1.5 wt% EDTA, Salinity : 8469 ppm (Hardness: 1350 ppm)
Initial Oil Saturation	0.78

Table 4-6: Different experimental parameters for the Estaillades Limestone static imbibition experiments.

Core	Texas Cream Limestone
Diameter	1.5 in/4 in
Height	11.5 in / 5.75 in
Permeability	8.4 mD
Porosity	26%
Soi	0.78
Expt. Temperature	23° C
Oil	Reservoir crude oil
Viscosity at RT	13.5 cp
API gravity	39
Surfactant	C12-13-7PO-Sulphate (0.25 wt% , Type I), IFT : 0.6 dyne/cm
Brine Salinity	8469 ppm

Table 4-7: Different experimental parameters for the Texas Cream Limestone static imbibition experiments.

Core	Estaillades limestone
Diameter	1.5 in
Height	5.75 in
Permeability	150mD
Porosity	0.28
Injection Flow Rate	0.01 ml/min (2.4 ft/day)
Soi	0.78
Expt. Temperature	23° C

Table 4-8: Experimental parameters for the Estaillades Limestone static/dynamic imbibition experiments.

Core	Estaillades Limestone
Diameter	1.5 in / 4 in
Height	5.75 in
Permeability	150mD/40 mD
Porosity	0.28/0.26
Injection Flow Rate	0.01/0.026 ml/min (2.4 ft/day)
Soi	0.78
Oil	Reservoir crude oil
Oil viscosity at RT	13.5 cp
Oil API gravity	39
Brine Salinity	8469 ppm
Expt. Temperature	23° C

Table 4-9: Parameters for Estaillades Limestone dynamic imbibition experiments for variable diameter

Parameter	**Values**
Brine Salinity	72973 ppm
Hardness	6183 ppm
Reservoir Temperature (RT)	52° C
Oil	Reservoir crude oil
Oil viscosity at RT	6.9 cp
Core	Carbonate Reservoir Core
Length	3.2 in
Diameter	1.5 in
Pore volume	29.91 ml
Porosity	31.30%
Soi	0.87
Oil permeability at Soi	5.25 mD
Brine permeability	7 mD
Injection Flow Rate	1 ft/day (0.05 ml/min)
Surfactant	15-S-20 (0.2 wt%)
Experiment Temperature	52° C

Table 4-10: Fluid and core properties along with experimental conditions for coreflood -1

Parameter	Values
Brine Salinity	57670 ppm
Hardness	2760 ppm
Reservoir Temperature (RT)	95 ° C
Oil	Reservoir Crude Oil
Viscosity @ RT	0.68 cp
Core	Carbonate Reservoir Core
Length	5.75 in
Diameter	1.5 in
Pore volume	41 ml
Porosity	0.24
Soi	0.71
Oil permeability at Soi	10 mD
Injection rate	1 ft/day
Surfactant	0.2 wt% NP-10 + 0.2 wt% D-TAB
Experiment Temperature	95° C

Table 4-11: Fluid and core properties along with experimental conditions for Coreflood-2

Parameter	Waterflood	Secondary Surfactant Flood	Tertiary Surfactant Flood (Coreflood-1)
Injection Scheme	IB	0.5 PVSS --> IB (2.5 PV)	(0.5 PV) IB --> (0.5 PV) SS --> (2 PV) IB
Initial Oil saturation	0.88	0.88	0.87
Flow rate	1 ft/day	1ft/day	1 ft/day
Oil recovery after 3 PV injection (% OOIP)	50	66	61
Incremental oil recovery (%OOIP) over waterflood		16	11

Table 4-12: Comparison of oil recovery under different injection schemes for Carbonate Reservoir 1

Parameter	Water flood	Secondary Surfactant Flood	Tertiary Surfactant Flood (Coreflood - 2)
Injection Scheme	5 PV IB	1.2 PV (SS) --> 3.8 PV (IB)	0.5 PV IB --> 1 PV SS --> 2 PV IB
Flow rate	1 ft/day	1ft/day	1 ft/day
Initial Oil Saturation	0.7	0.71	0.72
Oil recovery after flood completion (% OOIP)	29	40	54 (Initial 0.5 PV waterflood:47)
Incremental oil recovery (%OOIP) over waterflood	--	11	7

Table 4-13: Comparison of oil recovery under different injection schemes for Carbonate Reservoir 2

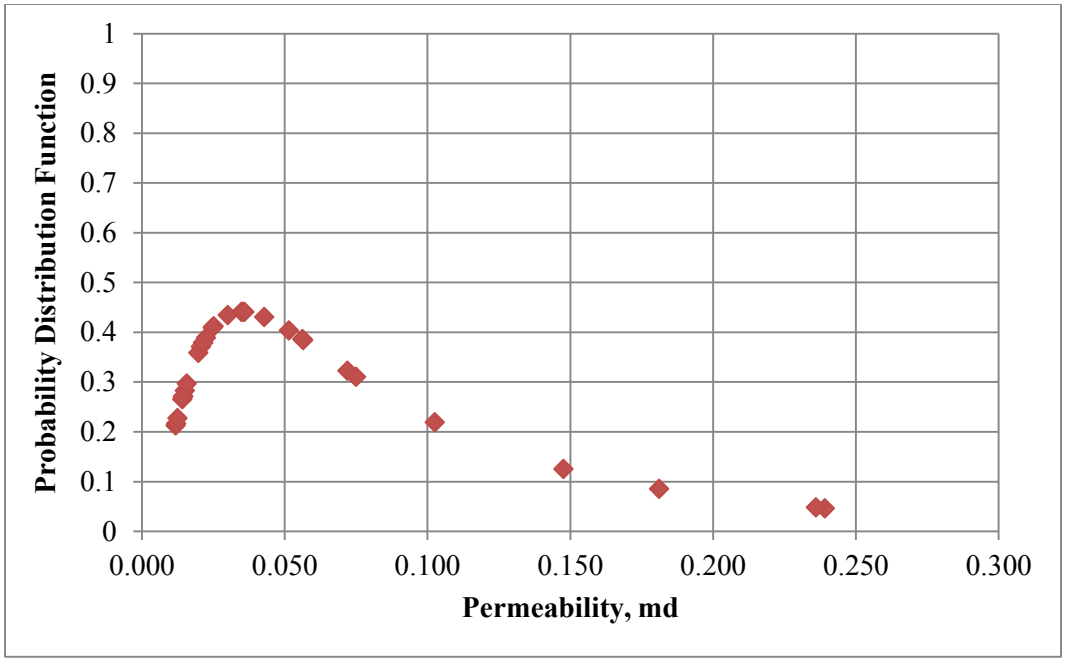

Figure 4-1: Distribution of brine permeabilities for the reservoir core plugs received

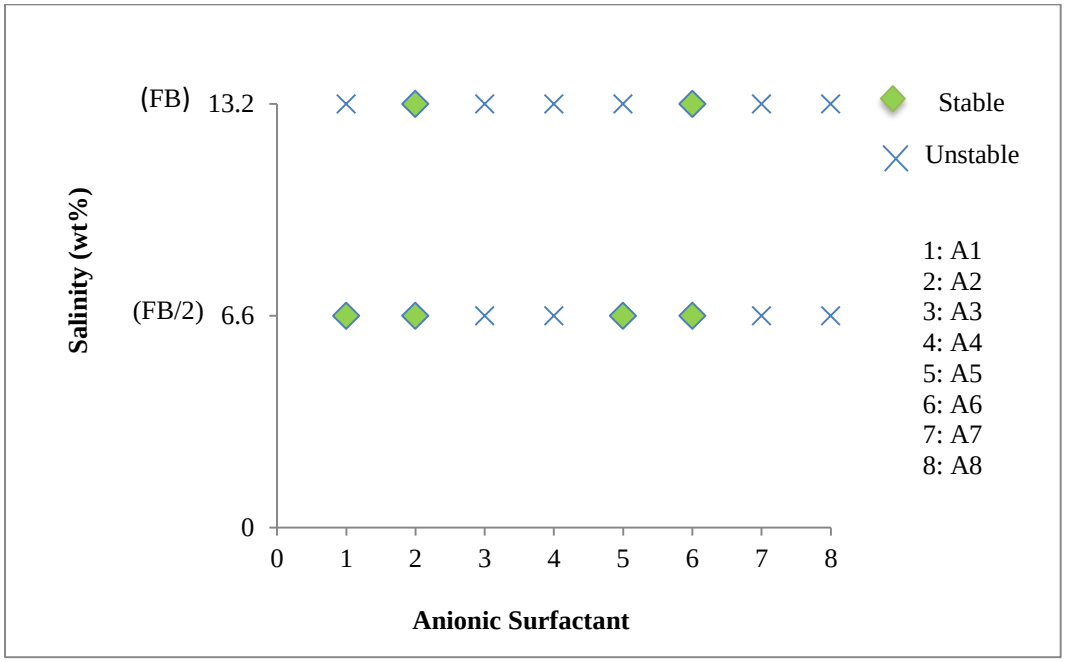

Figure 4-2: Aqueous stability results for anionic surfactants

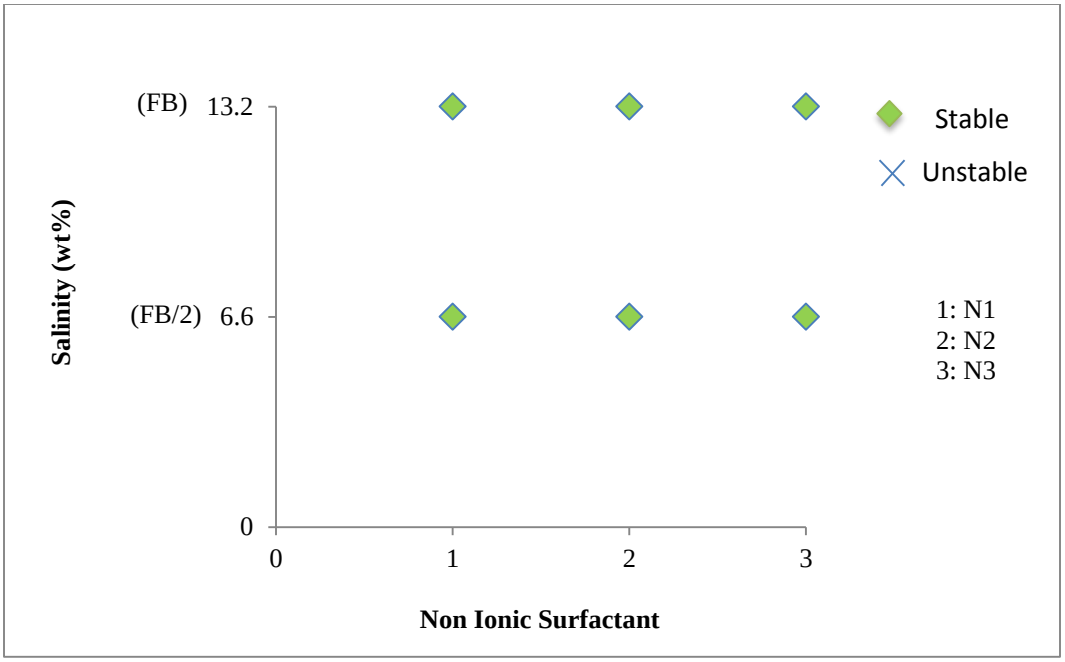

Figure 4-3: Aqueous stability results for non-ionic surfactants

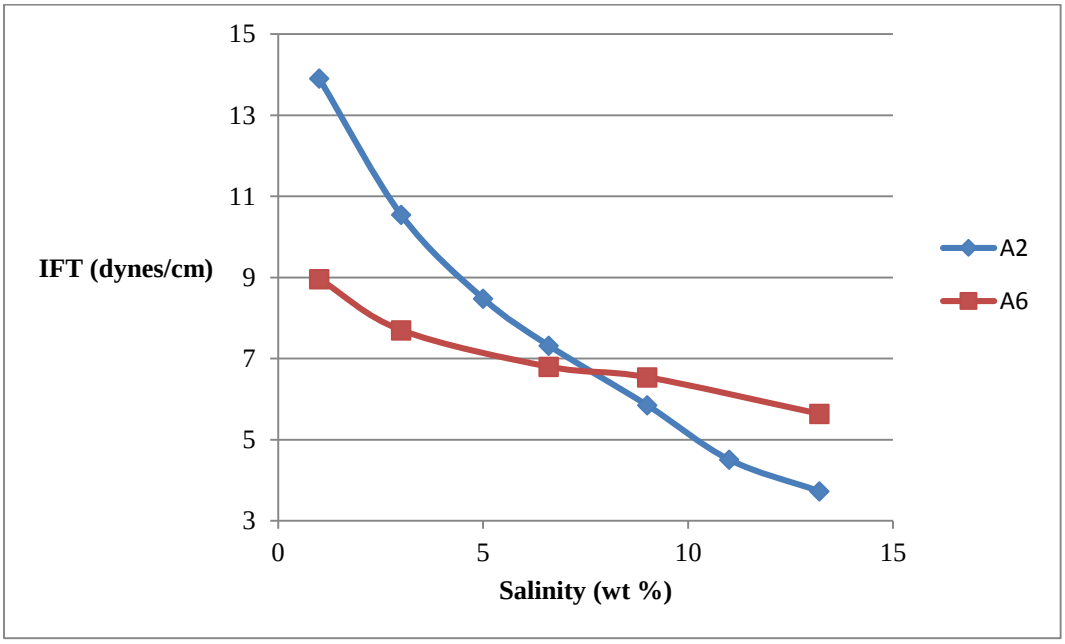

Figure 4-4: IFT values for surfactant A2 and A6 with varying salinity.

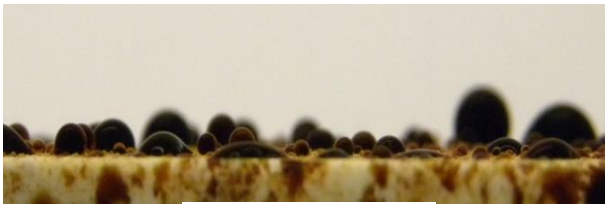

Formation Brine

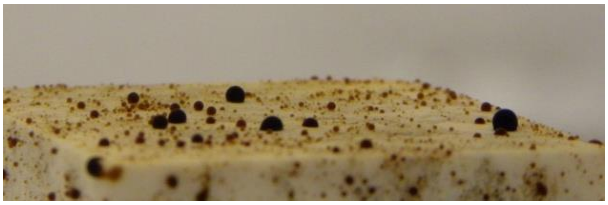

0.1 wt% A2 in FB/2

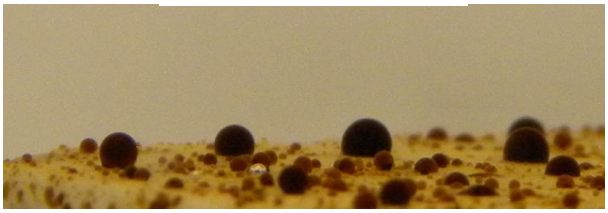

0.1 wt % A1 in FB/2

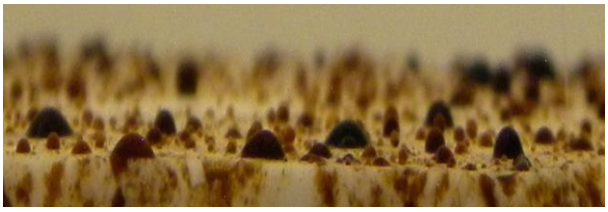

0.1 wt% A5 in FB/2

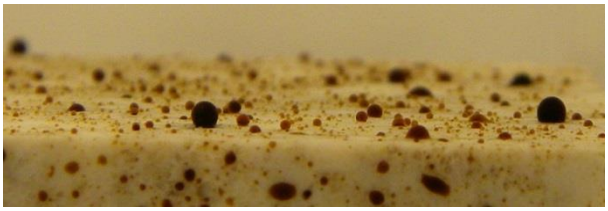

0.1 wt% A6 in FB/2

Figure 4-5: Oil droplets on Cristobalite plates submerged in half the formation brine salinity. The top picture is for oil-wetness of the aged-plate in formation brine.

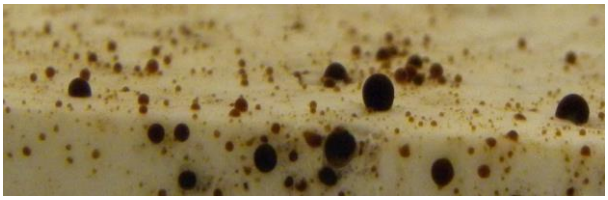

0.1 wt% A6 in FB

0.1 wt% A2 in FB

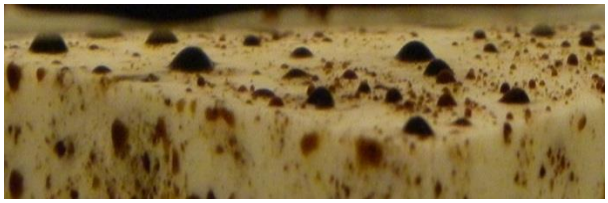

0.1 wt% N1 in FB

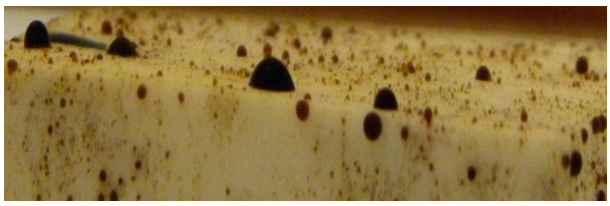

0.1 wt% N2 in FB

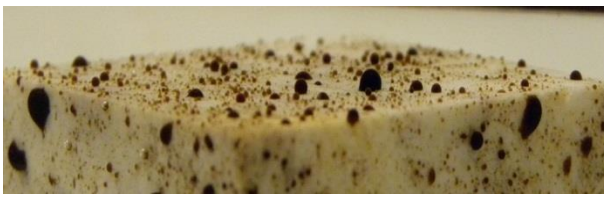

0.1 wt% N3 in FB

Figure 4-6: Oil droplets on Cristobalite plates submerged in surfactant solutions in formation brine

Figure 4-7: A water drop on top of an aged core showing its oil wettability

Figure 4-8: Oil droplets at the outer surface of the cylindrical core plug during spontaneous imbibition experiment in surfactant solution.

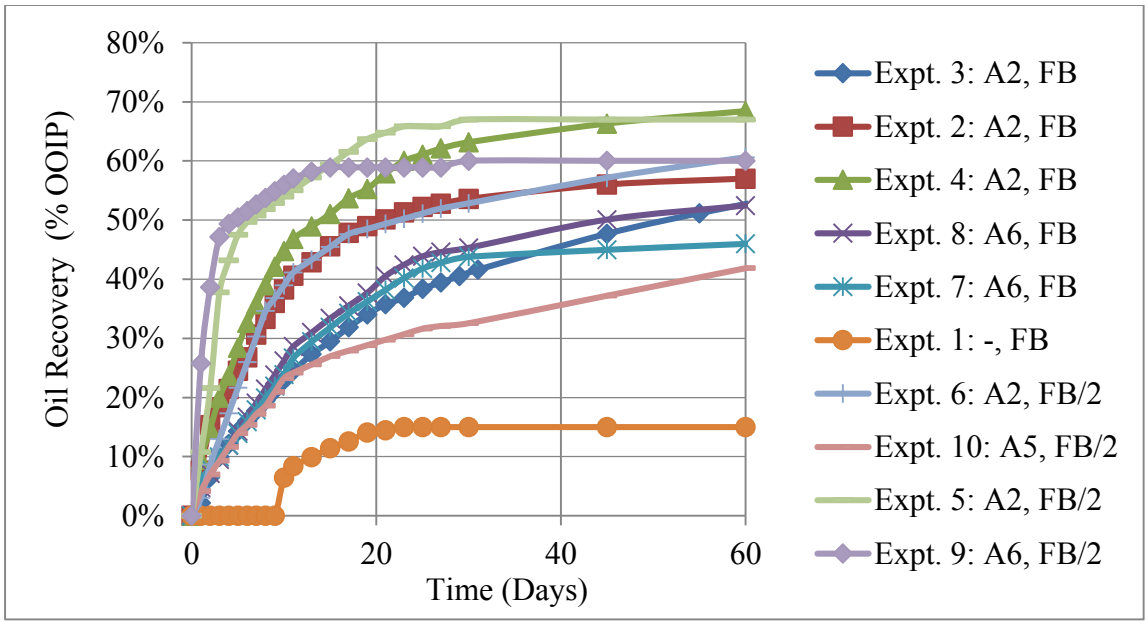

(a)

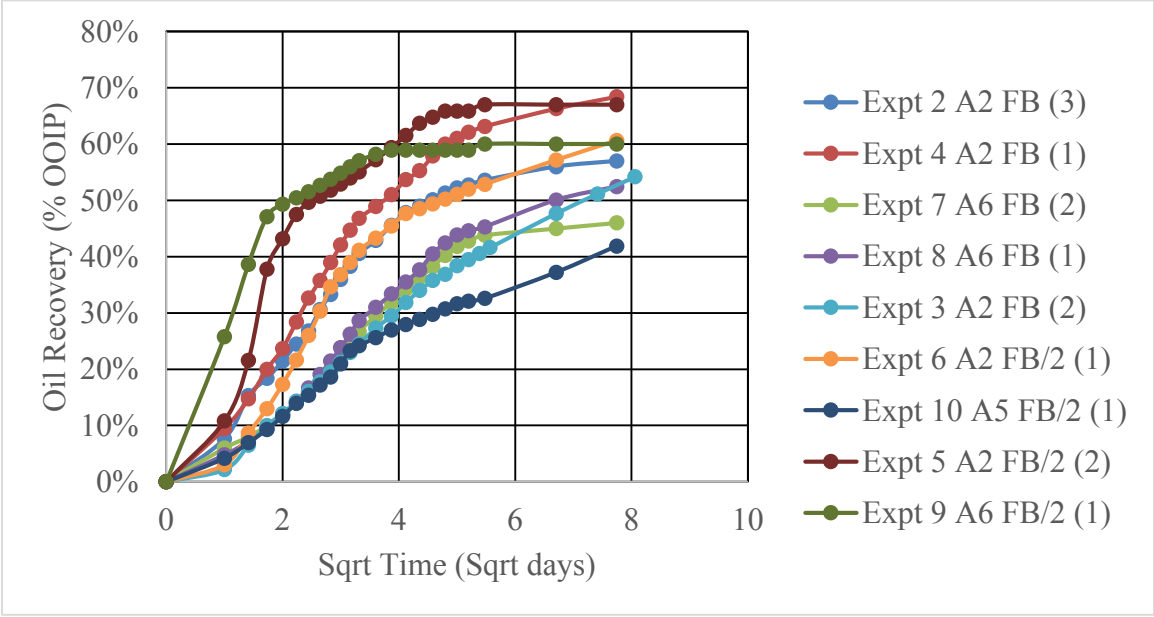

(b)

Figure 4-9: (a) Spontaneous imbibition oil recovery plotted with time. (b) Spontaneous imbibition oil recovery plotted with square root of time.

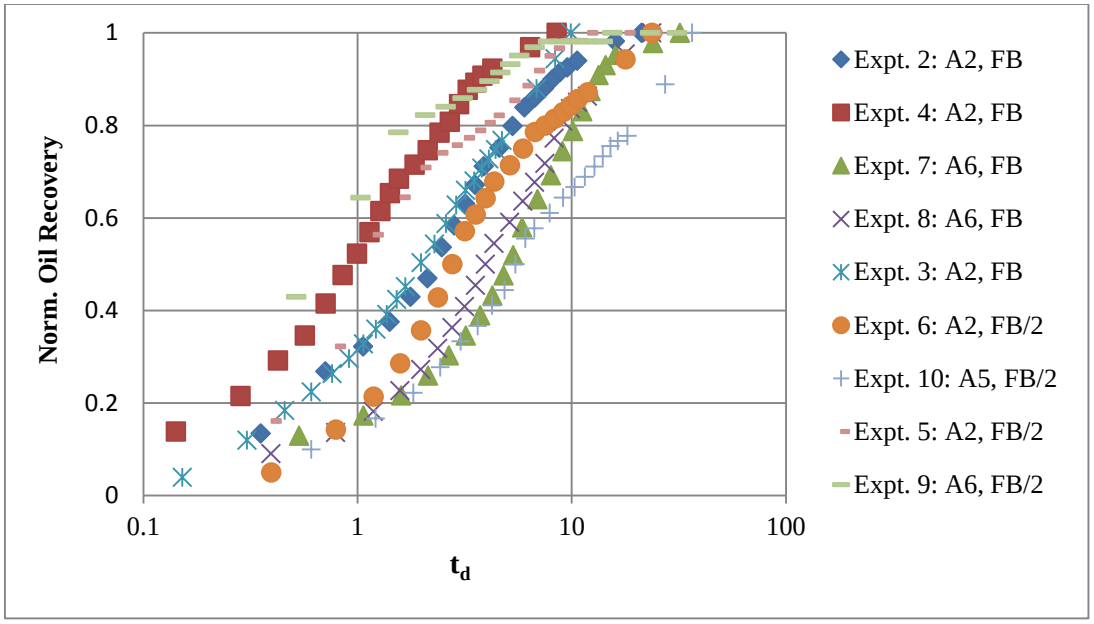

Figure 4-10: Imbibition data plotted with Mattax and Kyte dimensionless time.

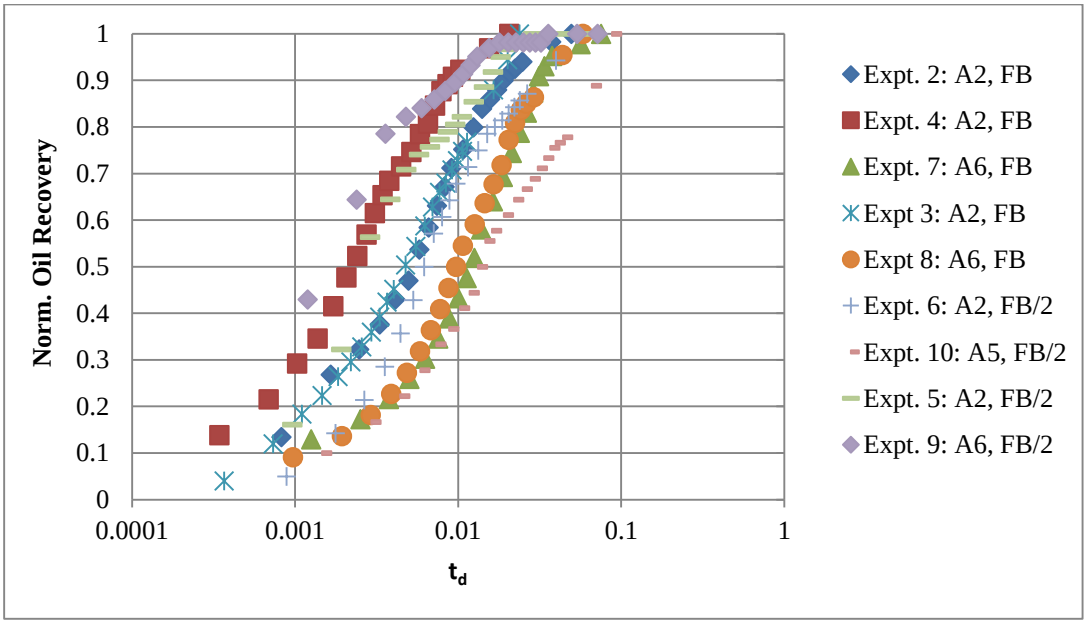

Figure 4-11: Imbibition data plotted with dimensionless time given by Ma et al. (1997)

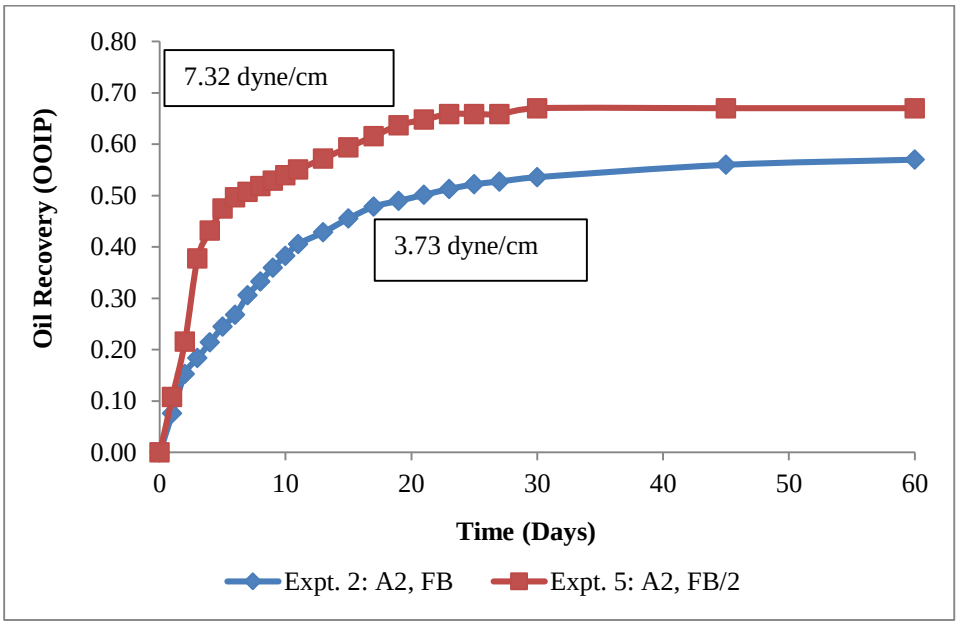

Figure 4-12: Recovery rate comparison for surfactant A2

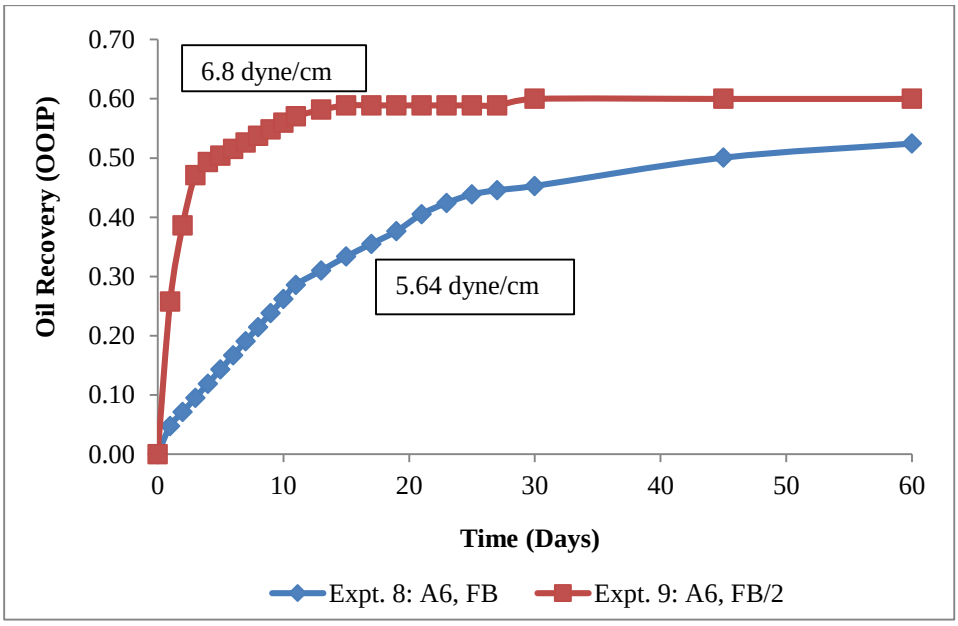

Figure 4-13: Recovery rate comparison for surfactant A6

Figure 4-14: Strongly oil-wet Estaillades Limestone Plate in Formation Brine (8469 ppm). The plate is immersed in brine after the aging process.

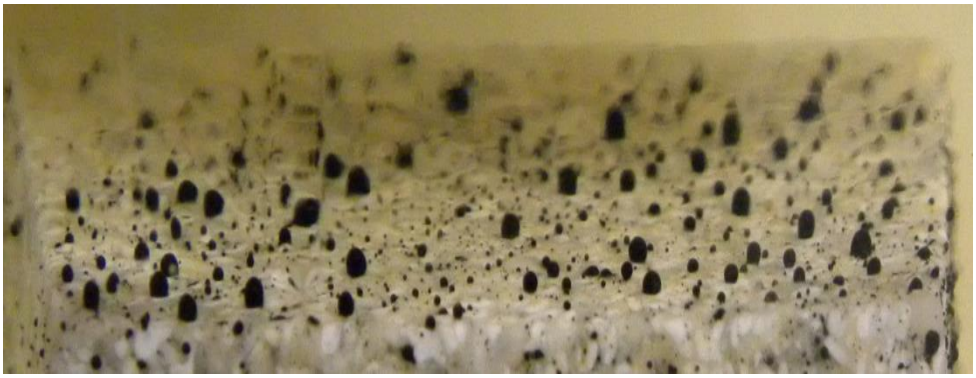

Estaillades Limestone plate in 0.25 wt% surfactant solution

Figure 4-15: Change in wettability of Estaillades Limestone in different surfactants. Wettability is changed from oil-wet to water-wet for the anionic surfactant mentioned in the table.

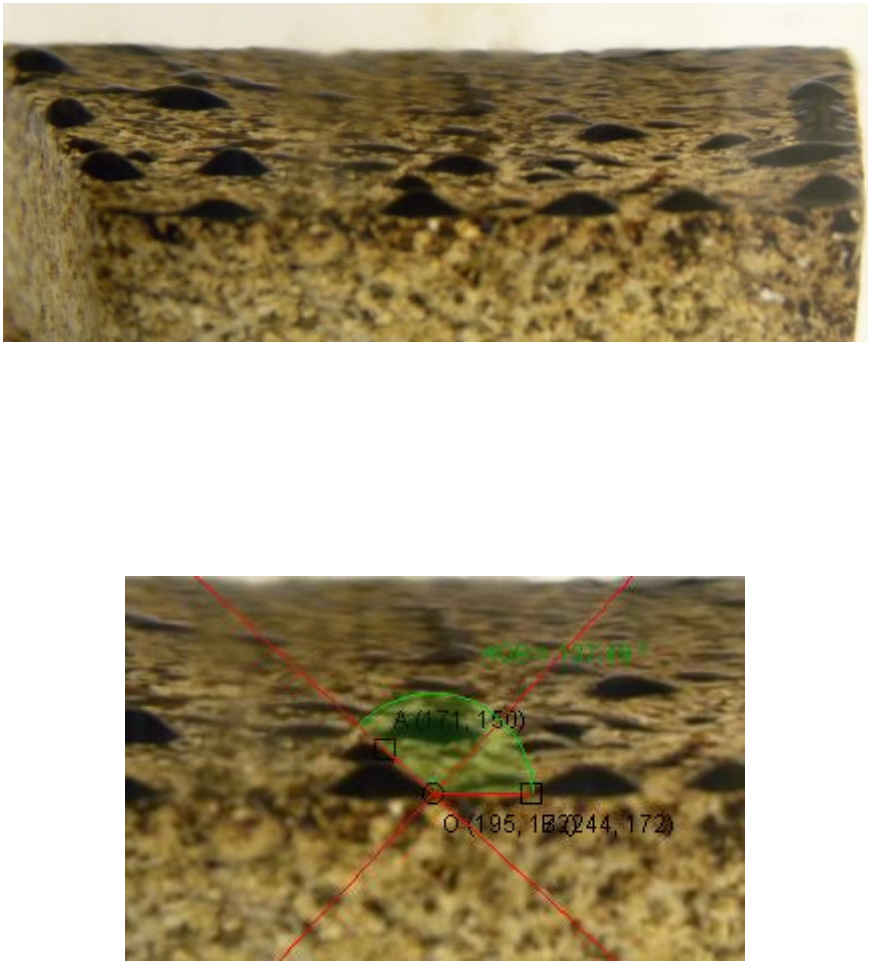

Figure 4-16: Estaillades Limestone plate in 0.5 wt% DTAB solution. The plate remains oil-wet in the surfactant solution.

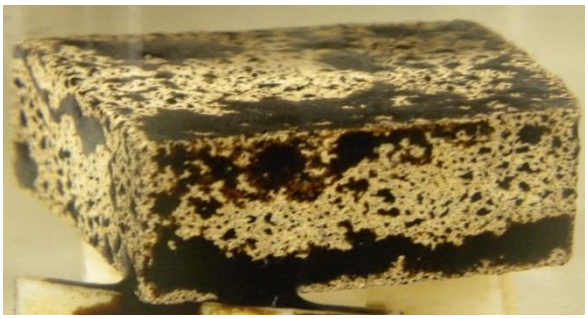

Figure 4-17: Oil-wet Texas Cream Limestone plate in formation brine

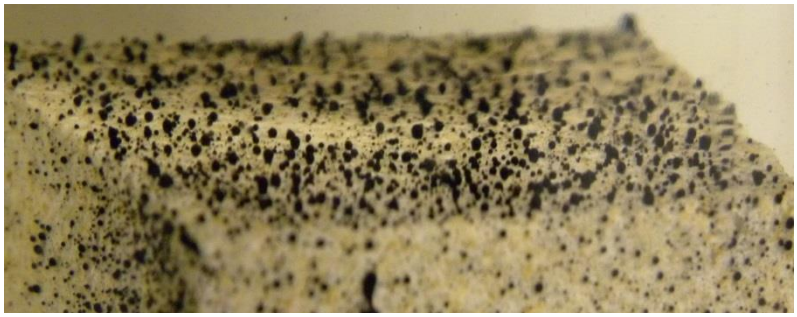

Figure 4-18: Change in wettability of Texas Cream Limestone from oil-wet to water-wet for 0.25 wt% anionic surfactant C12-13-7PO-SO_4.

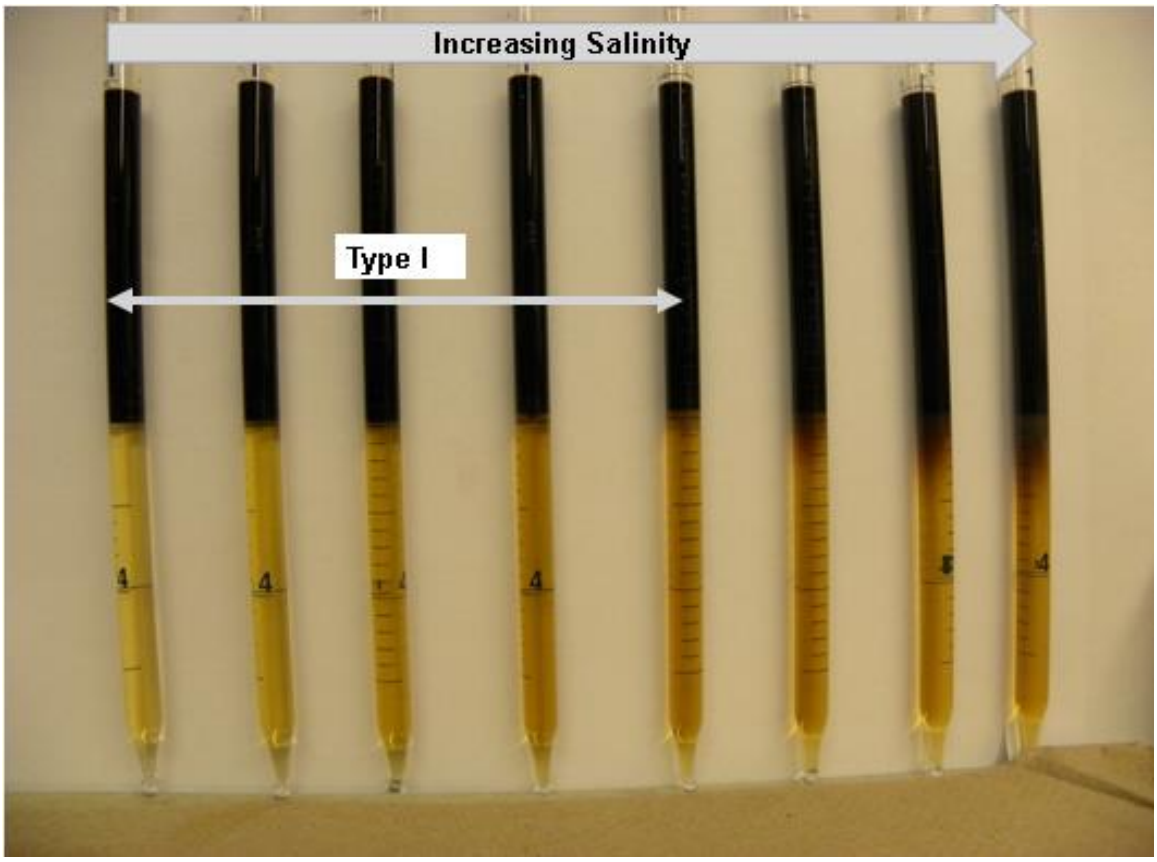

Figure 4-19: Phase behavior with increasing sodium chloride concentration. Experiments performed in this study are in the Type I salinity region

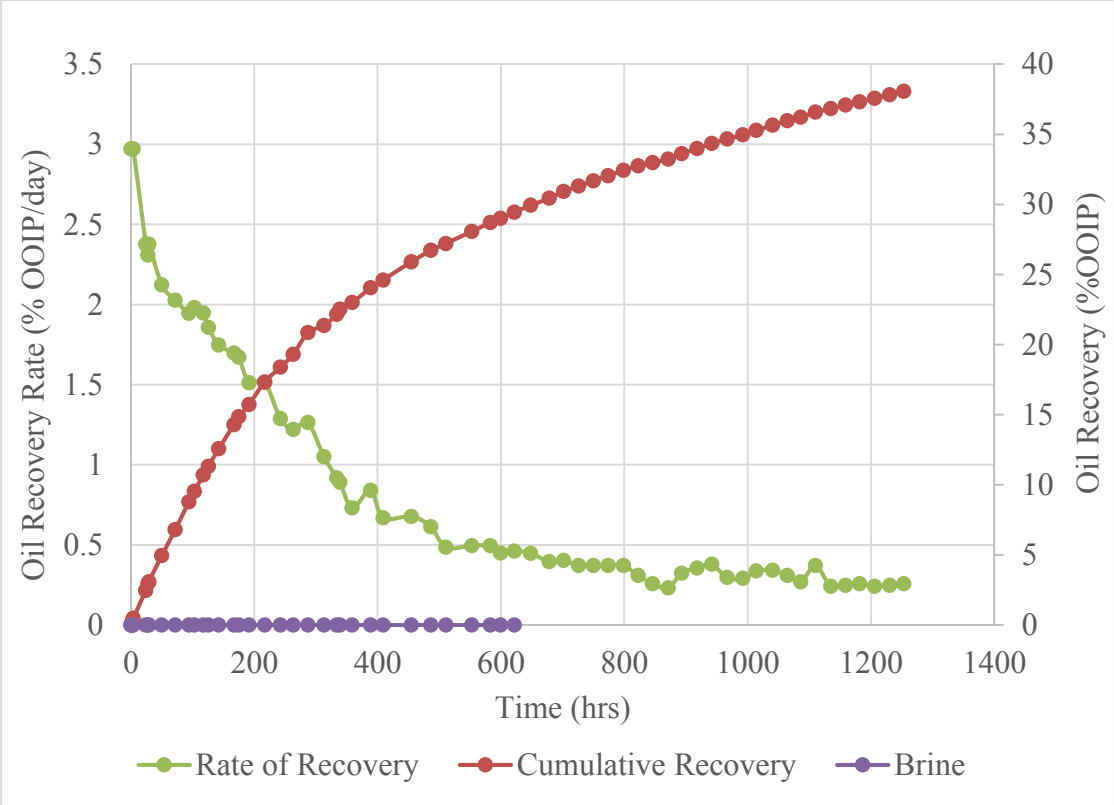

Figure 4-20: Oil recovery rate decay and cumulative recovery with time for the Estaillades Limestone static imbibition experiment on core with 1.5 in diameter and 5.75 in height.

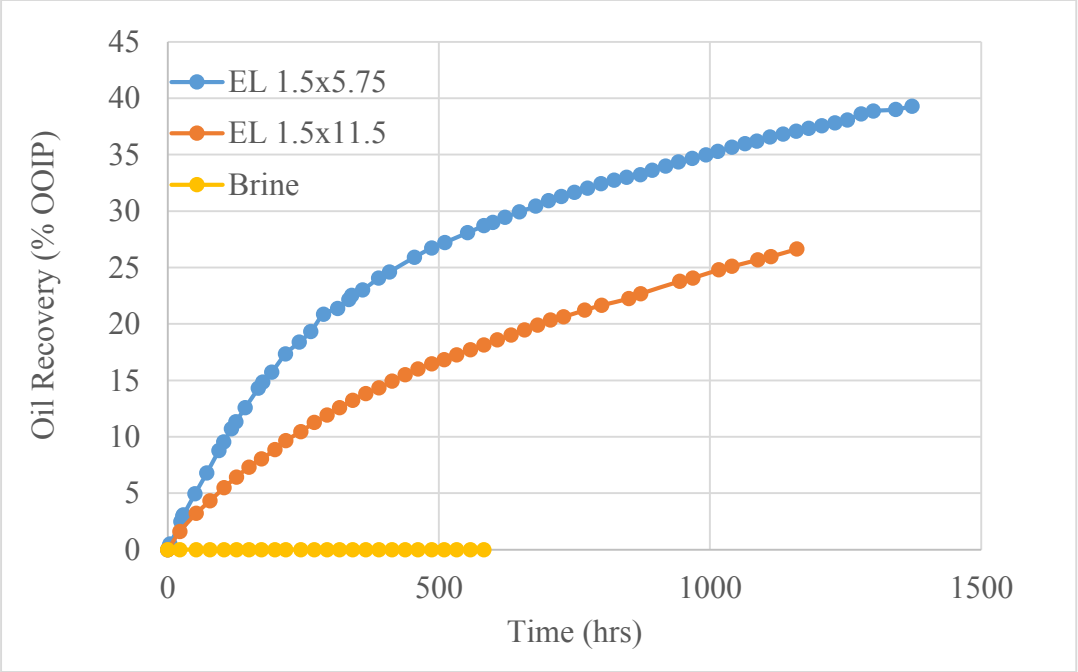

Figure 4-21: Comparison of oil recovery with height in a static imbibition setup on Estaillades Limestone core.

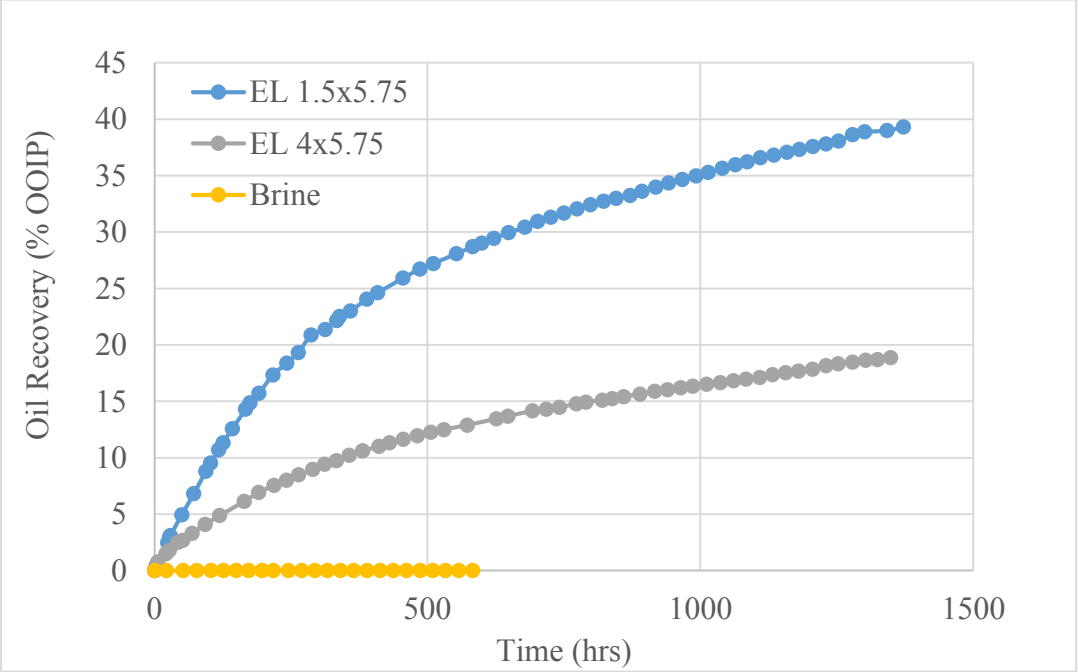

Figure 4-22: Comparison of oil recovery with diameter in a static imbibition setup on Estaillades Limestone core.

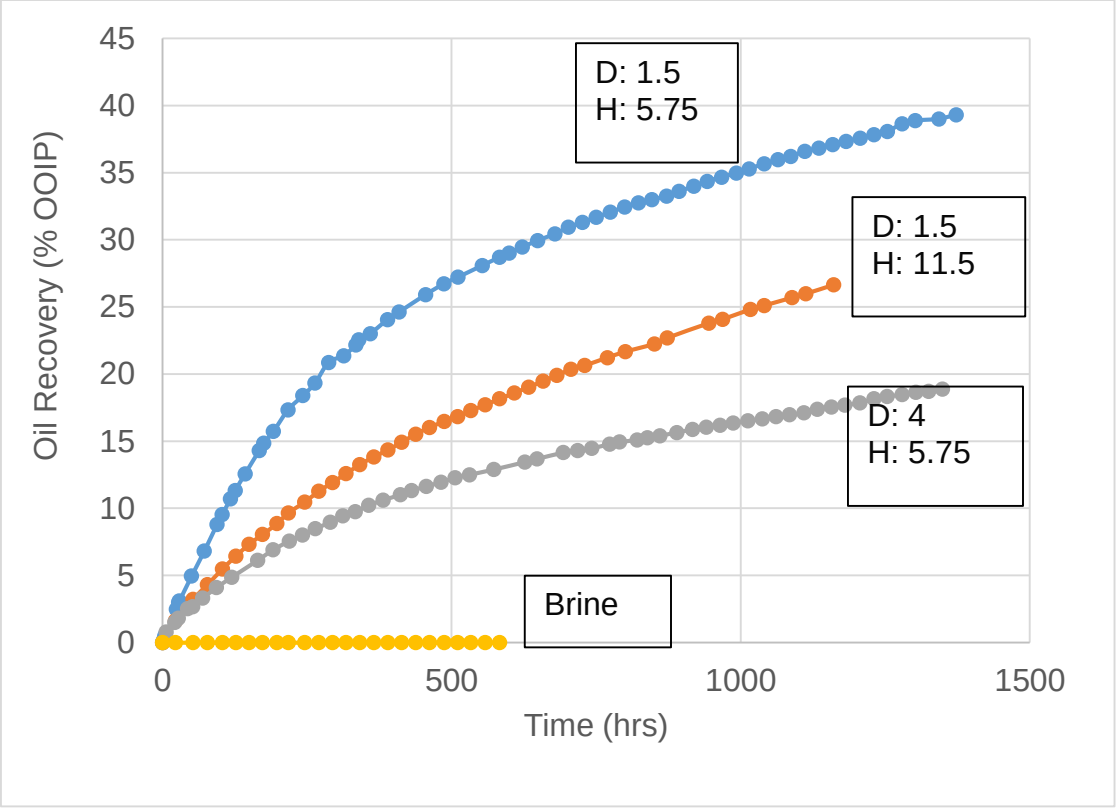

Figure 4-23: Comparison of oil recovery for Estaillades Limestone cores of varying dimensions with time.

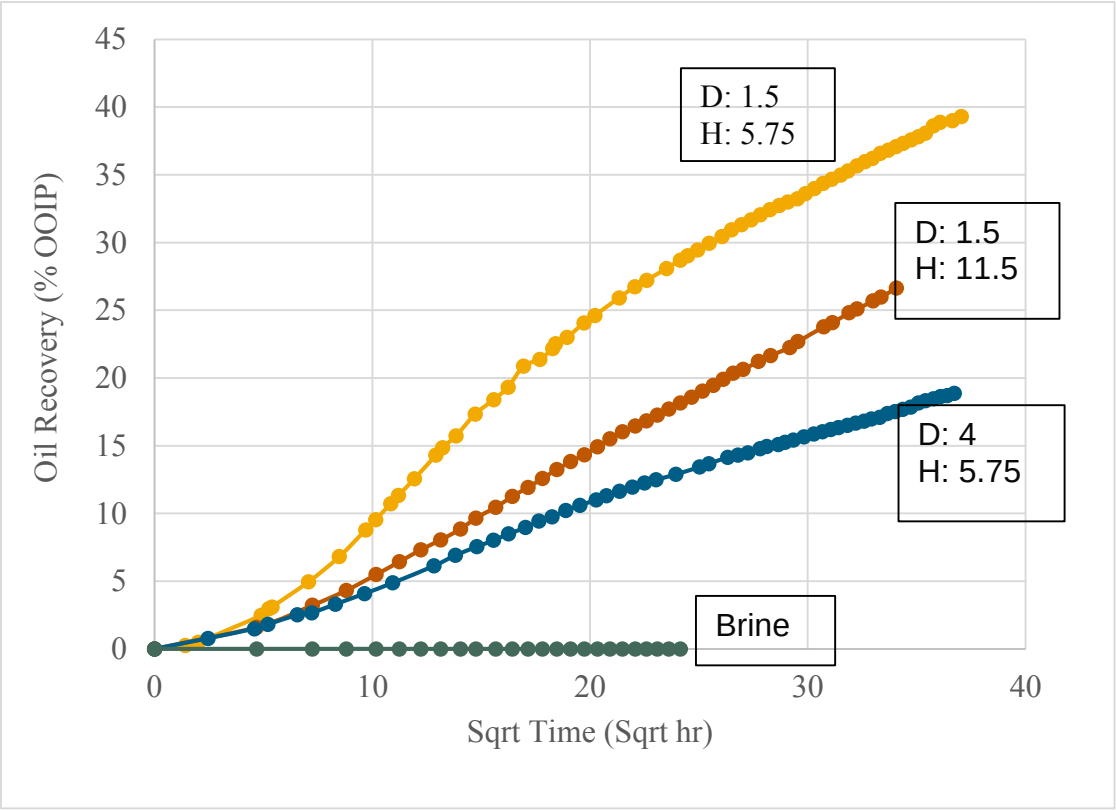

Figure 4-24: Comparison of oil recovery for Estaillades Limestone cores of varying dimensions with square root of time.

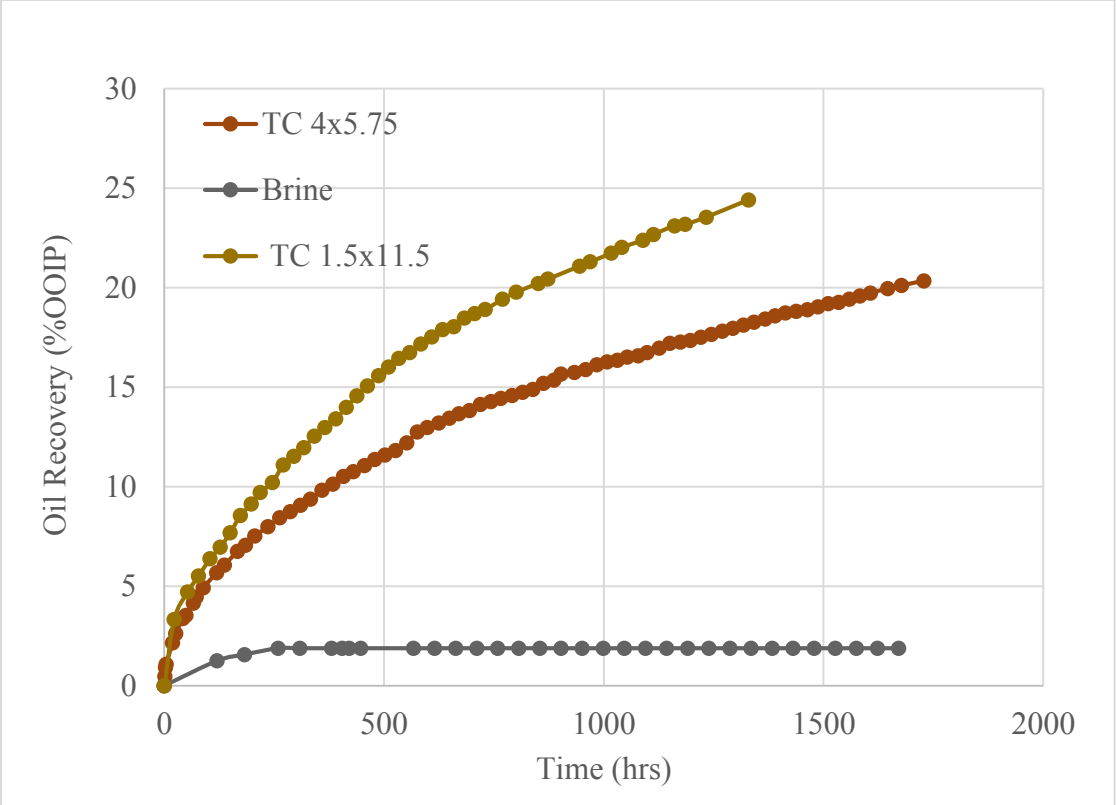

Figure 4-25: Static Imbibition Oil Recovery in Texas Cream Limestone Cores.

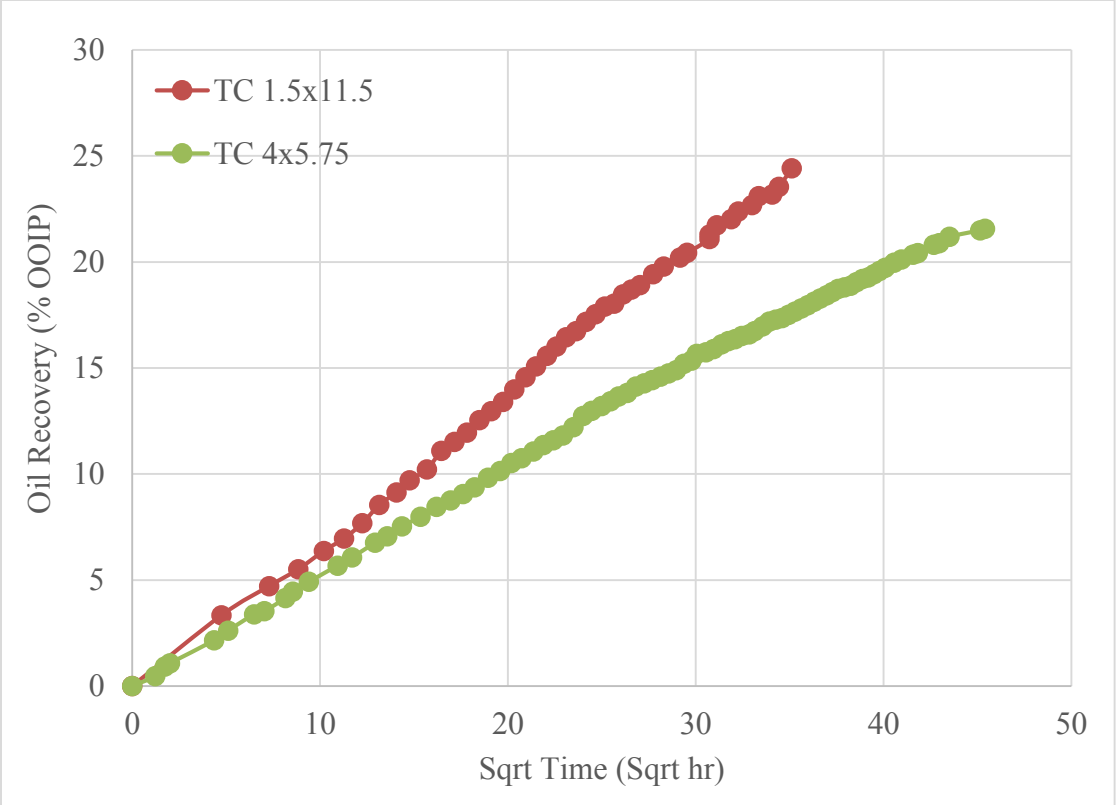

Figure 4-26: Oil Recovery plotted with square root of time for Texas Cream Limestone Experiments.

Figure 4-27: Fracture surface and epoxy coated lateral and top surface of the cylindrical Estaillades Limestone core used for the static versus dynamic imbibition comparison.

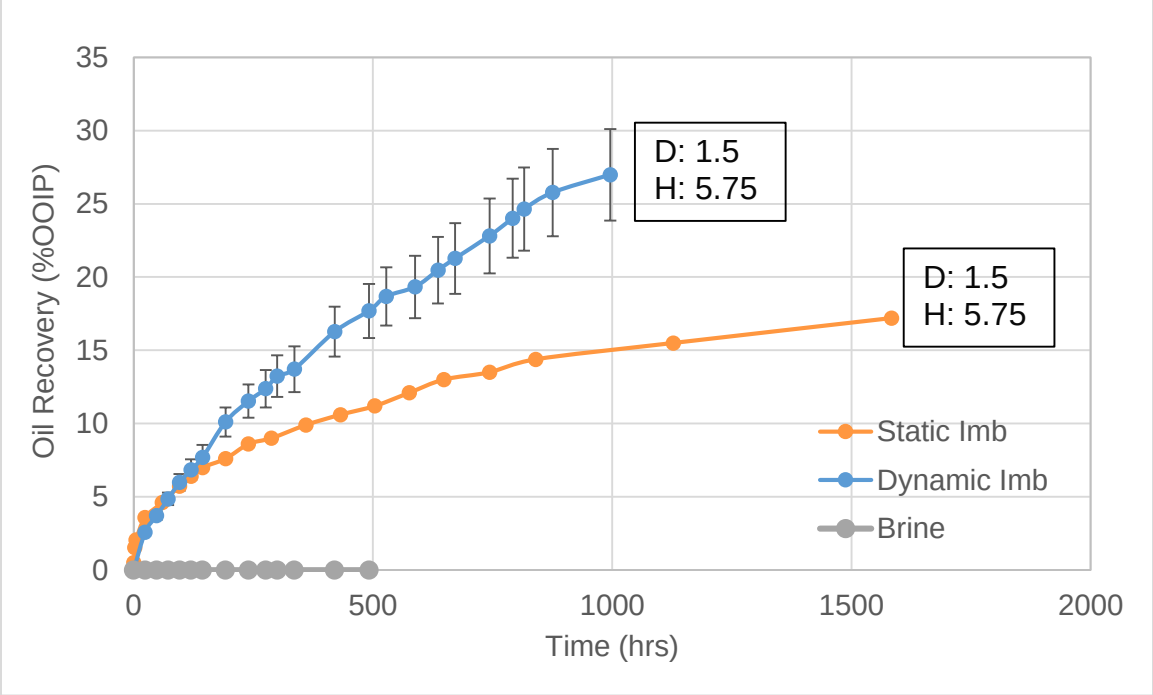

Figure 4-28: Comparison of static and dynamic imbibition recovery under same boundary condition and same rock/oil/fluid system.

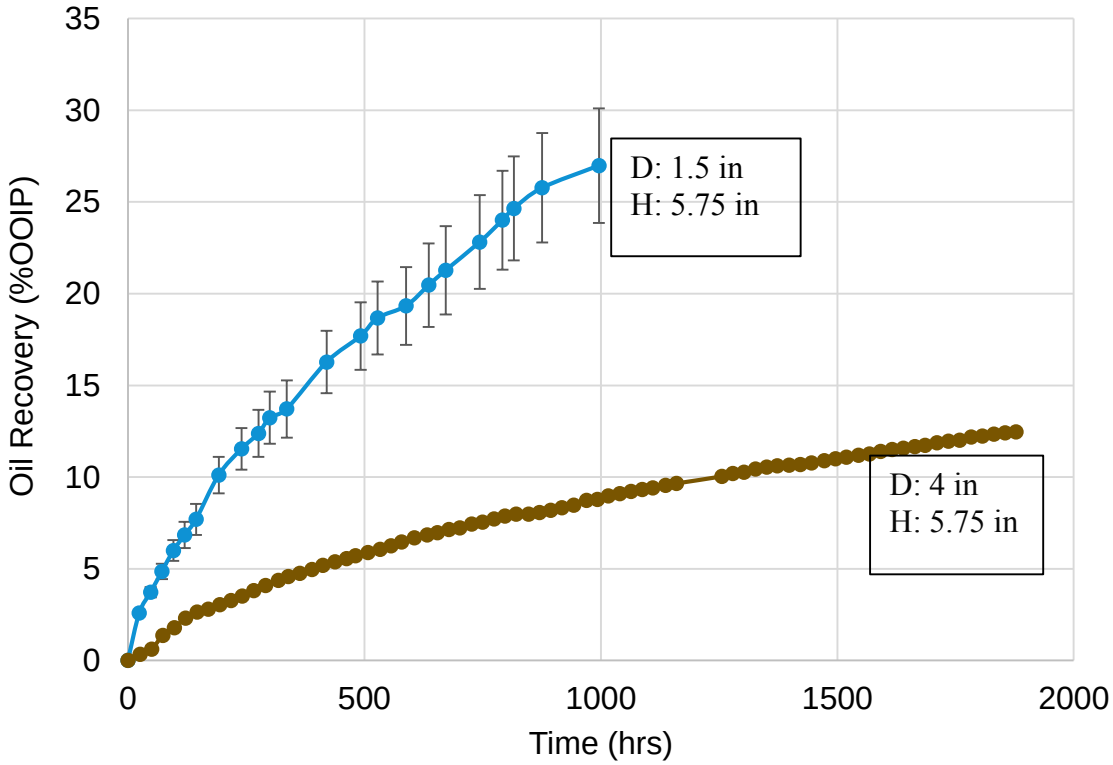

Figure 4-29: Dynamic imbibition oil recovery for cores of same height but varying diameter plotted with time

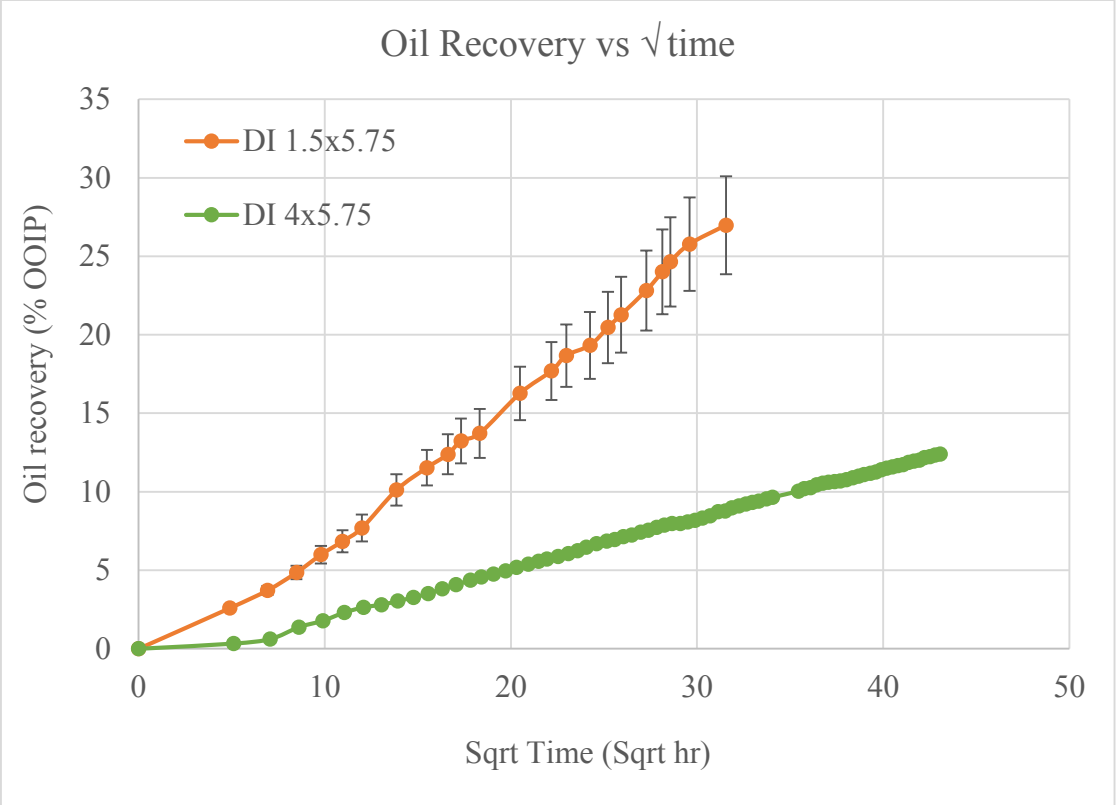

Figure 4-30: Dynamic imbibition oil recovery for cores of same height but varying diameter plotted with square root of time.

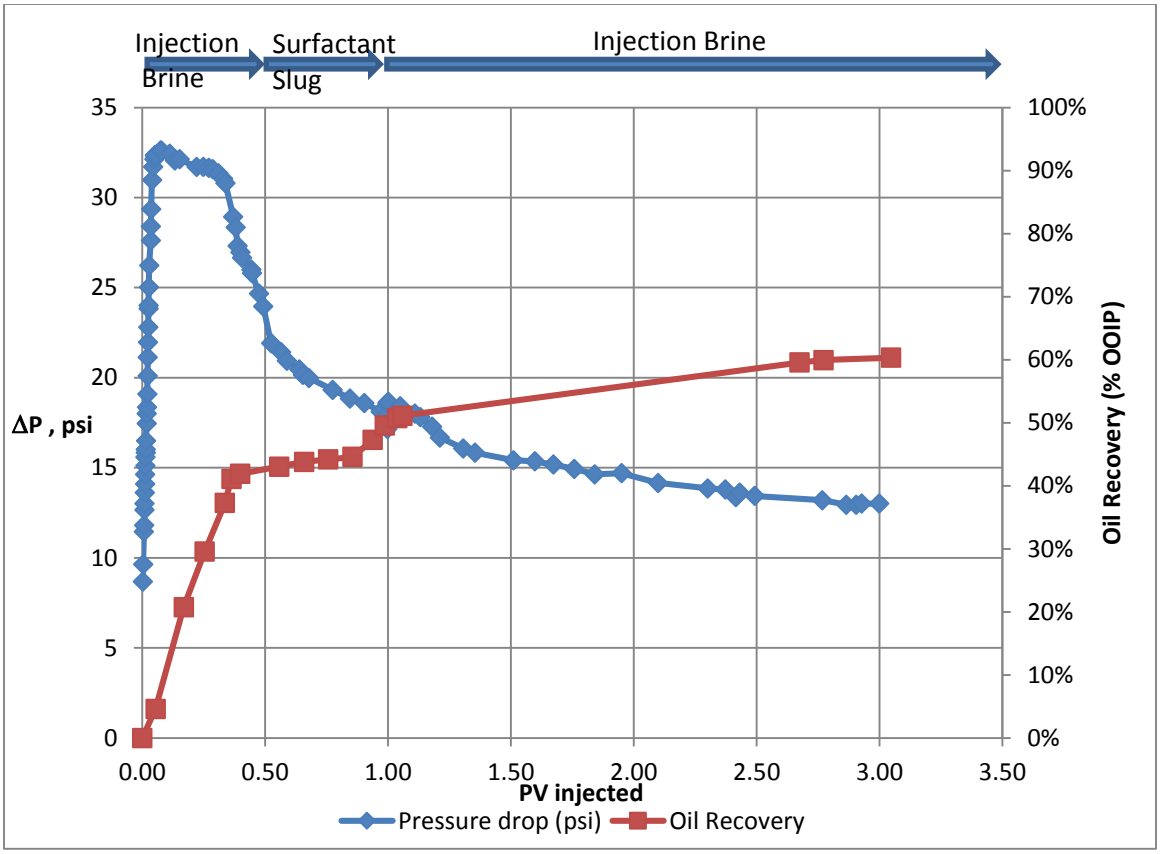

Figure 4-31: Pressure drop and cumulative oil recovery plotted against pore volume injected for Coreflood – 1

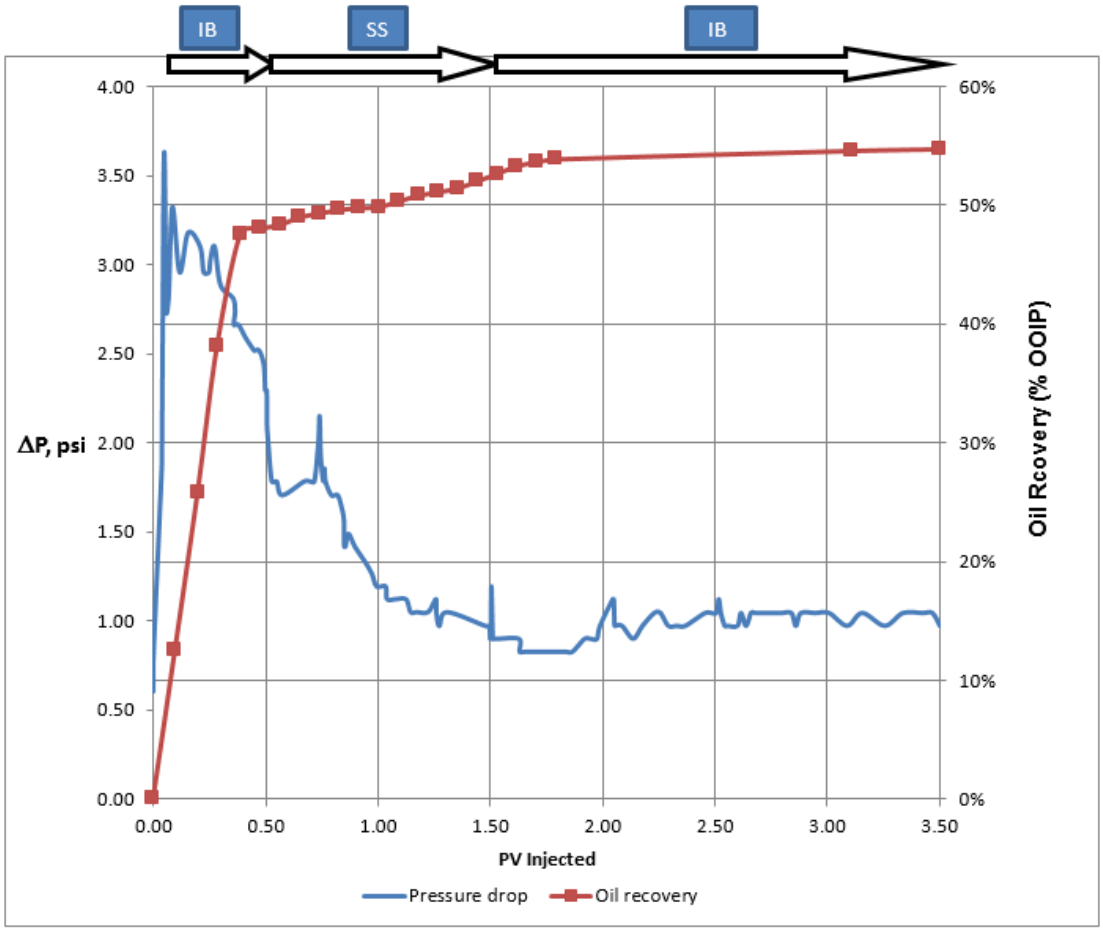

Figure 4-32: Pressure drop and cumulative oil recovery plotted against pore volume injected for Coreflood – 2. IB is injection brine and SS is Surfactant Slug.

Chapter 5: Recovery Mechanisms

5.1 Introduction

A mechanistic simulator developed in previous studies (Adibhatla et al. 2008) was used to perform numerical simulations in order to better understand the recovery processes. The simulator uses a 3D finite volume, two-phase, four-component implicit numerical scheme. It is compiled on FORTRAN and the output data files are analyzed via MATLAB. There is no third phase formation observed during oil/brine/surfactant phase behavior experiments performed in this study; hence the system is essentially two-phase. The numerical model takes into account surfactant convection/diffusion, consequent IFT and contact angle changes. The injected surfactant moves into the matrix because of flow caused by wettability alteration and IFT reduction.

Capillary pressure between the oil and brine phase, the relative permeabilities and the residual saturations of both phases were considered as functions of wettability and IFT. The effect of hydraulic dispersion is neglected and it is assumed that overall mass flux of each component is summation of convection and molecular diffusion. For an initially oil-wet reservoir, the improved oil recovery by introduction of surfactant into brine is achieved due to the alteration of flow functions, including capillary pressure, relative permeability and residual saturations. For the systems on which experiments are performed in this study the trapping number is not high enough to induce a change in residual saturation. Surfactant can lower the IFT and also alter the wettability of matrix to intermediate-wet or water-wet through removal of oil-wetting components from the matrix surface.

In this chapter, mechanistic simulations are performed for the capillary and gravity dominated imbibition experiments with an aim to study the recovery mechanisms.

Input parameters are validated by obtaining a match with the experimental data. Velocity and saturation profiles are then analyzed to understand and contrast the behavior of the two (capillary and gravity dominated) processes.

5.2 MODEL DESCRIPTION

In this section, the key equations and assumptions governing the mass transfer of different components are described. A detailed description of the model can be found in Adibhatla et al. (2008). According to the experimental observations, the following assumptions were made regarding the distribution of components (water, salt, hydrocarbon and surfactant) among different phases (aqueous and oleic):

- Hydrocarbon can exist in oil phase and aqueous phase;
- Water can exist in aqueous phase and oil phase;
- Surfactant can exist in aqueous phase and oil phase, and on the solid surface;
- Salt can exist in aqueous phase and can be absorbed onto matrix surface

Based on these assumptions, the mass balances at any position can be described with:

$$w_a^w + w_a^h + w_a^{sf} + w_a^{st} = 1 \tag{5-1}$$

$$w_o^w + w_o^h + w_o^{sf} = 1 \tag{5-2}$$

$$\phi C^{sf} = \phi(\rho_a S_a w_a^{sf} + \rho_o S_o w_o^{sf}) + A_s C_r^{sf} \tag{5-3}$$

$$\phi C^{st} = \phi(\rho_a S_a w_a^{st}) + A_s C_r^{st} \tag{5-4}$$

where the superscript "w" represents the water component, "h" represents the hydrocarbon component, "sf" represents the surfactant and "st" refers to the salt component. ϕ is the porosity; ρ_j is the density of phase j, w_j^i is the mass fraction of component i in phase j; C^{sf} (kg/m3) is overall concentration of surfactant and C^{st} is overall concentration of salt,

C_r^{sf} and C_r^{st} (kg/m2) are the concentrations of surfactant and salt absorbed on matrix surface in kg per unit area; A_s is the specific matrix surface area (m2/m3 matrix).

In this study, we neglected the effect of hydraulic dispersion and assumed that the overall mass flux ($\vec{F}_i$) of each component 'i' is a linear summation of convection and molecular diffusion:

$$\vec{F}_i = \rho_a \vec{v}_a w_a^i + \rho_o \vec{v}_o w_o^i - D_a^{i,e} \nabla w_a^i - D_o^{i,e} \nabla w_o^i \tag{5-5}$$

The phase velocity $\vec{v}_j$ is given by Darcy's law as:

$$\vec{v}_j = -\frac{k_{rj}}{\mu_j} \vec{\vec{K}} . (\nabla p_j + \rho_j \vec{g}) \tag{5-6}$$

$\vec{\vec{K}}$ is the absolute permeability tensor, k_{rj} is the relative permeability of phase j, μ_j is the viscosity of phase j, p_j is the pressure of phase j. In a system of two-phase (oil-aqueous phase) flow, the pressure difference between oil and aqueous phase is the capillary pressure. The mass balance equations for all the components can be written as:

$$\frac{\partial}{\partial t}\left[\phi(\rho_a S_a w_a^h + \rho_o S_o w_o^h)\right] + \nabla . \overline{F}^h = q^h \tag{5-7}$$

$$\frac{\partial}{\partial t}\left[\phi(\rho_a S_a w_a^w + \rho_o S_o w_o^w)\right] + \nabla . \overline{F}^w = q^w \tag{5-8}$$

$$\frac{\partial(\phi C^{sf})}{\partial t} + \nabla . \vec{F}^{sf} = q^{sf} \tag{5-9}$$

$$\frac{\partial(\phi C^{sf})}{\partial t} + \nabla . \vec{F}^{st} = q^{st} \tag{5-10}$$

We neglected any in-situ source for any component, e.g., the in-situ generation of surfactant, so the source term q^i is determined solely by boundary conditions. Equations 5-7 to 5-10 were spatially discretized with a finite volume method. One-point upstream averaging was employed in the evaluation of phase mobility. The backward Euler method

was used to approximate the partial derivative of time. This discretization method generated a fully implicit scheme in which 4n nonlinear algebraic equations were solved simultaneously. Here n is the number of grid blocks into which the medium is discretized. For each grid block, four unknowns were solved. The oil phase pressure (P_o), oil phase saturation (S_o), overall surfactant concentration (C^{sf}) and overall salt concentration (C^{st}) are the primary unknowns solved directly from the governing equations. Newton-Raphson method was employed to solve the system of equations. A linear solver based on the iterative methods was used to solve the sparse linear system.

The capillary pressure between the oil and brine phase, relative permeabilities and residual saturations of both phases were considered as functions of wettability and IFT. Capillary pressure is assumed to depend on saturation through a power-law model.

$$P_C(S_{DW}) = P_{CA} + P_{CB}(S_{DW})^{n_c} \tag{5-11}$$

P_{CA} and P_{CB} determine the endpoints of the capillary pressure curve, n_c is the exponential parameter and S_{DW} is the dimensionless water saturation defined by

$$S_{Dj} = \frac{S_j - S_{jr}}{1 - S_{wr} - S_{or}} \quad . \tag{5-12}$$

According to the Leverett J-function, the effects of interfacial tension σ and contact angle θ on capillary pressure are described with the following equation:

$$P_C = P_{C0}(S_{DW})\frac{\sigma\cos\theta}{\sigma_0\cos\theta_0} \quad . \tag{5-13}$$

The subscript ‘0’ on capillary pressure, interfacial tension and contact angle indicates values for an initial oil-wet system. Relative permeability curves are described by a modified Brooks-Corey model, i.e.,

$$k_{rj} = k_{rj}^0 (S_{Dj})^{n_j} \tag{5-14}$$

where k_{rj}^0 is the end point relative permeability of phase *j* and n_j is the relative permeability exponent of phase *j*. The end point relative permeability and exponent vary with contact angle as presented below:

$$k_{rj}^0 = k_{r,wet}^0 + \frac{\cos\theta_j - \cos\theta_0}{\cos(\pi - \theta_0) - \cos\theta_0}(k_{r,nw}^0 - k_{r,wet}^0) \tag{5-15}$$

$$n_j = n_{wet} + \frac{\cos\theta_j - \cos\theta_0}{\cos(\pi - \theta_0) - \cos\theta_0}(n_{nw} - n_{wet}) \tag{5-16}$$

θ_j is the contact angle measured through phase j, $k_{r,wet}^0$ corresponds to the wetting phase endpoint relative permeability and $k_{r,nw}^0$ corresponds to the non-wetting phase endpoint relative permeability. For considering the effect of IFT on change in residual saturations and consequent change in relative permeability parameters, the above equations can be modified with the trapping number. Interfacial tension and contact angle variation with surfactant concentration is modeled as polynomial and linear functions, respectively, with endpoint parameters obtained from experimental data. Residual saturation can be modified with the trapping number to account for the reduction in residual saturation with increase in trapping number. The trapping number is defined as:

$$N_{Tj} = \frac{|\bar{\bar{k}}.(\nabla p_j + \bar{g}(\rho_a - \rho_o))|}{\sigma} \tag{5-17}$$

where N_T is the trapping number and ∇p_j is the pressure gradient across phase j.

The effect of capillary number and bond number is combined in the trapping number and it is a more accurate means of accounting for change in residual saturation

rather than just taking the capillary number to account for change in residual saturation. The following equation is used to correlate the residual saturation with trapping number.

$$S_{rj} = \frac{S_{rj}^{low}}{1 + T_j N_T} \tag{5-18}$$

where S_{rj} is the residual saturation of phase *j* and T_j is the trapping parameter for phase *j*. The superscript 'low' refers to the saturation value at low trapping number. In this study the trapping number is not high enough since the interfacial tension is not reduced to ultra-low (0.001 dyne/cm) values. Hence, residual saturation is assumed as constant for the simulations performed.

5.3 CAPILLARY DOMINATED FLOW

Imbibition experiments were performed on low permeability oil-wet/mixed-wet sandstone reservoir cores (section 4.1) using a dilute (0.1 wt%) wettability altering surfactant solution. The surfactant formulation altered the wettability towards water-wet which resulted in high imbibition oil recovery. The inverse bond numbers for these experiments are above 240 suggesting that the oil recovery is dominated by capillary forces. Preparation of cores for these experiments is described in section 3.2. The initial oil saturation achieved by flooding oil in the core was on an average between 0.7 to 0.8. Experiment 2 (Table 4-3) was used for validation of the simulator inputs. Details about the experimental parameters are listed in Table 5-1.

Simulations were performed using a cylindrical grid block system for accuracy in representing the experiments which were performed on cylindrical cores. All surfaces of the core (lateral, top and bottom) were open to imbibition and in contact with the imbibing fluid. 13x55 grid blocks were used to model the core with 13 grid blocks in the radial direction and 55 grid blocks in the vertical direction rendering radial and vertical grid block

dimensions of 1mm. The cylindrical coordinate system dimension theta was taken as 2π. Constant permeability, porosity and initial saturation were assigned to each grid-block (values in Table 5-1). The brine surfactant weight percent is imposed as a boundary condition. For this imbibition experiment 0.1 wt% surfactant solution is used. Relative permeability, capillary pressure parameters and residual saturation were altered to get a match with the experimental data. The values of these parameters are mentioned in Table 5-2. Relative permeability variation with wettability is shown Figure 5-2. With increase in water-wetness, the water relative permeability decreases and oil relative permeability increases.

To study the mechanisms governing the recovery process, the simulator inputs were validated with data from Experiment 2 (Table 4-3). Figure 5-3 shows a comparison of the simulator generated recovery curve with the experimental recovery curve. The velocity vectors were plotted for the oil phase in Figure 5-5. These are the resultant vectors for the radial and vertical interstitial velocity

$$v_{Net} = \sqrt{v_r^2 + v_z^2} \tag{5-19}$$

where v_{Net} is the resultant velocity, v_r is the velocity in the radial direction, v_z is the velocity in z direction (vertical). Figure 5-5 shows radially outward pointing oil velocity vectors which are inclined in nature. The inclination is more at the top and bottom which indicates counter current imbibition at all the surfaces in contact with the surfactant solution at the boundary.

Figure 5-6 shows the core on which this experiment was performed. Oil recovery through sides is depicted in the image which was captured by the simulation results as well. The IFT in this surfactant-oil-brine system is lowered from 21.8 dyne/cm to 3.7 dyne/cm. Even at the lowest value of IFT for this system the inverse bond number is very high (248).

High inverse bond numbers indicate high capillary forces compared to gravity forces. High capillary forces lead to counter-current imbibition where oil is recovered from all faces compared to gravity dominated recovery where majority of oil is recovered through the top. The velocity vectors at the outer face of the core are large compared to the vectors towards center which suggests that the core is imbibed radially inward from the boundary.

To study the development of saturation profile with time, saturation in grid-blocks at the same cross section was averaged to obtain a single value of saturation at each height. These values were then plotted with the normalized height of the core (Figure 5-6). The profiles indicate faster invasion of aqueous phase at the top and bottom of the core. This is due to the fact that the top and bottom of the core are closer to surface area contacting the surfactant solution. Also, the profile is symmetrical indicating flow largely dominated by capillary forces with little contribution from gravity. The tapered region at the top and bottom of the profile becomes smaller with time as the imbibition front moves and invades the core radially. At later times the front is almost linear with small tapered region at the top and bottom.

Figure 5-7 shows the two dimensional saturation profiles as a contour plot. The color-bar shows the values of saturation, with the X axis being the radius (The value '0' being the center of the core) and Y axis is the normalized height of the core. Figure 5a shows the profile at initial stages (at 3.2 days). The boundaries of the core show the highest aqueous saturation with a gradual decrease towards the interior of the core. The saturation is highest at the corners because of accessibility to larger area in contact with the surfactant solution. Figure 5b shows profile after 13.5 days. The profiles are symmetrical with the least drained area being at the center of the core and away from the faces. At later times

(Figure 5-7c, 30.7 days) the nature of the profile remains the same, but it invades a larger region of the core and there is a higher aqueous phase saturation.

5.4 GRAVITY DOMINATED FLOW

In this section, static imbibition experiments performed on an outcrop rock, Estaillades Limestone, using a dilute wettability altering surfactant solution (0.25 wt%) are analyzed. For these experiments, the inverse bond number values are around 1 which indicate a flow where gravitational forces are also important (compared to the previous study of capillary dominated flow where inverse bond numbers are very high, ~250). This experimental data set hence provides a good opportunity to compare the recovery mechanisms for the two processes using numerical simulation. The surfactant formulation altered the wettability of initially strongly oil-wet core towards water-wet and lowered the IFT to 0.6 dynes/cm. Details about core preparation is described in section 3.2. The permeability of the core is 40 mD, porosity is 0.26 and initial oil saturation is 0.78. Experimental details are mentioned in Table 5-3.

Simulations are performed on cylindrical grid block system representing the core. All surfaces of the core (lateral, top and bottom) were open to imbibition and in contact with the imbibing fluid. The fluid surrounding the core contains surfactant and is static. Simulations were performed using a fine grid consisting of 10x70 radial cross vertical grid blocks with 10 grid blocks in the radial direction and 70 grid blocks in the vertical direction rendering radial and vertical grid block dimensions of 2 mm. The cylindrical coordinate system dimension theta was taken as 2π. Constant permeability, porosity and initial saturation is assigned to each grid-block (values in Table 5-3). Relative permeability, capillary pressure and residual saturation were altered to get a match with the experimental data. Residual oil saturation of 0.34 is used in the simulation validation case with the

experimental data (Figure 5-8). Initial water saturation (0.22) and residual water saturation are assumed to be same. Table 5-4 provides the values of relative permeability and capillary pressure parameters which give a match with the experimental data. Figure 5-8 shows the validation match using this data.

Figure 5-9 (a) to (d) show the oil phase velocity vectors at different points of time for the simulation match in Figure 5-8. Velocity vectors are aligned in vertical direction indicating strong co-current flows dominated by gravity forces. Observations during the imbibition experiment also confirm that majority of the oil is recovered from the top surface. (Figure 5-10). At the beginning (Figure 5-9 a), the velocity vectors with largest magnitude are at the outer periphery of the core. With increase in time (Figure 5-9 b-d), the velocity vector with largest magnitude move gradually towards the center of the core. Larger velocity is observed at the bottom of the core because of larger gravitational potential at the bottom.

Figure 5-11 shows the development of saturation profile with height. These values are obtained by taking the average of saturation values in grid blocks at the same radius. The profiles indicate faster invasion of aqueous phase at the bottom compared to the top. Maximum water invasion is at the bottom of the core and the saturation front gradually decreases from bottom with a slight aberration at the top. Water saturation at the top is more because of its proximity to area in contact with the surfactant solution. Similar CT scanned saturation profiles were observed by Mirzaei et al. (2013) in their dynamic imbibition experiments (Figure 5-17).

Figure 5-12 shows two dimensional saturation profiles as contour plots. The color bar shows the values of saturation, with the X axis being the radius (The value ‘0’ being the center of the core) and Y axis is the vertical dimensions of the core measured from bottom and normalized by the height of the core. Figure 5-12 (a) shows the profile at 14.7

days. Highest aqueous saturation can be seen at the bottom of the core with a gradual decrease in saturation upwards and then increase in saturation in the area adjacent to the top face of the core. Figure 5-12 (b) shows profile at 42.6 days. It can be inferred from this figure that at late times the saturation front moves vertically upwards sweeping the core after radially invading the core in the initial period. The profiles are symmetrical around the axis of the core (or the no flow boundary of the cylindrical core), but asymmetric at the top and bottom of the core. The volume of core near its axis and towards the top is invaded last by the surfactant solution.

5.5 SUMMARY

Oil recovery mechanisms in capillary dominated flow are analyzed by numerical simulation. To validate the input parameters, a simulation match is obtained with the experimental data for imbibition experiments on low permeability reservoir sandstone cores. Velocity profiles, one dimensional and two dimensional saturation profiles are plotted to better understand the process. Velocity profiles show counter-current imbibition as the dominant mechanism for oil recovery when capillary forces are high and gravitational forces can be neglected in comparison to capillary forces. In capillary dominated flows, the saturation profile is symmetrical at top and bottom of the core.

For gravity dominated imbibition process, simulation input parameters were validated by obtaining a recovery match with the experimental data for the Estaillades Limestone outcrop. The velocity vectors are vertical indicating co-current flows with the magnitude of the vectors decreasing radially inward. Saturation profiles show more invasion of aqueous phase at the bottom then at the top. The area of the core located around the axis towards the top is drained last by the imbibing fluid.

Parameter	Value
Diameter	2.5 cm
Length	5.5 cm
Permeability	0.24 mD
Porosity	0.133
S_{oi}	0.75
Oil Viscosity	2.3 cp
Oil-Water IFT	21.8 dynes/cm
Oil-Surf Sol IFT	3.7 dynes/cm

Table 5-1: Experimental data for validation with numerical simulation inputs for capillary dominated flow.

Parameter	Value
S_{or}	0.25
$k^0_{r,wet}$	0.2
$k^0_{r,nw}$	0.9
n_{wet}	4.5
n_{nw}	2.25
θ_0 (rad)	0
P_{CA}(Pa)	10342
P_{CB} (Pa)	30000000
n_c	1.3

Table 5-2: Simulation parameters for achieving the history match with the experimental data for capillary dominated flow

Parameter	Value
Diameter	3.81 cm
Length	14.6 cm
Permeability	40 mD
Porosity	0.26
S_{oi}	0.78
Oil Viscosity	13.5 cp
Oil-Water IFT	24.1 dynes/cm
Oil-Surf Sol IFT	0.6 dynes/cm

Table 5-3: Experimental data for capillary dominated flow validation case

Parameter	Value
S_{or}	0.34
$k^0_{r,wet}$	0.25
$k^0_{r,nw}$	0.9
n_{wet}	4
n_{nw}	2.25
θ_0 (rad)	0
P_{CA} (Pa)	10000
P_{CB} (Pa)	300000
n_c	1.5

Table 5-4: Simulation parameters used for obtaining a match with the experimental data

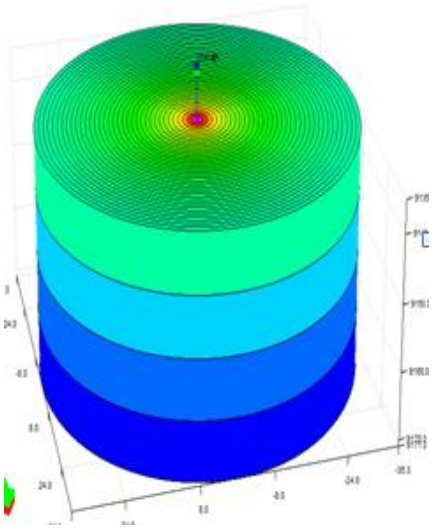

Figure 5-1: Representation of a cylindrical grid block system used in numerical simulations

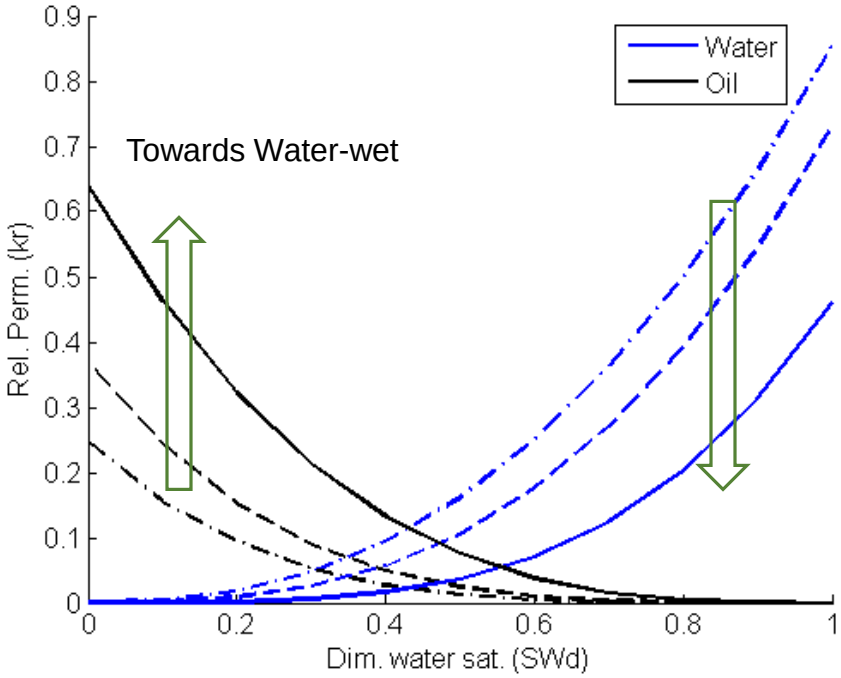

Figure 5-2: Simulator generated relative permeability curves for changing wettability.

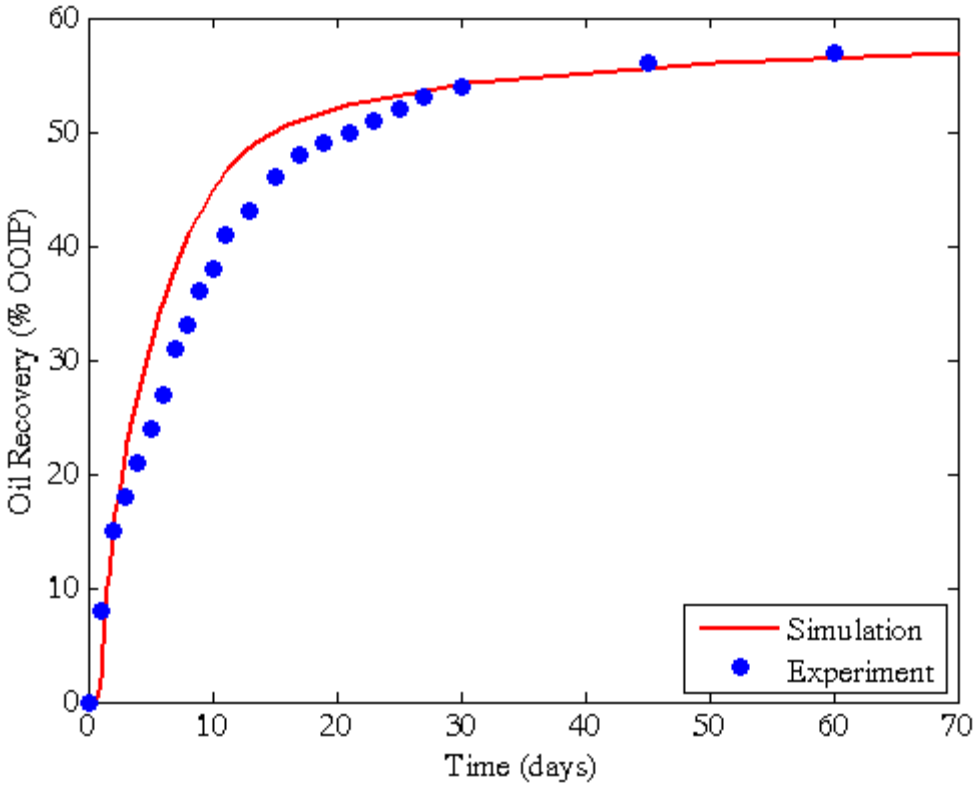

Figure 5-3: Validation match for capillary dominated flow: Imbibition experiment performed on low permeability sandstone reservoir cores.

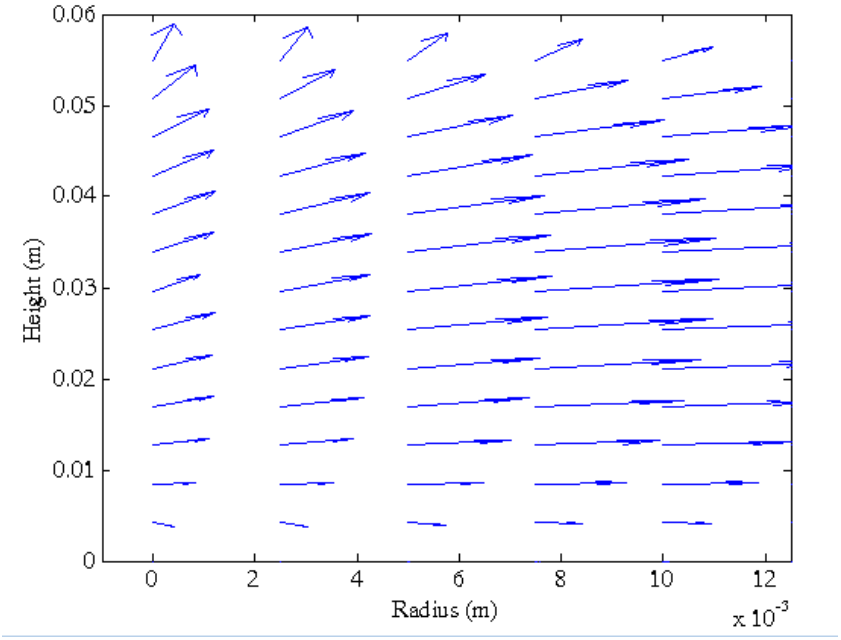

(a)

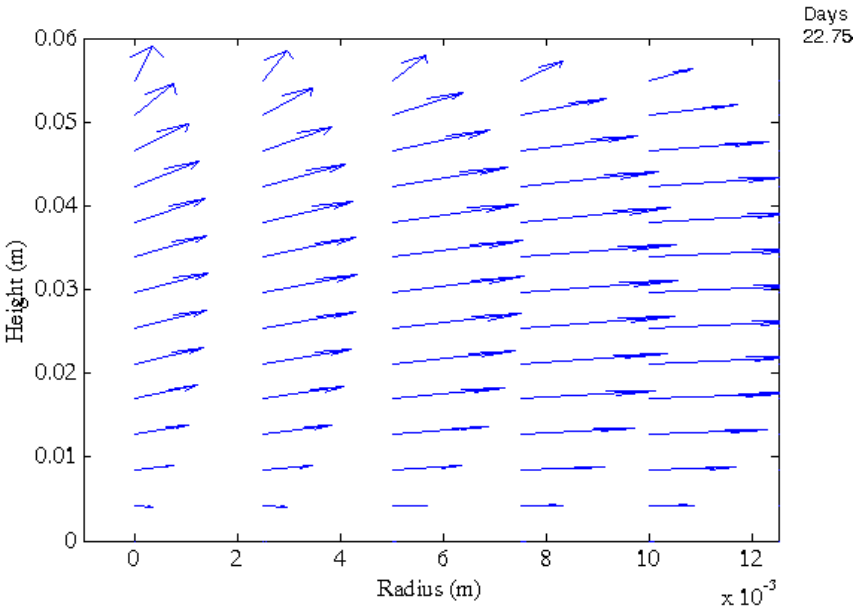

(b)

Figure 5-4 (a) and (b): Oil phase velocity vectors for surfactant induced capillary dominated flow in low permeability reservoir cores after 16.1 and 22.7 days respectively.

Figure 5-5: Oil recovery from lateral side of the core in capillary dominated flow experiments.

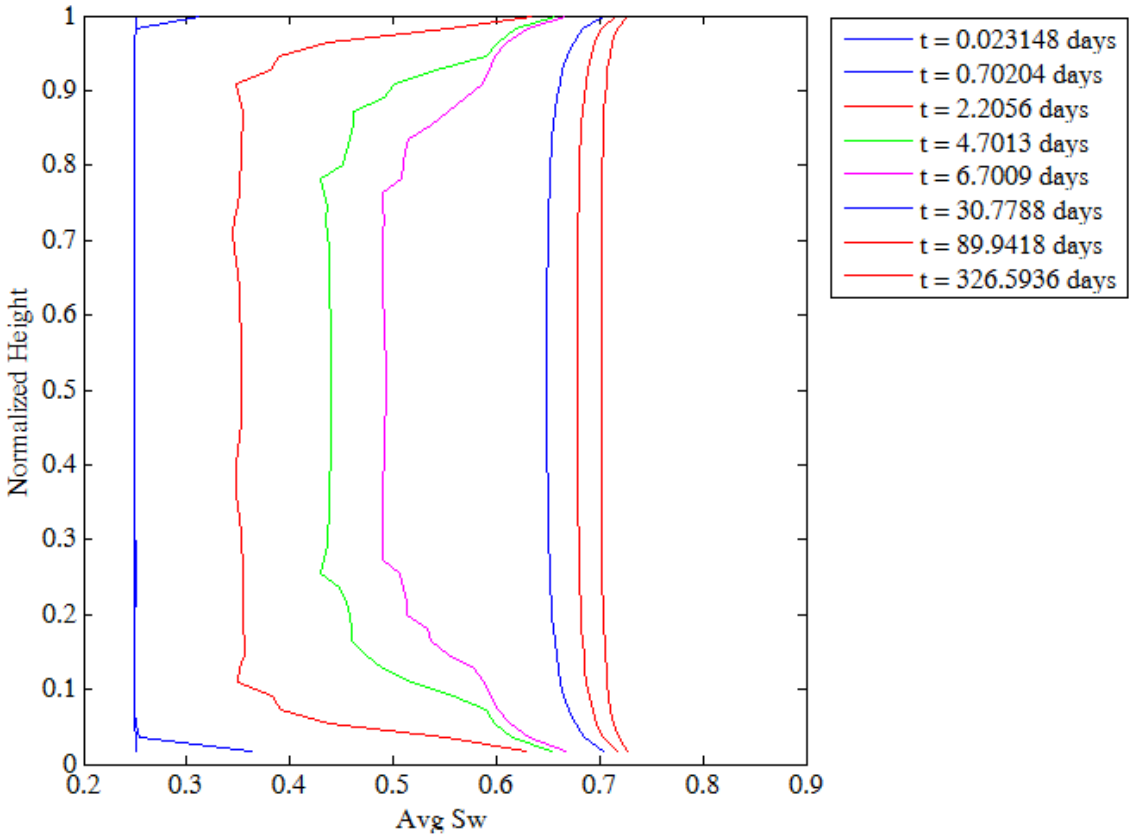

Figure 5-6: Saturation profiles averaged across core cross-section for capillary dominated flow

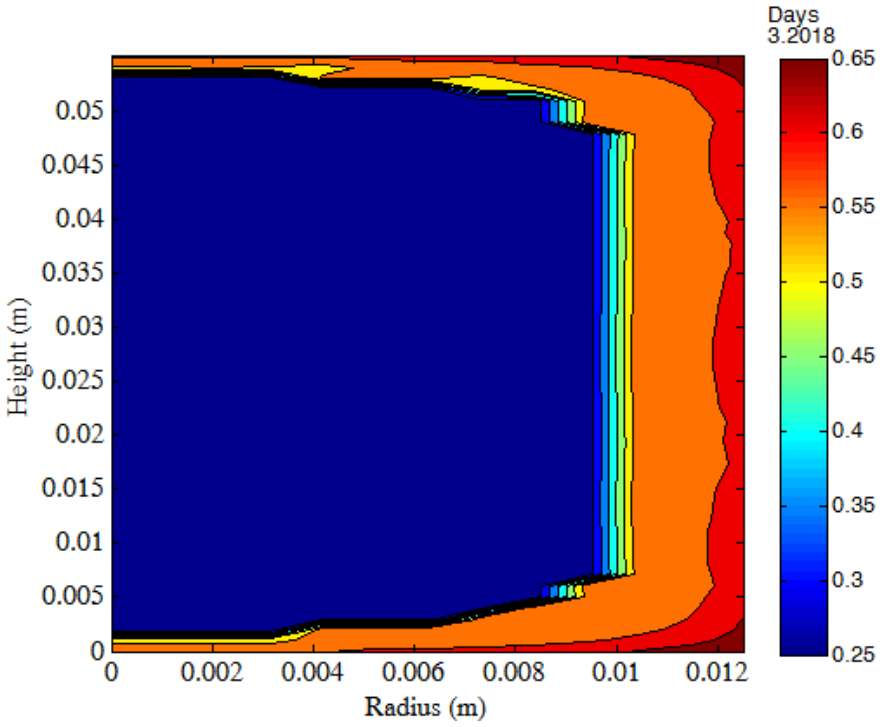
Days
3.2018
0.65
0.6
0.55
0.5
0.45
0.4
0.35
0.3
0.25
0.05
0.045
0.04
0.035
0.03
0.025
0.02
0.015
0.01
0.005
0
Height (m)
0
0.002
0.004
0.006
0.008
0.01
0.012
Radius (m)

(a)

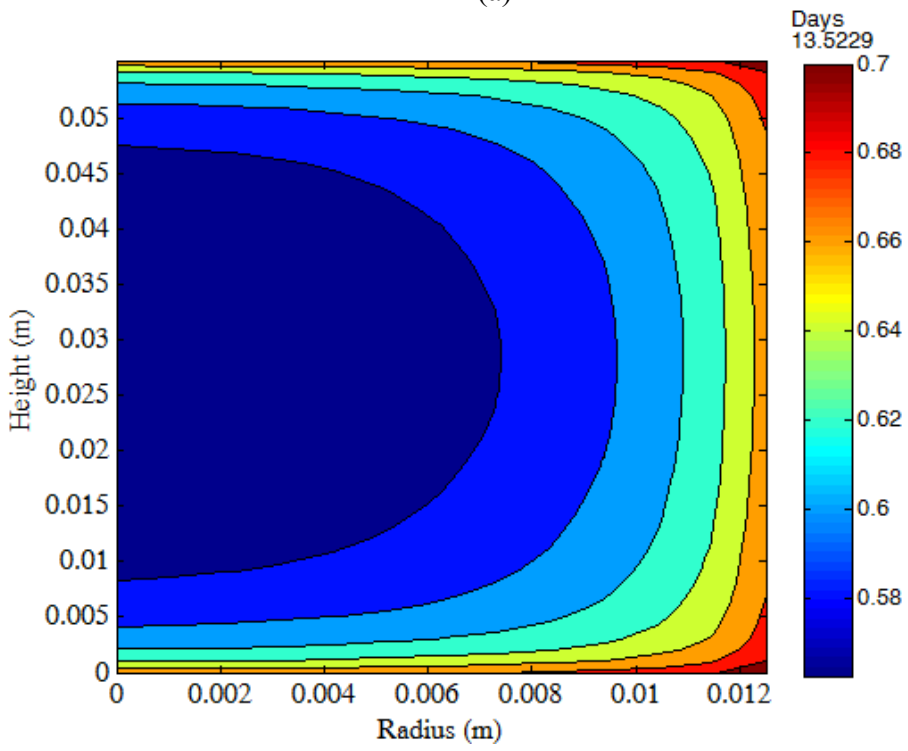
Days
13.5229
0.7
0.68
0.66
0.64
0.62
0.6
0.58
0.05
0.045
0.04
0.035
0.03
0.025
0.02
0.015
0.01
0.005
0
Height (m)
0
0.002
0.004
0.006
0.008
0.01
0.012
Radius (m)

(b)

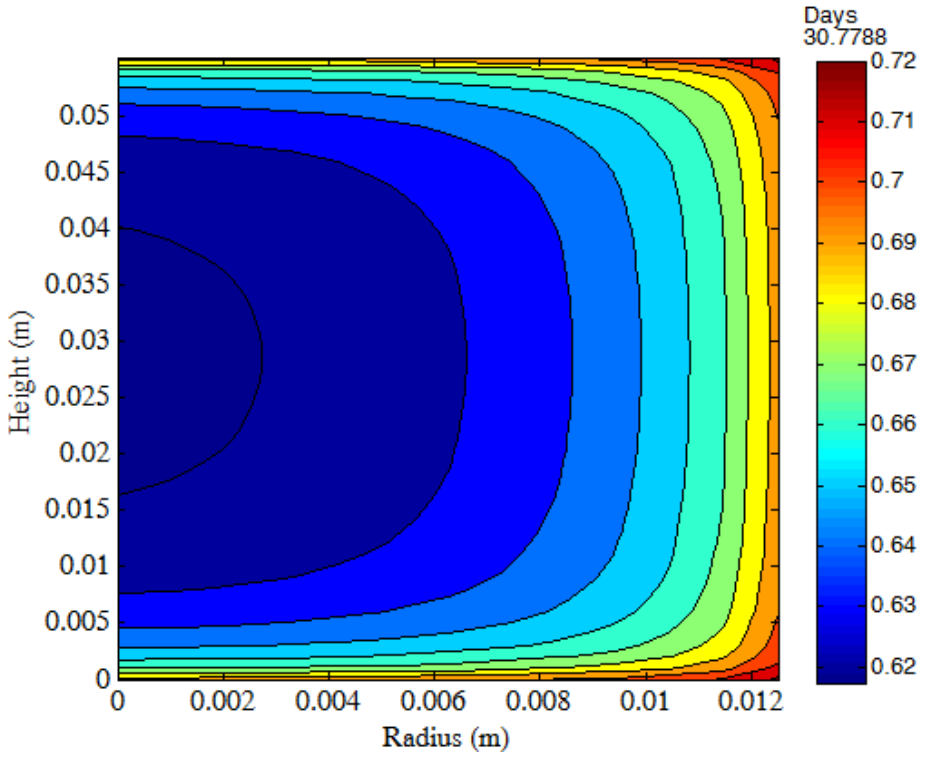

(c)

Figure 5-7 (a), (b) and (c): Saturation profiles after 3.2, 13.5 and 30.7 days respectively. There is gradual invasion of the core in the radial direction, the profiles indicate strong counter-current flow.

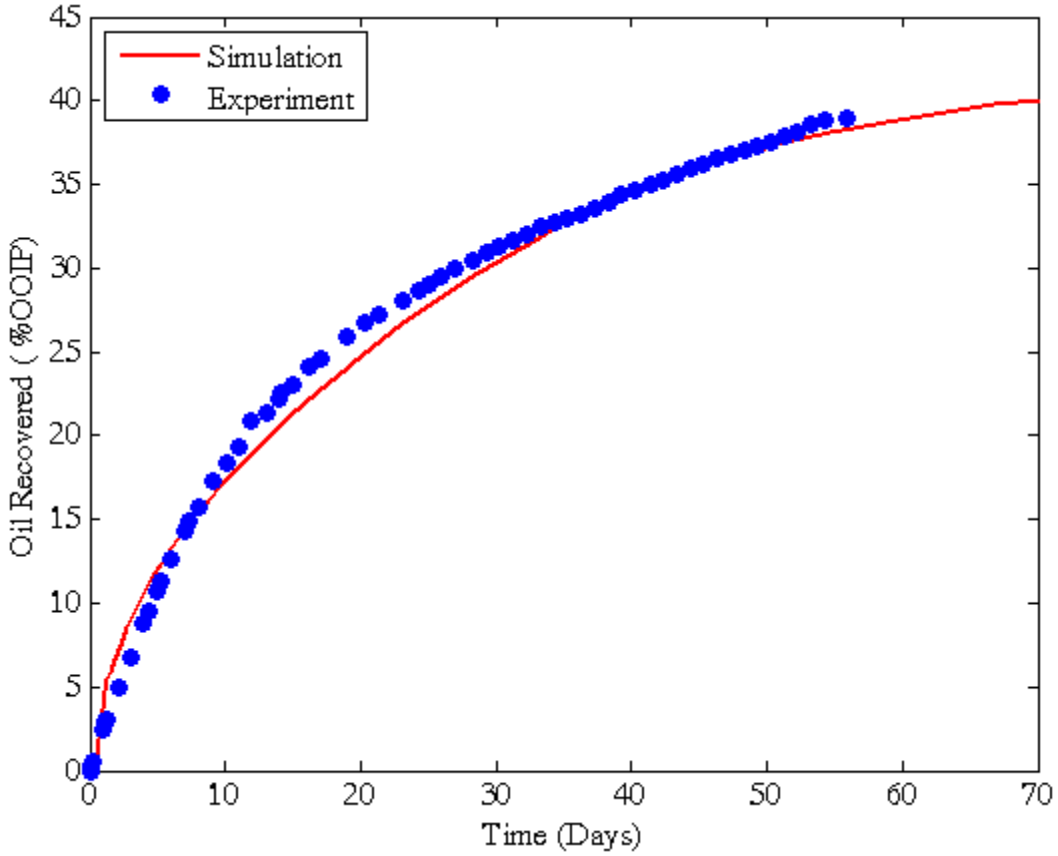

Figure 5-8: Validation match for Estaillades Limestone experiment (Diameter: 1.5 inch, Height: 5.75 inch) using the parameters mentioned in Table 5-3 and 5-4

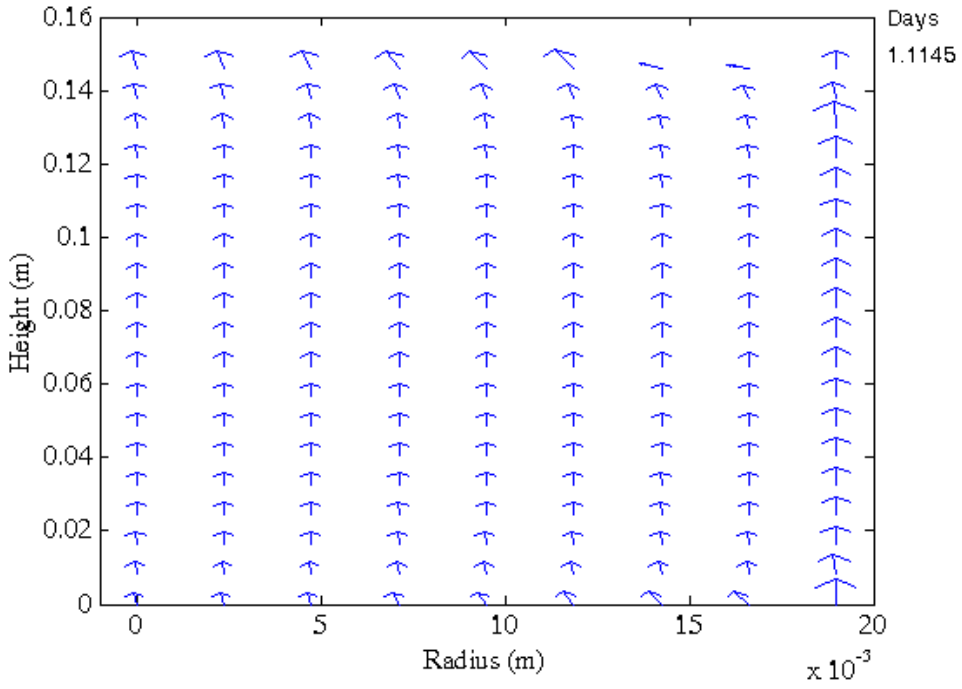
Days
1.1145
Height (m)
0.16
0.14
0.12
0.1
0.08
0.06
0.04
0.02
0
0
5
10
15
20
Radius (m)
x 10^-3

(a)

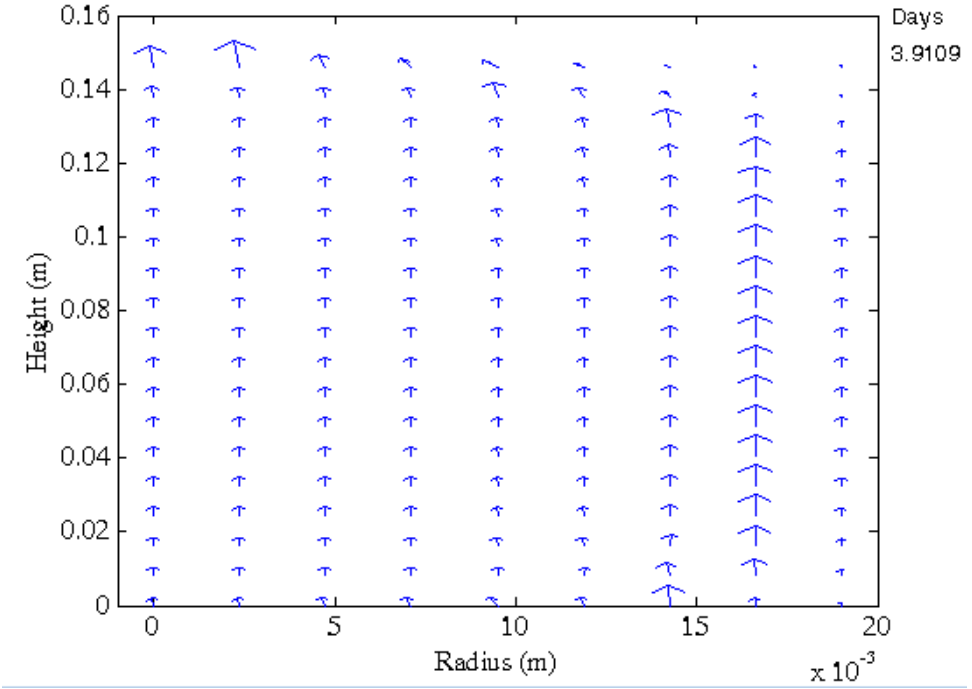
Days
3.9109
Height (m)
0.16
0.14
0.12
0.1
0.08
0.06
0.04
0.02
0
0
5
10
15
20
Radius (m)
x 10^-3

(b)

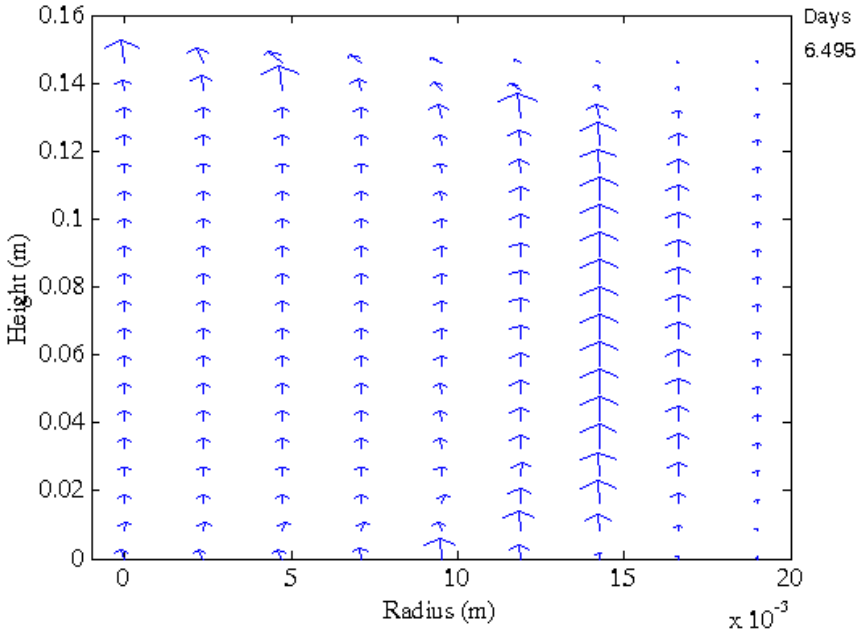

(c)

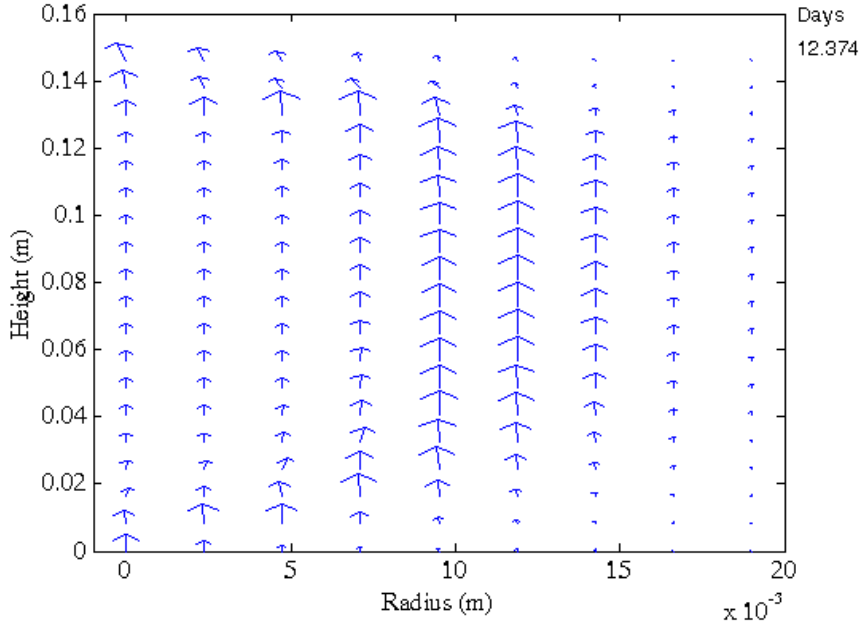

(d)

Figure 5-9 (a), (b), (c) and (d): Oil phase velocity vectors after 1.1, 3.9, 6.4 and 12.3 days. The vectors are resultant of the vertical and radial flow. A gradual increase in the vector arrows radially inward indicates the movement of the imbibition front radially inward as demonstrated by the saturation profile.

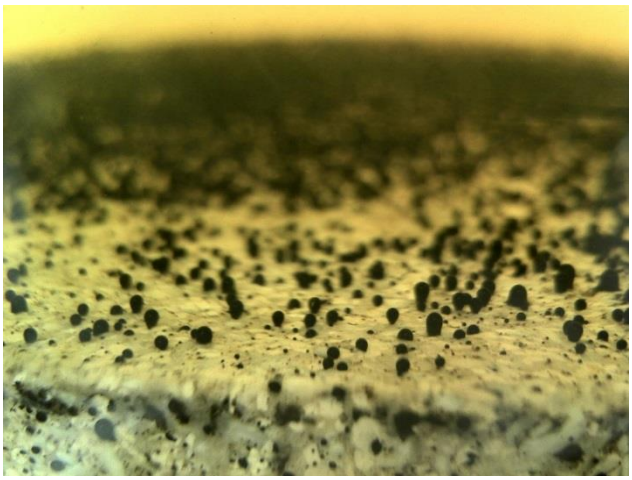

Figure 5-10: Top surface of the Estaillades Limestone Core. Majority of the oil is recovered from top surface.

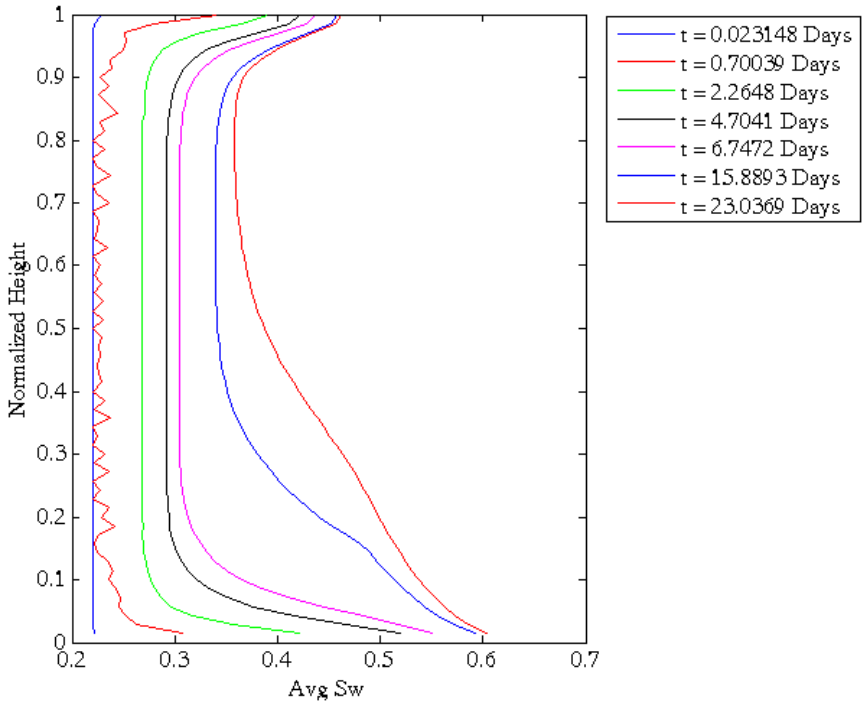

Figure 5-11: Saturation profiles averaged across core cross section with increasing time.

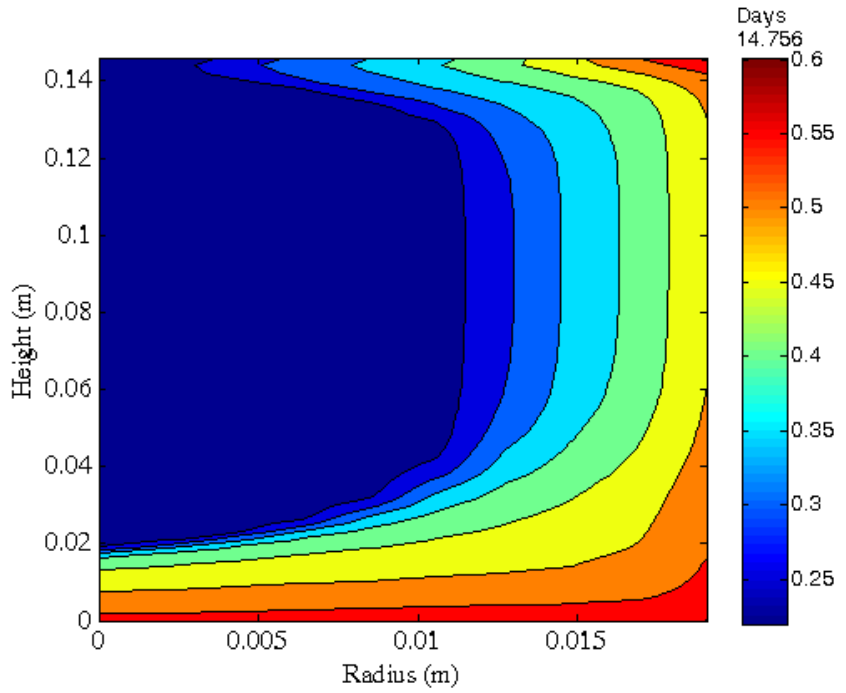

(a)

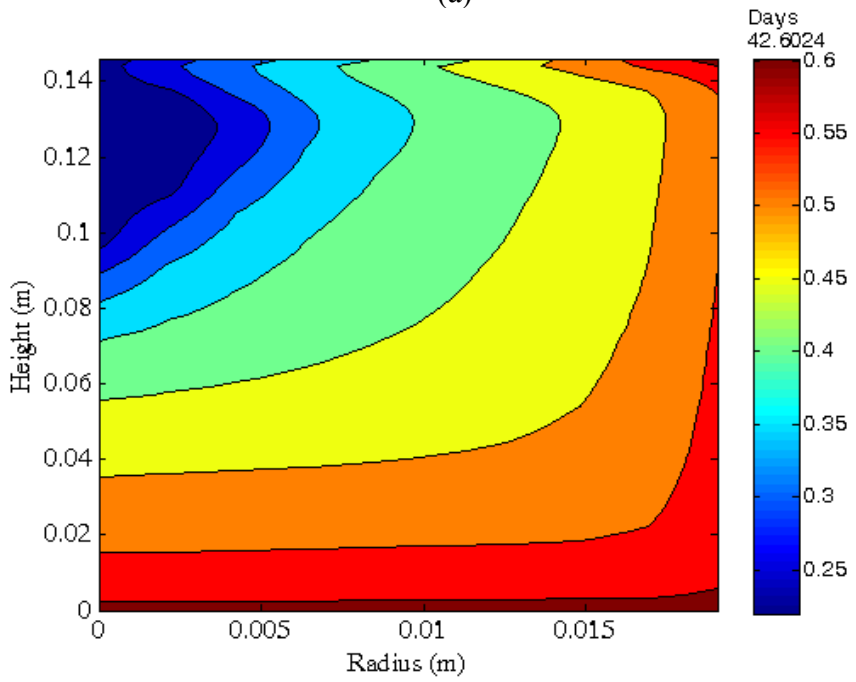

(b)

Figure 5-12 (a) and (b): Saturation front after 14.7 and 42.6 days. The bottom part of the core is imbibed faster than top because of higher gravity potential at bottom.

Chapter 6: Scaling Analysis

Oil recovery through imbibition processes is slow and it has been of particular interest among researchers to study scaling of these processes with regard to feasibility of oil recovery rate at larger scales as well as for optimization of these processes. Scaling rules facilitate studying of imbibition processes with increased understanding of the physics and the first order mechanisms dictating the process. They are an important means to predict recovery in larger dimension matrix blocks in a matrix-fracture system. They can serve as an effective tool to determine the sensitivity with different parameters like absolute and relative permeability, porosity, viscosity etc.

Using the scaling relationships, recovery behavior for a large reservoir matrix block can be estimated from an imbibition test on a small core sample. Many researcher's (Mattax and Kyte 1962, Hagoort et al. 1980, Schechter et al. 1994, Li and Horne 2002 & 2006, Schmidt et al. 2012) have proposed dimensionless time for scaling of experimental data. Figure 2-17 shows a plot where the data from different experiment sets collapses to a single curve indicating a good correlation with the dimensionless time.

In this chapter different scaling rules are analyzed and their applicability is tested with respect to the surfactant aided gravity dominated imbibition experiments. Main focus here is to determine the relationship with respect to time and dimensions of the system. To this effect a new scaling function is proposed with no fitting parameters involved. It is shown that the new space time scaling function correlates the data well at early times for initially oil-wet surfactant aided gravity driven processes with the same boundary conditions, rock, fluids and varying dimensions.

6.1 ANALYTICAL MODELS FOR GRAVITY DOMINATED FLOW

In this section, analytical models developed at The University of Texas at Austin in studies by Mirzaei et al. (2013) and Chen et al. (2014) in communication with Dr. Pope will be presented and tested for their ability to scale the data with height and diameter. First a description and assumptions of the models will be presented followed by validation of models against experimental data from this study. The model is based on profile of the imbibition front (Figure 6-1). In Figure 6-1 the dashed line at the center represents the no flow boundary because of symmetry of the cylindrical core. The assumptions, key steps in derivation and main equations are presented in the following sections.

6.1.1 Assumptions

1. Incompressible oil and water which implies volume of water entering the core is equal to volume of oil produced.
2. The IFT of the oil-brine system is sufficiently low so that capillary forces are negligible in comparison to buoyancy forces. As a consequence of this gravity is the only driving force for recovery.
3. The aqueous phase containing the surfactant enters only in the x direction and oil is displaced only in the z direction.
4. The imbibition process leads to the development of the imbibition shock front as shown in Figure 6-1. Behind the front (region to the left of the front) there is aqueous phase at residual oil saturation and ahead of the front oil is at initial oil saturation.
5. Homogeneous distribution of porosity and permeability as well as uniform saturation throughout the core.
6. The aqueous phase velocity at the imbibition front changes linearly with height z (Figure 6-1) before imbibition front reaches the center of the core ($x_{wb} =< R$). When

water front at the bottom of the core advances beyond the center the velocity becomes same everywhere.

6.1.2 Important Equations and Derivation Steps

Based on the imbibition profile in Figure 6-1, for $x_{wb} =< R$ oil recovery can be estimated as:

$$\eta = \frac{\Delta V_0}{V_o} = \frac{x_{wb}}{R} - \frac{1}{3}\left(\frac{x_{wb}}{R}\right)^2 \tag{6-1}$$

where η is oil recovery in terms of fraction of recoverable oil, V_o is the recoverable volume of oil in the core, ΔV_o is the change in volume of oil or the volume of oil recovered, x_{wb} is the position of the front at the base of the core and R is radius of the core.

Important derivation steps and results are mentioned below for $x_{wb} =< R$ or before the imbibition front sees the no flow boundary at the radius. The frontal velocity at height z is given by

$$v_w(z) = v_{wb}(1 - \frac{z}{H}) \tag{6-2}$$

where v_{wb} is the water phase interstitial velocity at the bottom of the core. The imbibiton rate of surfactant solution into the core between z and z + dz is $\phi^* v_w(2\pi R)dz$ where $\phi^* = \phi(S_{oi} - S_{or})$. The flow rate of oil at any given height is the cumulative flow from the bottom to that height. The fluids being incompressible, the cumulative oil flow rate at a given height z, can be expressed through mass balance as:

$$Q_o(z) = \int_0^z (\phi^* v_w 2\pi R) dz \tag{6-3}$$

Also, oil flow rate (Q_o) is given by Darcy's law as:

$$Q_o(z) = \frac{k k_{ro}}{\mu_o} A \frac{d\Phi_o}{dz} \tag{6-4}$$

where A is area open to flow, which as per the assumed imbibition profile can be estimated as:

$$A = \pi \left[R - x_{wb}(1 - \frac{z}{H}) \right]^2 \tag{6-5}$$

From the above equations, oil phase pressure drop over the vertical height H can be given as:

$$\int_0^H d\Phi_o = \frac{\mu_o \phi^* H^2 v_{wb}}{k k_{ro}} (\frac{2}{3R} + \frac{1}{2} \frac{x_{wb}}{R^2}) \tag{6-6}$$

Similarly we can compute pressure drop across the water phase

$$v_w(z) = -\frac{k k_{rw}}{\phi^* \mu_w} \frac{d\Phi_w}{dx} \tag{6-7}$$

$$\int_0^{x_{wb}} d\Phi_w = \frac{v_{wb} \mu_w \phi^*}{k k_{rw}} x_{wb} \tag{6-8}$$

It is assumed that capillary forces are negligible and can be ignored, hence the combined pressure drop of water and oil phases at a point at the base of the cylindrical geometry (Figure 6-1) should be equal to $\Delta \rho g H$ which is given by the following equation:

$$\int_0^{x_{fb}} d\Phi_w + \int_0^{H} d\Phi_o = \Delta\rho g H \tag{6-9}$$

Based on the assumptions listed before, ratio of average pressure drop between water and oil phase can be given by Equation 6-10 (Mirzaei et al. 2013) for a rectangular block.

$$\frac{\Delta P_w^v}{\Delta P_o^v} = \frac{x_{fb} R}{H^2} \frac{\frac{k_{ro}}{\mu_o}}{\frac{k_{rw}}{\mu_w}} \tag{6-10}$$

It can be inferred from this equation that there can be cases where the pressure drop in one phase is negligible in comparison to the other phase based on the geometry and the mobility of the phases. Even after the effect of geometry is considered, the difficulty in estimating the mobility ratio leads to uncertainty in determining the ratio of pressure drops across the two phases. Hence, three cases are described in the subsequent sections. In the first case only pressure drop across water phase is considered, the second case considers pressure drop only in the oil phase and for the final case pressure drop is considered in both the phases. The different cases are analyzed to check their ability to predict recovery with changing dimensions after a base case match is obtained with reasonable values of the model fitting parameter. The model parameters for different cases are mentioned as well.

6.1.3 Pressure Drop across Water Phase (Case 1)

Assuming there is no significant pressure drop across oil phase (low values of aqueous phase mobility or very large diameter compared to height of the core), Equation 6-9 can be modified to account for all the gravitational driving potential dissipated in the water phase. In such a scenario the model is given by Equations 6-11 to 6-13. The

relationship between imbibition front position at base of the core and the dimensionless time is given by:

$$\frac{x_{wb}}{R} = \sqrt{t_D} \tag{6-11}$$

In this case the oil recovery is given by:

$$\eta = \frac{\Delta V_0}{V_o} = \frac{x_{wb}}{R} - \frac{1}{3}\left(\frac{x_{wb}}{R}\right)^2 = \sqrt{t_D} - \frac{1}{3}t_D \tag{6-12}$$

$$t_D = \frac{8kk_{rw}\Delta\rho gH}{\mu_w \phi^* D^2}t \tag{6-13}$$

In this model k_{rw} or $\frac{k_{rw}}{\mu_w}$ (mobility of water phase) is the fitting parameter. For the base case (Estaillades Limestone) a match was obtained for the imbibition experiment on core with diameter 1.5 inch and height 5.75 inch. Table 6-1 lists the model parameters for the match. Figures 6-2 shows the scaling with diameter. Solid lines represent the curves generated through the model (Equations 6-12, 6-13) and points represent the experimental data. A good match is obtained for cores with the same height and different diameters. Figure 6-3 shows comparison with height with the base case remaining the same as mentioned earlier. The model predicts an increase in oil recovery with increasing height which is contrary to the experimental observations. This is a major limitation of this model. Next, a comparison (Figure 6-4) was made for the Texas Cream Limestone data where diameter and length of the core were both changed to see the combined effect of these parameters on recovery prediction. The model was matched with experimental data for the core with 4 inch diameter and 5.75 inch height. The model recovery was then predicted for

the experiment with 1.5 inch diameter and 11.5 inch height. The model predicted recoveries two fold greater than the experimental data primarily because of the increased height which lead to increase in oil recovery,

This model gives an accurate prediction with the change in diameter, but with an increase in height it predicts higher recovery while the experimental data shows decrease in oil recovery. Hence, the model fails to predict oil recovery when there is a change in both height and diameter. As per the assumption that the aqueous phase enters only in x direction, an increase in diameter will result in more pressure loss in the aqueous phase and hence the validity of the assumption in this model holds better with increase in diameter. This is believed to be the reason for match obtained with the change in diameter.

6.1.4 Pressure Drop across Oil Phase (Case 2)

Large values of aqueous phase mobility (or high values of mobility ratio) and large height compared to the diameter of the core may lead to pressure drop in the aqueous phase being negligible in comparison to pressure drop across the oil phase. In this scenario the relationship between imbibition front position at base of the core and the dimensionless time is given by (Chen et al. 2014):

$$\frac{x_{wb}}{R} = \sqrt{t_D + \frac{16}{9}} - \frac{4}{3} \tag{6-14}$$

The corresponding oil recovery as per the imbibition profile is given by:

$$\eta = \frac{\Delta V_0}{V_o} = \frac{x_{wb}}{R} - \frac{1}{3}\left(\frac{x_{wb}}{R}\right)^2 = \frac{11}{3}\sqrt{t_D + \frac{16}{9}} - \frac{t_D}{3} - \frac{68}{27} \tag{6-15}$$

$$t_D = \frac{4kk_{ro}\Delta\rho g}{\mu_0 \phi^* H} t \tag{6-16}$$

Figures 6-5, 6-6 and 6-7 give a comparison for oil recovery at different scales using this model. The model fitting parameter is the oil phase relative permeability k_{ro} or the mobility of the oil phase $\frac{k_{ro}}{\mu_o}$ if there is uncertainty in estimation of oil phase viscosity due to emulsion formation. First a match is obtained by tuning the model fitting parameter k_{ro} for the Estaillades Limestone dataset with diameter 1.5 inch and height 5.75 inch. Details of all the values for the model variables is provided in Table 6-3. Figure 6-5 shows scaling comparison with diameter of the core. The diameter of the core is increased to 4 inch whereas the height remains the same compared to the base case. Only change made in the model is that of the diameter value and all other values remain same including the fitting parameter. The model is insensitive to changes in diameter hence the curves overlap or no change is observed in the model generated curve. Figure 6-6 shows scaling comparison with height. The height of the core is increased to twice (11.5 inch) the height of the base case and diameter remains same as the base case (1.5 inch). Only height is changed in the model parameters mentioned in Table 6-3 and rest all other values remain same. A good match of experimental data is observed with increase in height. Next, we compare data from Estaillades Limestone where there is deviation of length and height from the base case. Table 6-5 shows all the model parameter values including the fitting parameter k_{ro}. The model is first matched with the base case (diameter: 4 inch, height: 5.75 inch) and then prediction is done for core with diameter 1.5 inch and height 11.5 inch. The model predict a decrease in recovery because of increased height which is correctly captured by the model but the effect of decrease in diameter which would have increased recovery is not captured hence the overall model recovery is lower but the experimental data gives higher recovery.

This model gives good prediction with change in height but is insensitive to change in diameter. A reason for that can be due to the fact that during derivation of this model a

Taylor series expansion is made which is valid for (x_{wb} << R) hence by making this assumption we are effectively neglecting the effect of diameter. As a result of this the model fails to predict oil recovery when there is change in both height and diameter. As per the assumption that the oil is displaced only in z direction, an increase in height will result in more pressure loss in the oil phase and hence the validity of the assumption (pressure drop only in oil phase) in this model holds better with increase in height. This is believed to be the reason for match obtained with change in height of the core while the diameter remains the same.

6.1.5 Pressure Drop across Water and Oil Phases (Case 3)

For a more comprehensive analysis pressure drop across oil as well as water phase was considered in Equation 6-9. In this scenario the relationship between the dimensionless time and the imbibition front position at base of the core is given by:

$$t_D = \frac{1}{4}\left[\left(\frac{2}{M^o H'^2}+1\right)x_{wb}'^2 + \frac{8}{3}x_{wb}'\right] \tag{6-17}$$

Alternatively, equation 6-17 can be expressed as:

$$x_{wb}' = \frac{x_{wb}}{R} = \frac{\sqrt{\frac{64}{9}+16\left(\frac{2}{M^0 H'^2}+1\right)t_D}-\frac{8}{3}}{2\left(\frac{2}{M^0 H'^2}+1\right)} \tag{6-18}$$

$$M^o = \frac{k_{rw}{}^o \mu_o}{k_{ro}{}^o \mu_w} \qquad x_{wb}' = \frac{x_{wb}}{R} \qquad H' = \frac{H}{R} \tag{6-19}$$

$$t_d \equiv \frac{k k_{ro}{}^o \Delta\rho g}{\mu_o \varphi^* H} t \tag{6-20}$$

The oil recovery is then given by:

$$\eta = \frac{\Delta V_0}{V_o} = \frac{x_{wb}}{R} - \frac{1}{3}\left(\frac{x_{wb}}{R}\right)^2 \tag{6-21}$$

Figures 6-8, 6-9, 6-10 show the experimental and model curve comparison for this case. The fitting parameters for this scaling model are relative permeability of the oil k_{ro} (or $\frac{k_{ro}}{\mu_o}$) and water phases k_{rw} (or $\frac{k_{rw}}{\mu_w}$). Figures 6-8 and 6-9 give comparison with change in diameter and height of the cores for Estaillades Limestone data. The base case model match is established for core with diameter 1.5 inch and height 5.75 inch. The model parameters including the values of the model fitting parameter are mentioned in Table 6-5. Figure 6-8 shows the scaling comparison with diameter. Only the value of diameter is changed in the model parameters used for matching the base case. The model shows reduced recovery with increase in diameter which is in line with the experimental observation, but the model does not match the experimental data. The effect of oil recovery reduction due to decrease in diameter is not as pronounced as observed in experimental data. Figure 6-9 shows scaling comparison with increase in height over the base case (diameter of both curves remain the same), the model curve is generated by just changing the value of height from the model match parameters of base case mentioned in Table 6-5. A good model prediction with height is obtained compared to the experimental data, the model generated curves almost overlaps the experimental data for the initial part and deviates a bit at later times. The model generated recovery is then compared with the Texas Cream Limestone data Figure (6-10) where diameter and height both are changed in the experimental data. A base case model match is established for core with diameter 4 inch and height 5.75 inch. Table 6-6 shows the model parameter including the relative permeability values. On changing the

diameter and height of the core as per the second experiment (diameter: 1.5 inch, Height: 11.5 inch) the model predicted lower recovery compared to the experimentally observed higher recovery from the base curve.

One of the major positives of this model is that it predicts the correct trend with change in height and diameter of the core. Keeping the diameter of the core same, increase in height leads to decrease in recovery. An increase in diameter leads to decrease in oil recovery when height of the core is kept constant. Model match with the experimental recovery curve is much better for the height compared to the diameter. A reason for that can be due to the fact that during derivation for the pressure drop in oil phase a Taylor series expansion is made which is valid for ($x_{wb} << R$) hence by making this assumption we are effectively neglecting the effect of diameter. As a result of this the model fails to predict oil recovery when there is change in both height and diameter which is the case for the Texas Cream Limestone data. There is less sensitivity in the model to the diameter hence the predicted model recovery for the Texas Cream data shows opposite trend (predicts decrease in oil recovery compared to experimentally observed increase in recovery). Relative contribution of the diameter and height is not captured in the model as the recovery predicted is lower whereas experimentally observed recovery is higher. Overall, this model is better than the previous two models as it captures the correct recovery trends with diameter and height and captures sensitivity in oil recovery with variation in height fairly accurately.

6.2 Scaling with Space and Time

In this section, an attempt is made to determine the scaling with the two most critical parameters space (or the dimensions of the core) and time. These two parameters are important for estimating recovery in larger systems based on laboratory experimental data.

First, scaling of data with the conventional shape factor (Equation 6-23) is analyzed which results in scattering of data (Figure 6-12) or non-conformance with the shape factor. This shape factor is applied in several scaling groups including Ma et al. 1997, Li and Horne (2002, 2006), Zhou and Kovscek (2002) to account for changes in oil recovery with changes in dimensions and boundary conditions hence these scaling groups are ineffective to account for recovery with changing dimensions for the system studied here. Also, Figure 6-12 is plotted with logarithmic time scale on the X-axis which shows a concave upwards curvature.

New space time scaling functions are proposed and tested for surfactant aided gravity dominated processes. The scaling functions are tested with the static and dynamic imbibition experimental data in this study as well as with data from Mirzaei et al. (2013) where dynamic imbibition experiments were performed on oil saturated cores using surfactant solutions which result in ultra-low oil-water IFT (gravity dominated process).

It should be noted that as observed in the analytical models part of this chapter (section 6.1) oil recovery can be expressed as a function of dimensionless time (Equation 6-22). The scaling functions tested in this study are part of the dimensionless time. The complete expression for the dimensionless time will include the scaling function combined with the mobility terms, absolute permeability, porosity, density difference and constants like acceleration due to gravity. In this study an attempt is made to understand the combined effect of time and dimensions of the core. The relationship of oil recovery with diameter and height of the core separately cannot be drawn from the scaling function since oil recovery is an unknown function of dimensionless time (Equation 6-22) and scaling function is a part of the dimensionless time as stated earlier.

$$R = f(t_D) \tag{6-22}$$

where R is oil recovery and t_D is dimensionless time.

6.2.1 Scaling with Conventional Shape Factor

In oil production from fractured reservoirs, systems with different matrix sizes, shapes and boundary conditions give different mass-transfer rates between fractures and rock matrix. The smaller the ratio of volume to open surface area, the faster the imbibition rate. On the basis of the work by Warren and Root (1963) and Kazemi et al. (1976), a critical length L_c was proposed by Kazemi et al. (1992) to compensate for the effect of sample geometry. The critical length (L_c) is given as:

$$L_C = \sqrt{\frac{V_b}{\sum_1^n \frac{A_i}{S_{A_i}}}} \tag{6-23}$$

where V_b is bulk volume of the matrix, A_i the area open to imbibition in the ith direction, S_{A_i} is the distance from A_i to the no flow boundary, and n is the total number of surfaces open to imbibition. The shape factor is related to the critical length as:

$$F_s = \frac{1}{L_c^2} \tag{6-24}$$

This shape factor (or inverse squared critical length) is used in many scaling groups to account for change in oil recovery with changes in dimensions of the matrix block and under different boundary conditions. Ma and Morrow (1997) checked the applicability of the shape factor for water imbibition in water-wet media with cores of different dimensions and boundary conditions. Figure 6-11 shows strong correlation of data plotted from three studies: Mattax and Kyte, (1962), Zhang et al. (1996) and Haman and Vidal (1986) with the dimensionless time t_D which incorporates the shape factor.

To check the applicability of this shape factor, the Estaillades Limestone experimental data from this study was plotted with $\frac{t}{L_c^2}$ where t is time and L_c is the critical length. Figure 6-12 shows the scaling of data for different dimension cores with the same rock fluid system, details of which are given in Table 4-6. The Y axis is oil recovery in terms of fraction of oil recoverable and the X axis is time plotted in logarithmic scale. The data does not correlate indicating the need for better space-time scaling functions.

6.2.2 New Scaling Functions

New scaling functions (SF) are tested in this study which incorporate the dimensions of the core and time. The scaling functions are given by:

$$SF_1 = \frac{t}{DH} \tag{6-25}$$

$$SF_2 = \frac{t}{D^2 \mathrm{H}} \tag{6-26}$$

where D is the diameter of the core or the dimension perpendicular to the fracture and H is the height of the core or the dimension parallel to the fracture. The scaling functions do not have any fitting parameter and their ability to correlate the data with same boundary conditions, rock and fluids but with different dimensions is analyzed in this work. Scaling function 2 (Equation 6-26) is the combination of analytical model cases 1 and 2 (Equation 6-13 and 6-20) which were consistent for diameter and height scaling respectively. (Figures 6-13, 6-14, 6-15) are the different experimental datasets plotted with the variations of the space time scaling functions. For scaling function 2 all datasets are plotted with square root of the scaling function.

Static imbibition data for Estaillades Limestone and Texas Cream Limestone cores is plotted with the new scaling functions in Figure 6-13 (a, b & c). The data from the five experiments with varying diameter and height of the cores correlates well for the initial time with a slight scatter at later times for scaling function 1. For data plotted with square root of scaling function 2 better correlation is obtained at late times. The scaling functions are also validated with the dynamic imbibition experiments. Figure 6-14 a, b and c shows the scaling with the dynamic imbibition recovery for the Estaillades limestone rock. Experimental parameters are mentioned in Table 4-9. In this data set the two experiments are performed on cores with different diameter, permeability and porosity. To take the change of permeability and porosity into account a factor is introduced in the scaling function. The modified scaling function (MSF) is then given by:

$$MSF_1 = \sqrt{\frac{k}{\phi}}.SF_1 \tag{6-27}$$

$$MSF_2 = \sqrt{\frac{k}{\phi}}.SF_2 \tag{6-28}$$

The dynamic imbibition data is plotted with the modified scaling functions. A good correlation is obtained with the modified scaling function 1. Modified scaling function 2 does not give good correlation with the data.

Dynamic imbibition data from Mirzaei et al. (2013) is also plotted with the new scaling functions. Figure 6-15 a, b and c shows the different cases plotted with the scaling functions. Scaling function 1 gives reasonably better correlation compared to scaling function 2.

The experimental data sets show that oil recovery decreases with increase in height and diameter of the core. The new scaling functions capture this trend. The experimental

datasets show that the scaling function 1 can be applied to both static and dynamic imbibition cases at early times. A possible reason for this is that both static and dynamic imbibition cases for surfactant aided gravity dominated cases result in same nature of the imbibition profile. Mirzaei et al. (2013) captured this profile using CT scanner for the dynamic imbibition cases (Figure 6-16). Simulations were performed for the static imbibition experiments for gravity dominated flow where IFT is lowered (0.6 dyne/cm) as well as wettability is altered. The saturation profile obtained is shown in Figure 6-17. The two profiles are very similar except that for static imbibition experiments there is some recovery from the top as well. This is due to the fact that there is open flow boundary at top in static imbibition experiments and the surfactant formulation is wettability altering which leads to initial recovery at top face. In both the cases recovery is faster at the bottom and then tapers up as the gravity potential driving the flow is largest at bottom and then gradually reduces from bottom to top of the core.

In comparison to the conventional scaling group which is given by Equation 6-23, the new scaling function 1 in a way mathematically captures the retardation process compared to the case of water imbibition in a water-wet media which is a faster process. In the experiments performed here wettability is altered towards water-wet from oil-wet which leads to delay in oil recovery or making the process slower. Also the IFT is reduced which makes the process gravity dominated compared to the capillary dominated process of water imbibition in a water-wet media in which recovery rate is highly dependent on magnitude of capillary forces (or the permeability of the rock). The new scaling function 1 defined here can be obtained from Equation 6-23 if in the denominator geometric mean of surfaces open to imbibition is taken (symmetric surfaces are considered only once) instead of arithmetic sum as mentioned below:

$$L_c^2 = \frac{V_b}{\left(\prod_1^n \frac{A_i}{S_{A_i}}\right)^{1/n}} \begin{cases} = \left(L_x L_y L_z\right)^{2/3} & \text{(for a block of dimension } L_x \text{ , } L_y \text{ and } L_z \text{)} \\ = \dfrac{DH}{4} & \text{(for a cylindrical core of diameter D and Height H)} \end{cases} \quad (6\text{-}29)$$

As defined above the shape factor can be extended to three dimensions and to different geometries. This new definition of the shape factor can be implemented in dual porosity simulators to model the surfactant aided gravity dominated processes which is discussed in the next section.

6.3 APPLICABILITY OF SHAPE FACTOR IN DUAL POROSITY SYSTEM

Dual porosity systems are characterized by two porosities. A primary porosity which is that of the matrix and a secondary porosity corresponding to fractures in the media. The dual porosity approach was formulated by Barenblatt and Zheltov (1960) for single phase in naturally fractured reservoir composed of two superimposed media, a continuous fracture system and a discontinuous system of matrix blocks. When there is interaction between matrix blocks or matrix blocks are continuous then the representation is given by Figure 6-18 and the system is called dual porosity and dual permeability system.

Warren and Root (1963) presented a practical model for fractured systems (Figure 2-20). They considered an idealized case comprised of a set of identical rectangular parallelepipeds, representing the matrix blocks, which are separated by fractures. Kazemi et al. (1976) presented an extension of the dual-porosity model of Warren and Root (1963) to two-phase flow which could account for relative fluid mobilities, gravitational effects, imbibition, and variation in formation properties. The mass transfer equations for a given phase (components=phases case) in the matrix and fracture are coupled via a matrix

fracture term which in turn depends on a matrix fracture transfer function. The equation for flow of phase α in fracture (f) is given by:

$$\nabla.[\lambda_{\alpha f}(\nabla\Phi_{\alpha f})] = \frac{\partial(\phi S_\alpha)_f}{\partial t} + q_{\alpha f} + \tau_{\alpha m-f} \tag{6-30}$$

where the potential Φ is given as:

$$\Phi = P + \rho g H \tag{6-31}$$

$\lambda_{\alpha f}$ is the transmissibility of phase α in fracture, $\nabla\Phi_{\alpha f}$ is the potential gradient of phase α in fracture, $\frac{\partial(\phi S_\alpha)_f}{\partial t}$ represents the accumulation term for phase α in fracture, $q_{\alpha f}$ is the source/sink term and $\tau_{\alpha m-f}$ represents the matrix-fracture flow term and is given by:

$$\tau_{\alpha m-f} = -T_{\alpha m-f}[(\Phi_{\alpha f} - \Phi_{\alpha m})] \tag{6-32}$$

where $T_{\alpha m-f}$ is the matrix-fracture transfer function and is given by:

$$T_{\alpha m-f} = \sigma V_b \frac{k_m k_{r\alpha}}{\mu_\alpha} \tag{6-33}$$

where σ is the shape factor, V_b is the bulk volume, k_m is the permeability of the matrix, $k_{r\alpha}$ is the relative permeability of phase α and μ_α is the viscosity of phase α. The shape factor σ is given by the following equation:

$$\sigma = \frac{1}{L_c^2} = \frac{1}{V_b}\sum\frac{A_i}{S_{A_i}} \quad . \tag{6-34}$$

For surfactant aided gravity dominated processes the shape factor can be modified as:

$$\sigma_{new} = \frac{1}{L_c^2} = \frac{1}{V_b}\left(\prod_1^n \frac{A_i}{S_{A_i}}\right)^{1/n} \tag{6-35}$$

Farhadinia et al. (2010) studied wettability alteration and interfacial tension reduction due to surfactants in a dual porosity system using UTCHEM. To match the dual porosity UTCHEM simulation with explicit fracture simulations a numerical constant was multiplied to the transfer function to obtain a pseudo matrix transfer function. The values for the numerical constant were 1.15, 0.2 and 0.35 for water, alkali (wettability alteration agent) and alkali/surfactant floods (wettability alteration and ultra-low IFT) respectively.

Assuming that all other parameters in the transfer function can be correctly modeled by the physics incorporated in the wettability alteration model, the multiplication of a value less than 1 captures the retardation of the process. To compare this with the new shape factor (Equation 6-35) we find the ratio of the new shape factor with the old shape factor for a block (cartesian grid block system) with $L_x = L_y = 1.32$ inch and $L_z = 5.75$ inch which has the same volume as that of a cylindrical core with diameter: 1.5 inch and height: 5.75 inch (same as experiment performed in this study). A ratio of 0.18 was obtained which is very close to the value of transfer function multiplier of 0.2 for the alkaline process or the wettability altering agent process in the UTCHEM dual porosity match with the explicit fracture simulation. Along with the validation for the cylindrical cores which was achieved by comparison with different static and dynamic imbibition datasets, this comparison of ratio with the transfer function multiplier makes a strong case for the validity of the new shape factor.

6.4 SUMMARY

Analytical models were tested considering pressure drop only in water phase, pressure drop only in oil phase, and pressure drop across both water and oil phases. The model with pressure drop only in water phase gives an accurate prediction with the change in diameter, but with an increase in height it predicts higher recovery while the experimental data shows decrease in oil recovery. As per the assumption that the aqueous phase enters only in x direction, an increase in diameter will result in more pressure loss in the aqueous phase and hence the validity of the assumption in this model holds better with an increase in diameter. This is believed to be the reason for match obtained with the change in diameter.

The model with pressure drop in only in oil phase gives good prediction of oil recovery with change in height but is insensitive to the change in diameter. As per the assumption that the oil is displaced only in z direction, an increase in height will result in more pressure loss in the oil phase and hence the validity of the assumption (pressure drop only in oil phase) in this model holds better with increase in height. This is believed to be the reason for match obtained with change in height of the core while the diameter remains the same.

The model with pressure drop in both oil and water captures the decrease in recovery with diameter and height. Sensitivity to change in oil recovery with change in height is fairly accurate whereas the model over-predicts oil recovery with change in diameter. Model match with the experimental recovery curve is much better for the height compared to the diameter.

A new space-time scaling function (t/DH) is proposed for surfactant aided gravity dominated processes. Data with same boundary conditions, rock, fluids and varying dimensions can be correlated with the scaling function at early times with no fitting

parameters involved. A good correlation is obtained with the data from different studies indicating the effectiveness of the scaling function. The scaling is applicable to both static as well as dynamic imbibition cases. Applicability of the scaling rule in a dual porosity simulation model is described in the last section of this chapter.

Parameter	Values	Units
k_{rw}	0.00043	
μ_w	0.01	poise
Height	14.6	cm
Diameter	3.81	cm
ρ_w	1	g/cm^3
ρ_o	0.83	g/cm^3
$\Delta\rho$	0.17	g/cm^3
g	980	cm/s^2
Porosity	0.26	
Permeability	40	mD
S_{oi}	0.78	
S_{or}	0.34	

Table 6-1: Case 1 (pressure drop in water phase): Model parameters for the base case (Diameter: 1.5 inch, Height: 5.75 inch) Estaillades Limestone recovery curve match.

Parameter	Values	Units
k_{rw}	0.002	
μ_w	0.01	poise
Height	13.843	cm
Diameter	10.16	cm
ρ_w	1	g/cm^3
ρ_o	0.83	g/cm^3
$\Delta\rho$	0.17	g/cm^3
g	980	cm/s^2
Porosity	0.26	
Permeability	8.4	mD
S_{oi}	0.78	
S_{or}	0.34	

Table 6-2: Case 1 (pressure drop in water phase): Model parameters for the base case (Diameter: 4 inch, Height: 5.75 inch) Texas Cream Limestone recovery curve.

Parameter	Values	Units
k_{ro}	0.85	
μ_o	0.135	poise
Height	14.605	cm
ρ_w	1	g/cm^3
ρ_o	0.83	g/cm^3
$\Delta\rho$	0.17	g/cm^3
g	980	cm/s^2
Porosity	0.26	
Permeability	40	mD
S_{oi}	0.78	
S_{or}	0.34	

Table 6-3: Case 2 (pressure drop in oil phase): Model parameters for the base case (Diameter: 1.5 inch, Height: 5.75 inch) Estaillades Limestone recovery curve.

Parameter	Value	Units
k_{ro}	1	
μ_o	0.135	poise
Height	29.21	cm
ρ_w	1	g/cm^3
ρ_o	0.83	g/cm^3
$\Delta\rho$	0.17	g/cm^3
g	980	cm/s^2
Porosity	0.26	
Permeability	8.4	mD
S_{oi}	0.78	
S_{or}	0.34	

Table 6-4: Case 2 (pressure drop in oil phase): Model parameters for the base case (Diameter: 4 inch, Height: 5.75 inch) Texas Cream Limestone recovery curve.

Parameter	Value	Units
k_{rw}	0.003	Units
k_{ro}	1	
μ_o	0.135	poise
μ_w	0.01	poise
Height	14.605	cm
Diameter	3.81	cm
ρ_w	1	g/cm^3
ρ_o	0.83	g/cm^3
$\Delta\rho$	0.17	g/cm^3
g	980	cm/s^2
Porosity	0.26	
Permeability	40	mD
S_{oi}	0.78	
S_{or}	0.34	

Table 6-5: Case 2 (pressure drop in both phases): Model parameters for the base case (Diameter: 1.5 inch, Height: 5.75 inch) Estaillades Limestone recovery curve match.

Parameter	Value	Units
k_{rw}	0.01	
k_{ro}	1	
μ_o	0.135	poise
μ_w	0.01	poise
Height	29.21	cm
Diameter	3.81	cm
ρ_w	1	g/cm^3
ρ_o	0.83	g/cm^3
$\Delta\rho$	0.17	g/cm^3
g	980	cm/s^2
Porosity	0.26	
Permeability	8.4	mD
S_{oi}	0.78	
S_{or}	0.34	

Table 6-6: Case 2 (pressure drop in both phases): Model parameters for the base case (Diameter: 4 inch, Height: 5.75 inch) Texas Cream Limestone recovery curve match.

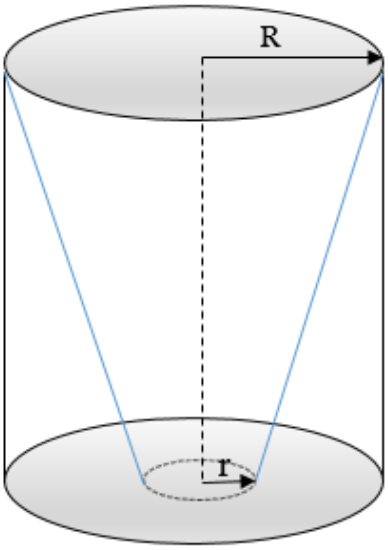

(a)

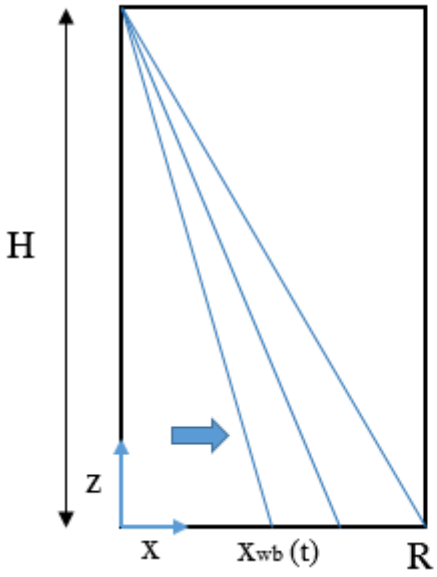

(b) $x_{wb} =< R$

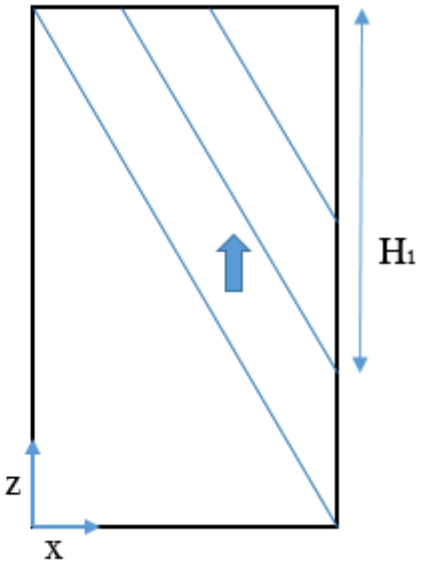

(c) $x_{wb} > R$

Figure 6-1: Schematic of imbibition front movement in a core for gravity driven flow: (a) Cylindrical core with axial no flow boundary (b) Imbibition front movement till it reaches no flow boundary ($x_{wb} =< R$). (c) Imbibition front movement after reaching no flow boundary ($x_{wb} > R$)

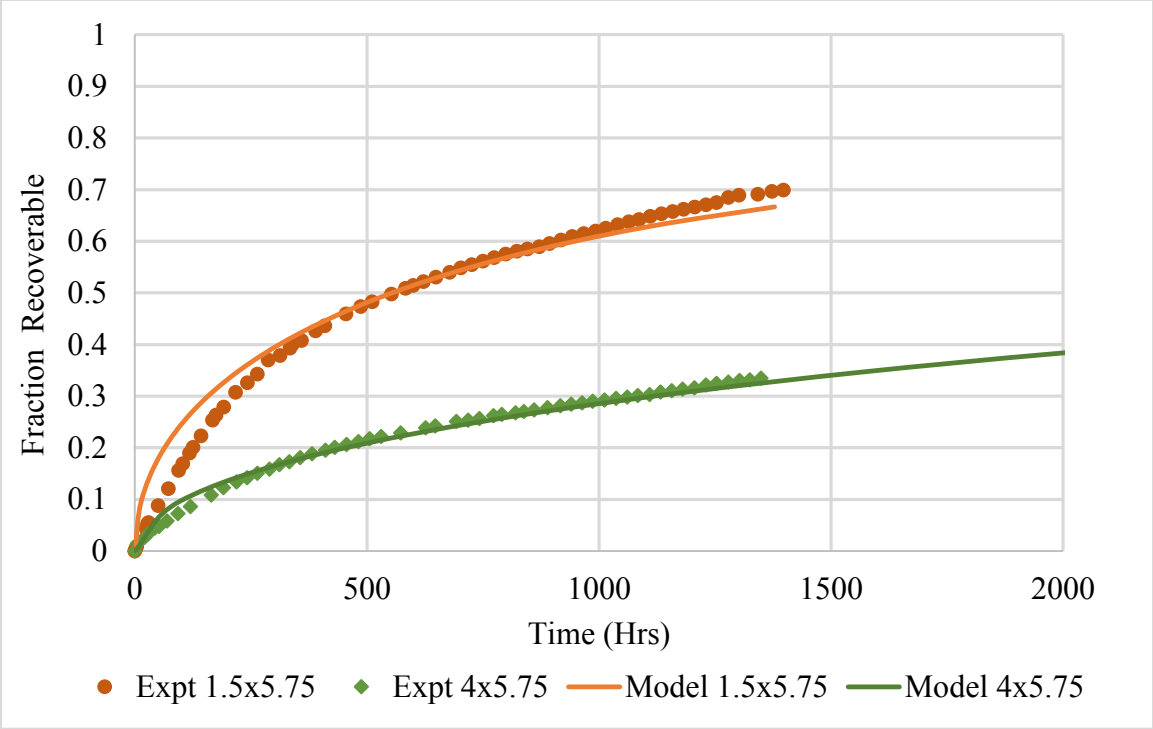

Figure 6-2: Case 1 (pressure drop in water phase): Scaling comparison with diameter. Solid lines denote the model generated curves, points denote the experimental curves.

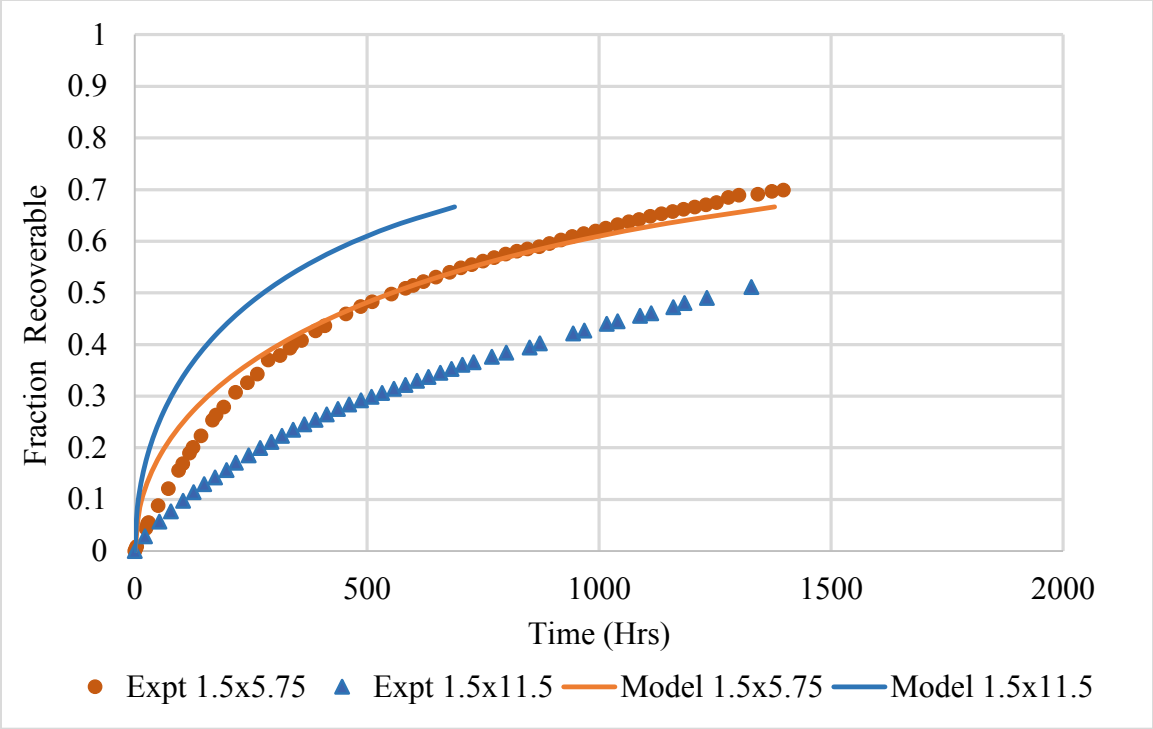

Figure 6-3: Case 1 (pressure drop in water phase): Scaling comparison with height for Estaillades Limestone Data. Solid lines denote the model generated curves, points denote the experimental curves.

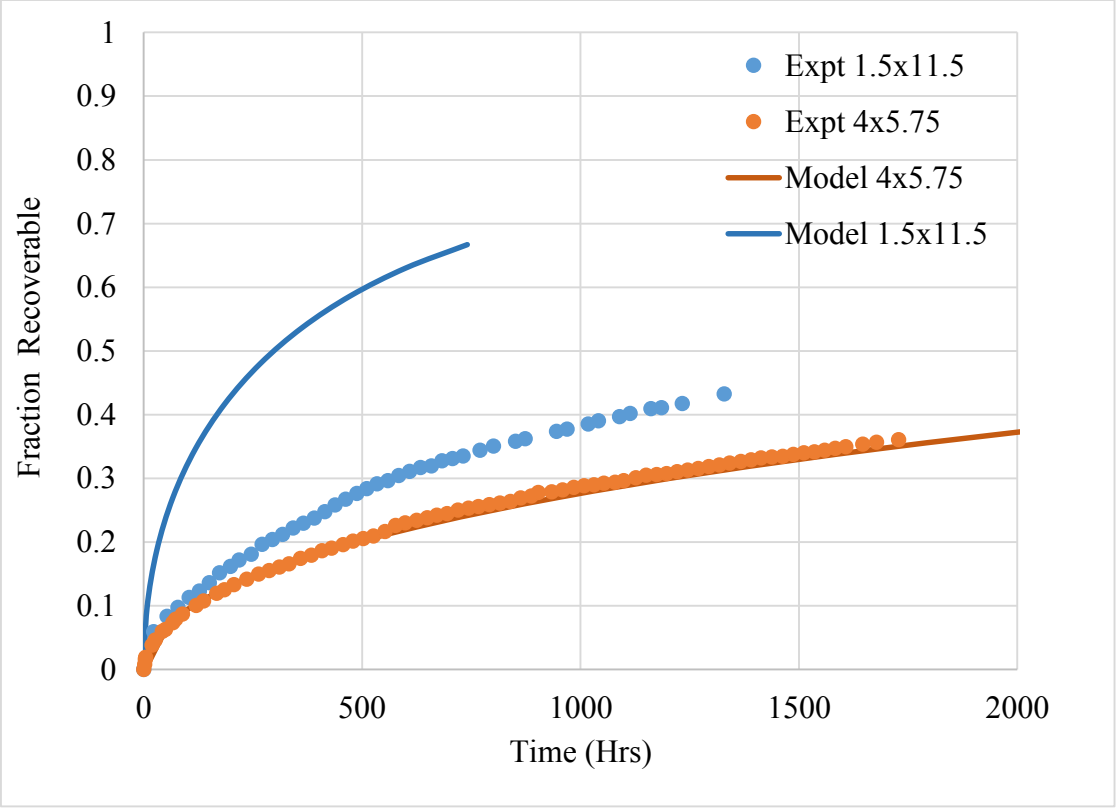

Figure 6-4: Case 1 (pressure drop in water phase): Scaling comparison with Texas Cream Limestone with variation of length and height of core. Solid lines denote the model generated curves, points denote the experimental curves.

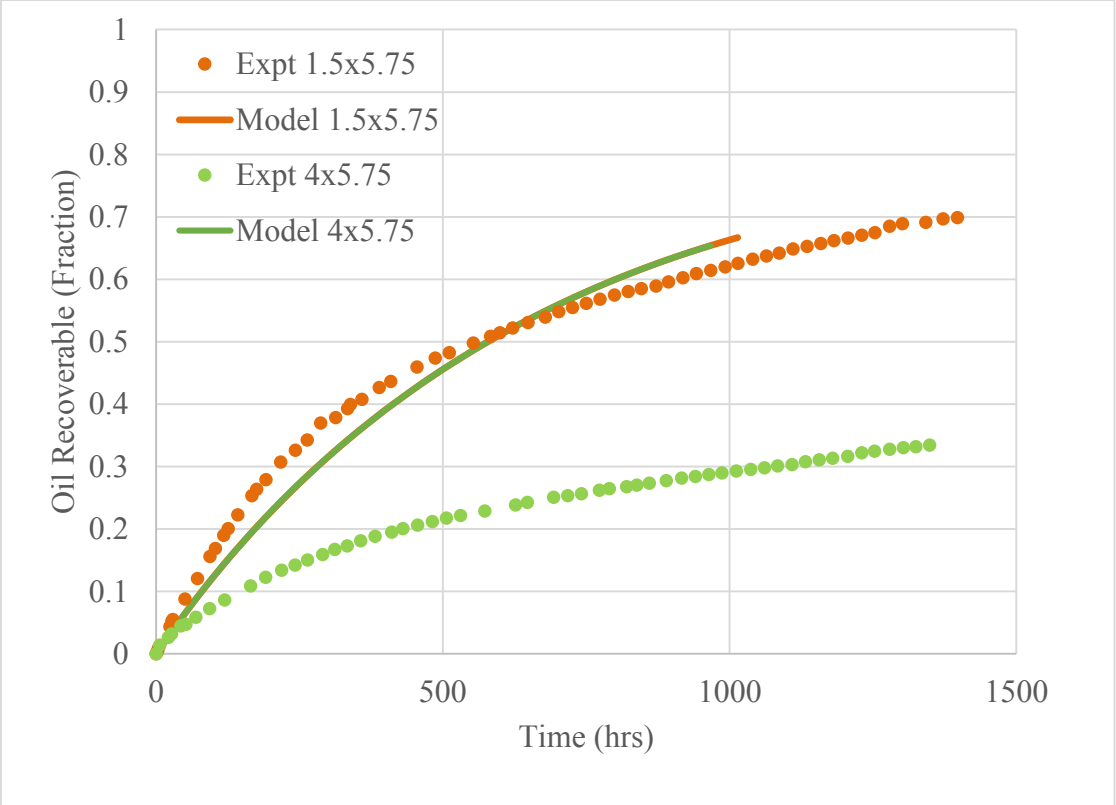

Figure 6-5: Case 2 (Pressure drop in oil phase): Scaling comparison with change in diameter of the core for Estaillades Limestone Data. Solid lines denote the model generated curves, points denote the experimental curves.

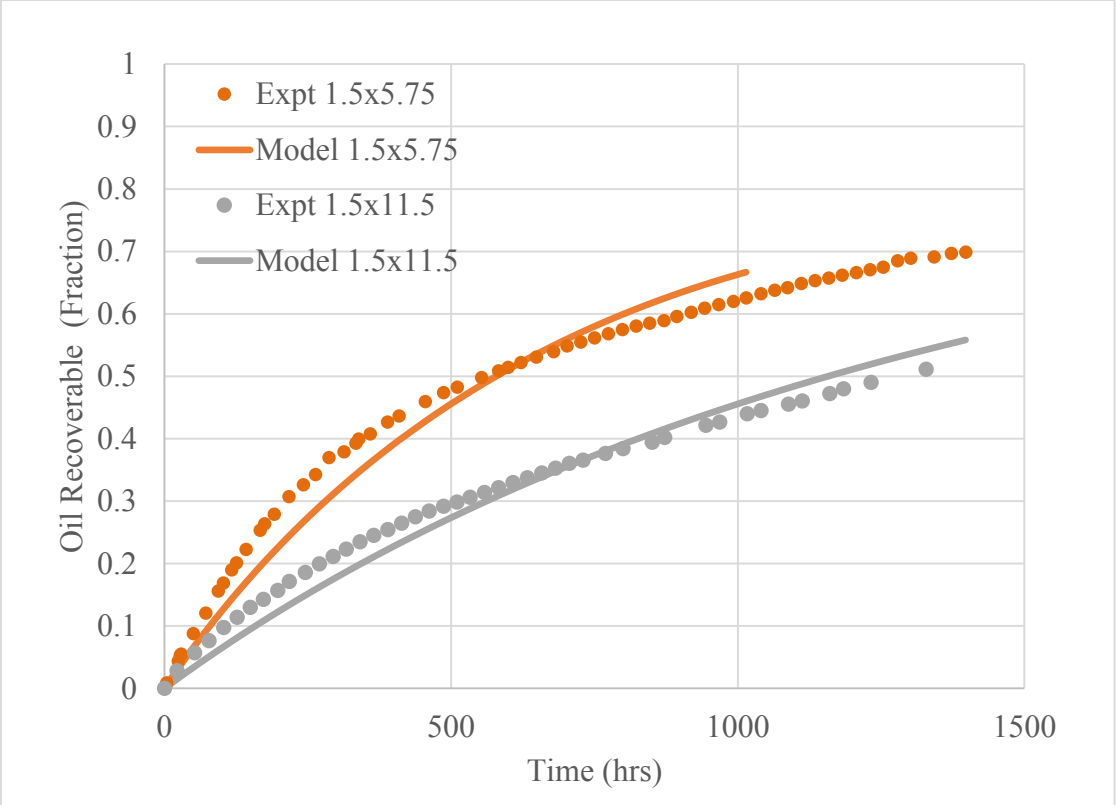

Figure 6-6: Case 2 (Pressure drop in oil phase): Scaling comparison with change in height of the core for Estaillades Limestone Data. Solid lines denote the model generated curves, points denote the experimental curves.

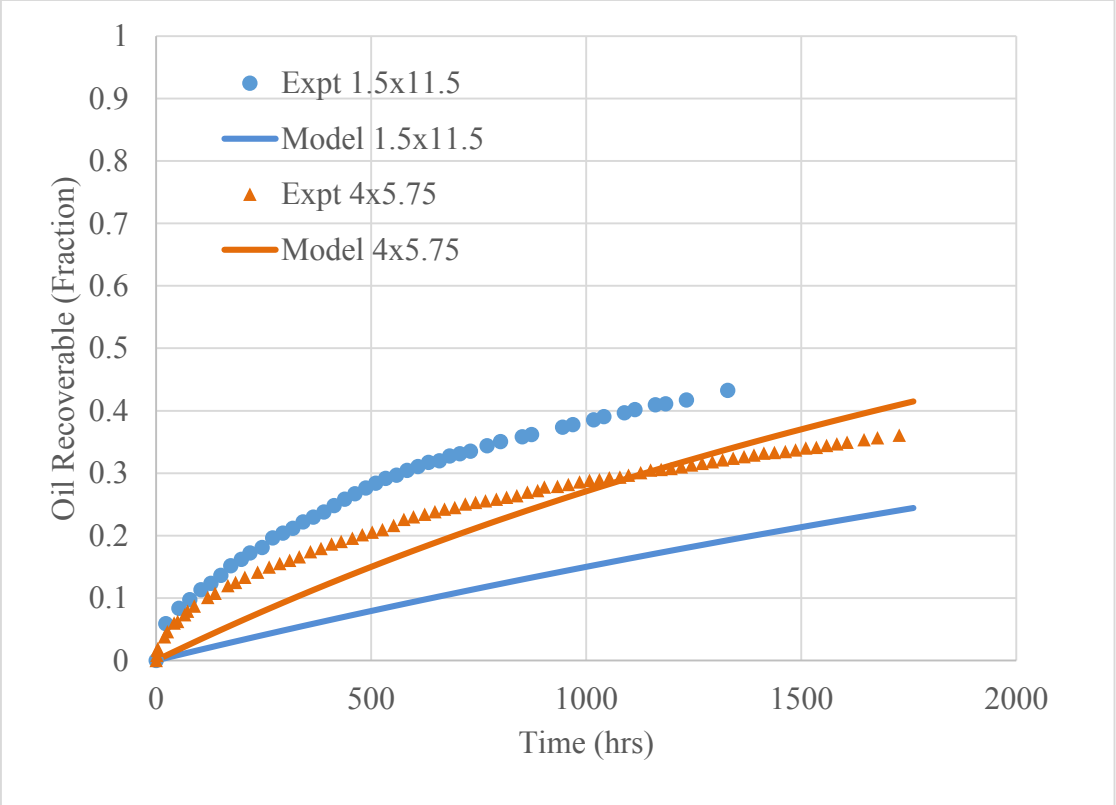

Figure 6-7: Case 2 (Pressure drop in oil phase): Scaling comparison with change in height and diameter of the core for Texas Cream Limestone Data. Solid lines denote the model generated curves, points denote the experimental curves.

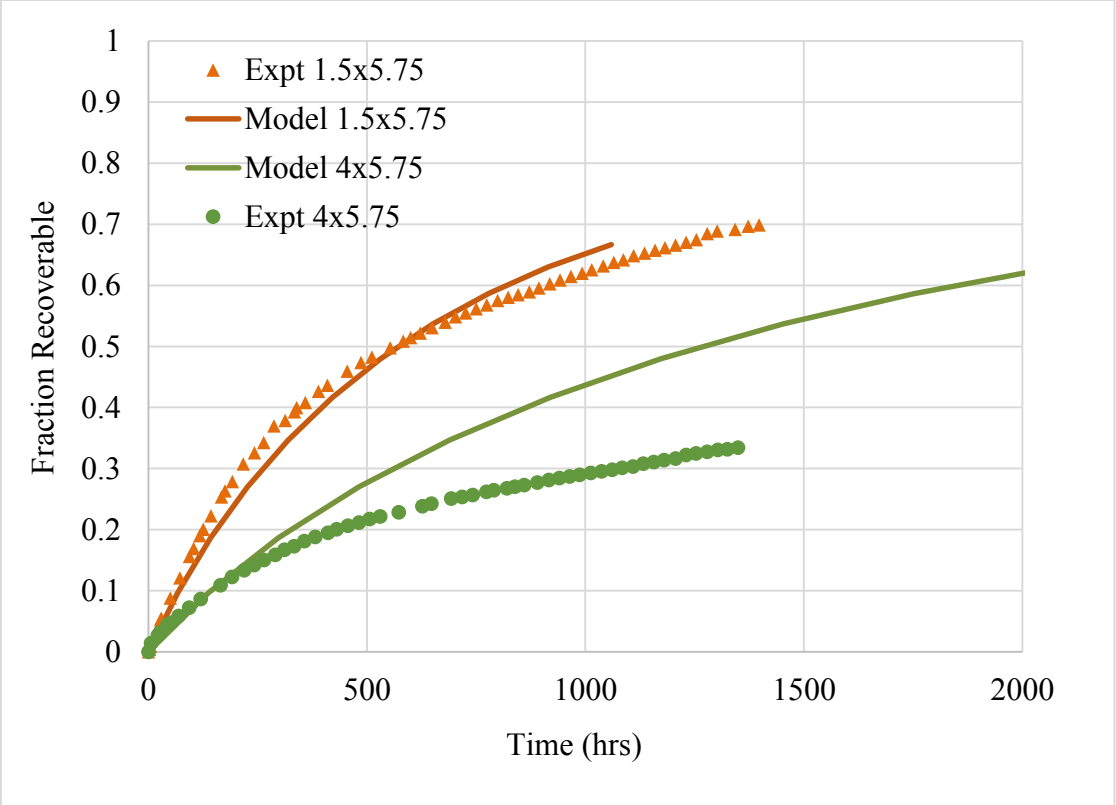

Figure 6-8: Case 3 (Pressure drop in both the phases): Scaling comparison with diameter of the core for Estaillades Limestone Data. Solid lines denote the model generated curves, points denote the experimental curves.

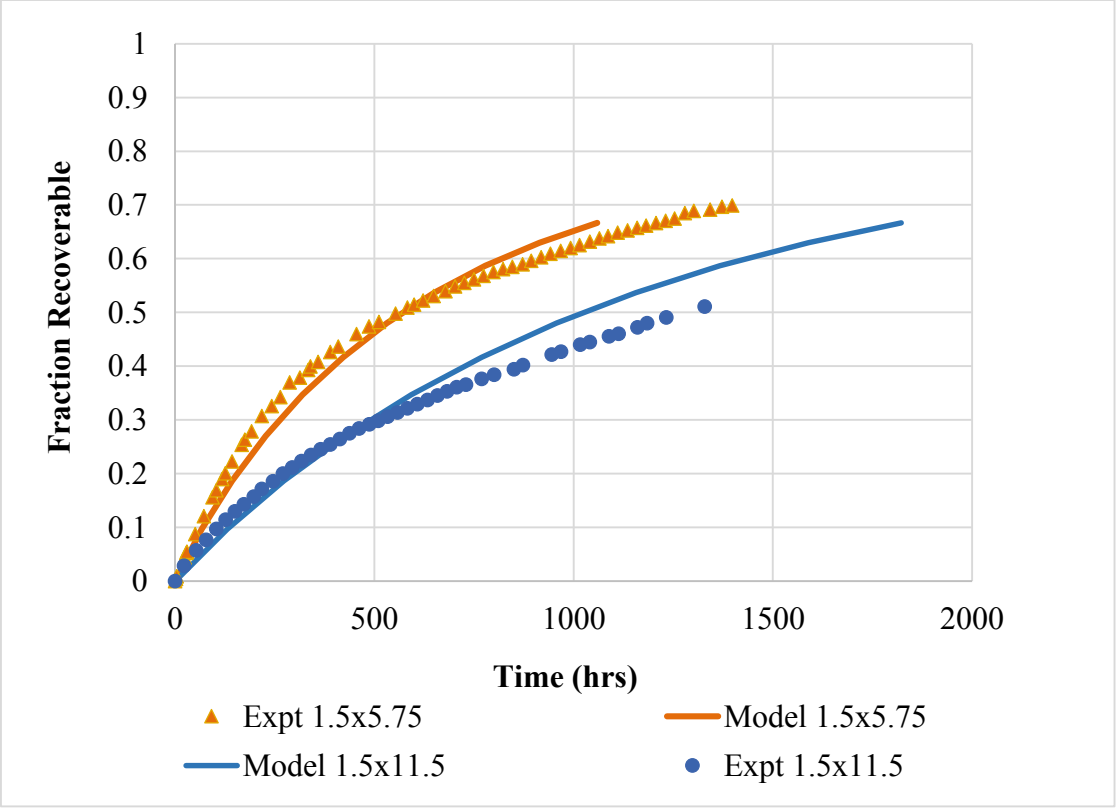

Figure 6-9: Case 3 (Pressure drop in both the phases): Scaling comparison with height of the core for Estaillades Limestone Data. Solid lines denote the model generated curves, points denote the experimental curves.

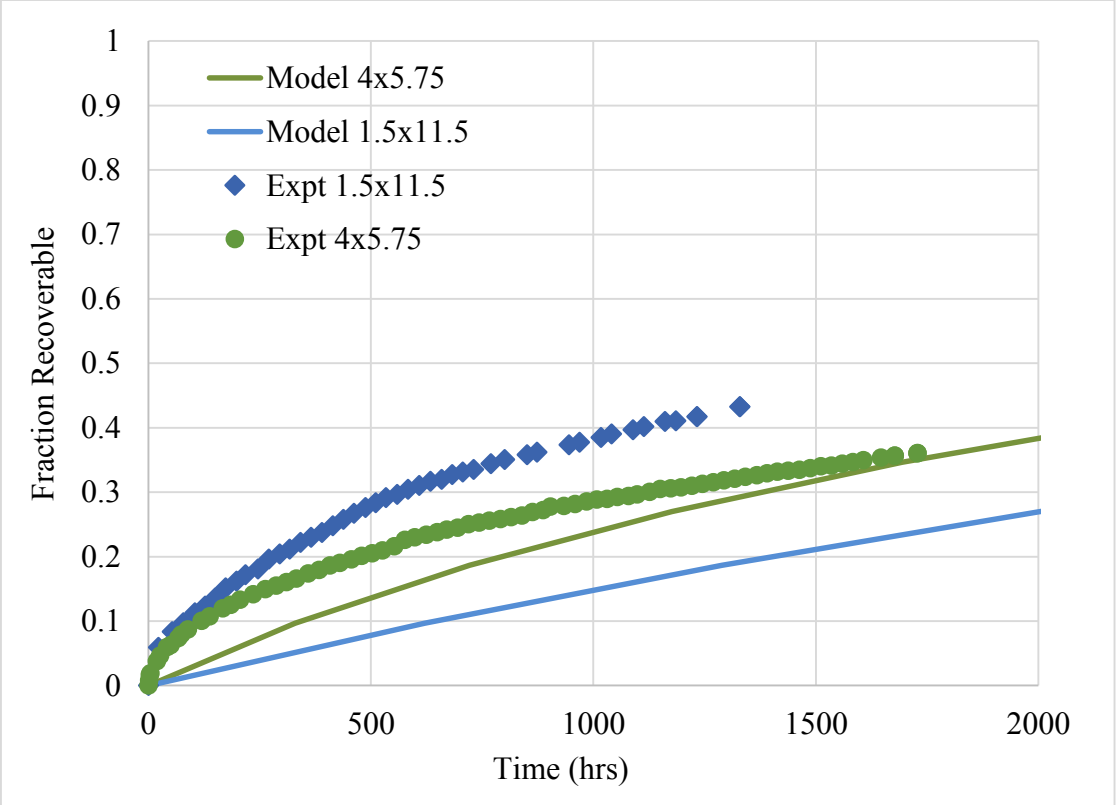

Figure 6-10: Case 3 (Pressure drop in both the phases): Scaling comparison for Texas Cream Limestone data with variation of length and height of the core. Solid lines denote the model generated curves, points denote the experimental curves.

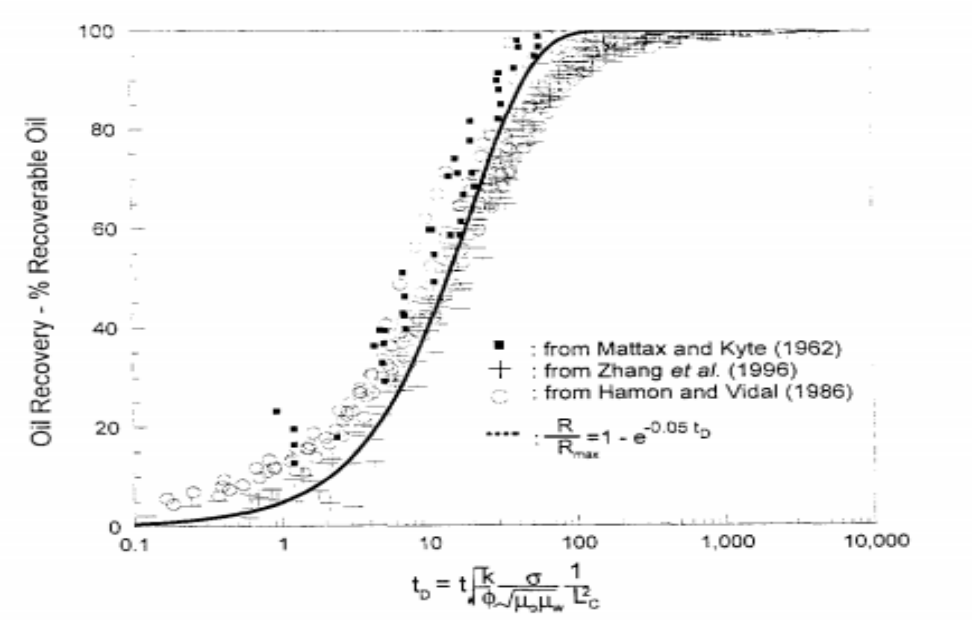

Figure 6-11: Correlation of data for imbibition in water-wet media (no surfactants) using Ma and Morrow (1997) dimensionless time which incorporates the critical length L_c .

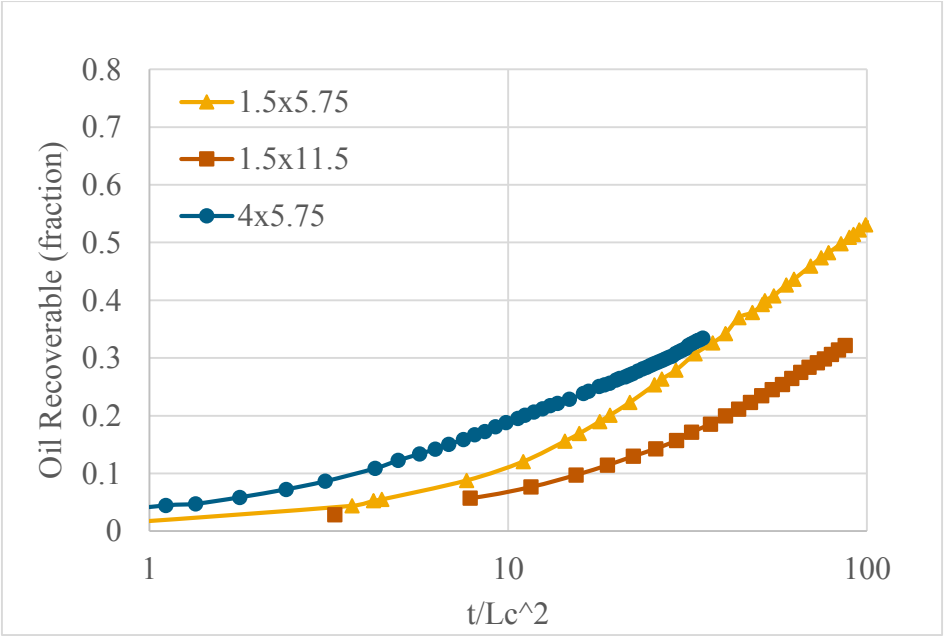

Figure 6-12: Scaling of Estaillades Limestone imbibition recovery curves with conventional critical length L_c.

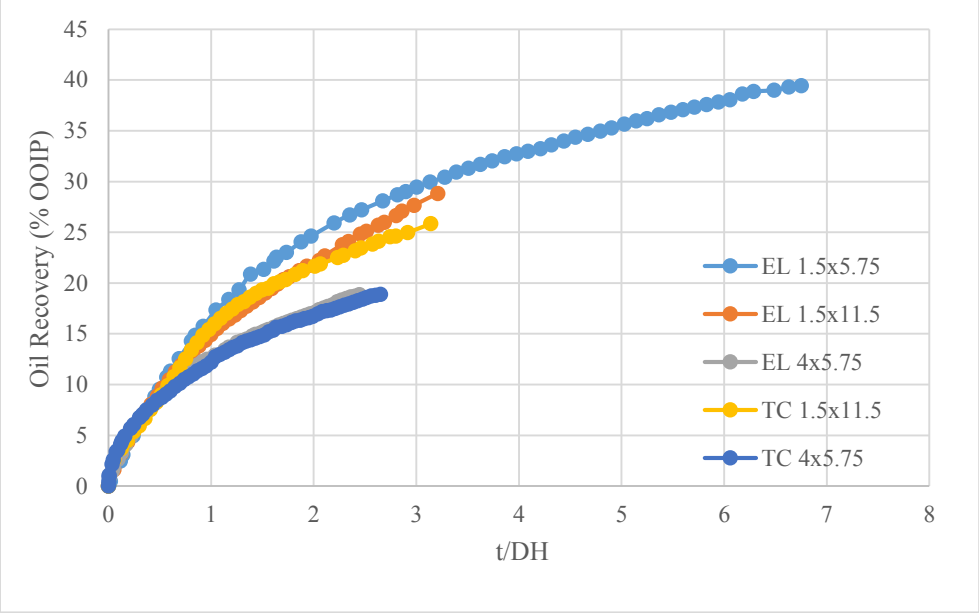
Oil Recovery (% OOIP)
t/DH
EL 1.5x5.75
EL 1.5x11.5
EL 4x5.75
TC 1.5x11.5
TC 4x5.75

(a)

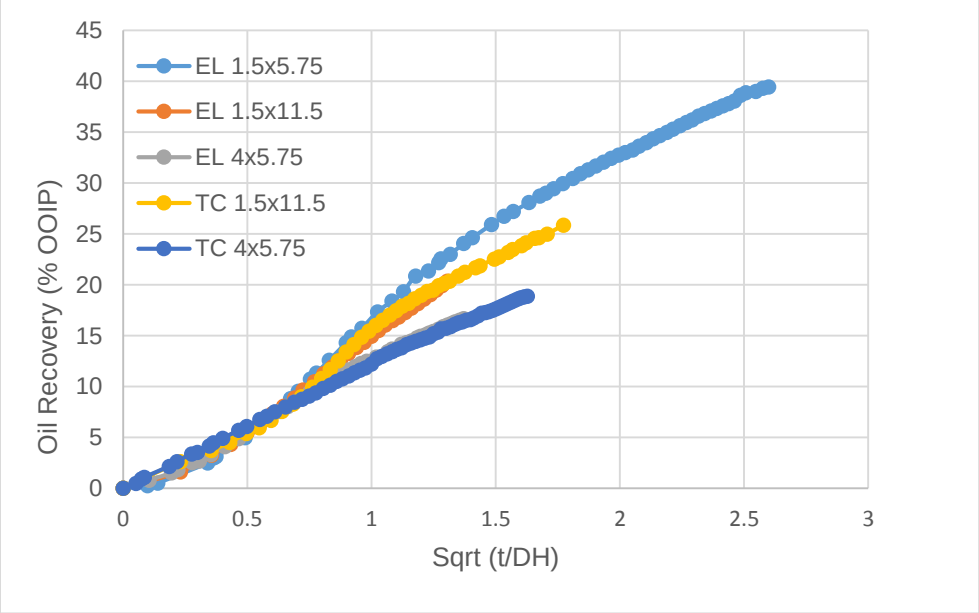
Oil Recovery (% OOIP)
Sqrt (t/DH)
EL 1.5x5.75
EL 1.5x11.5
EL 4x5.75
TC 1.5x11.5
TC 4x5.75

(b)

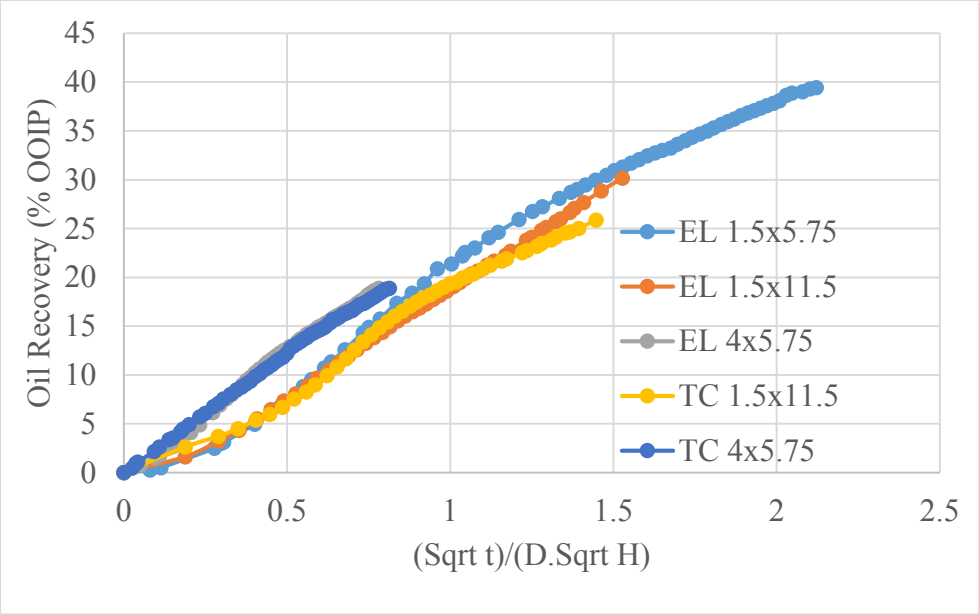

(c)

Figure 6-13 a, b & c: Scaling of Estaillades Limestone and Texas Cream Limestone static imbibition recovery curves with different scaling relationships.

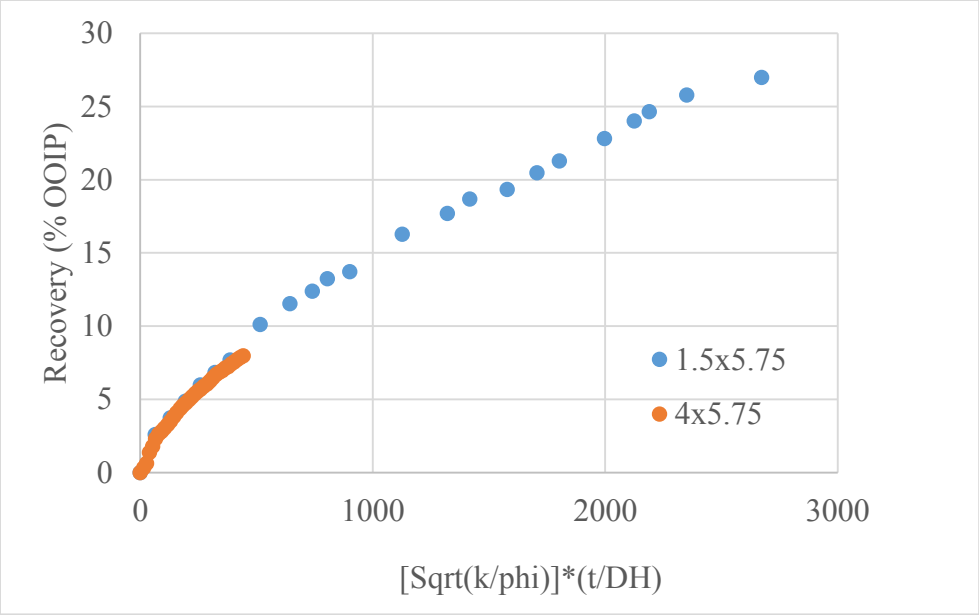
30
25
20
15
10
5
0
Recovery (% OOIP)
0
1000
2000
3000
[Sqrt(k/phi)]*(t/DH)
1.5x5.75
4x5.75

(a)

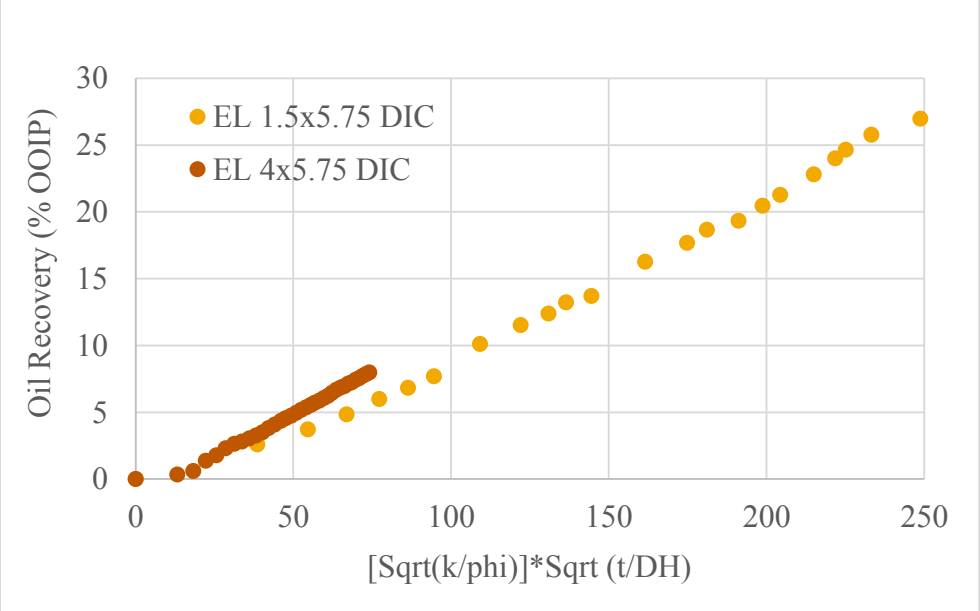
30
25
20
15
10
5
0
Oil Recovery (% OOIP)
0
50
100
150
200
250
[Sqrt(k/phi)]*Sqrt (t/DH)
EL 1.5x5.75 DIC
EL 4x5.75 DIC

(b)

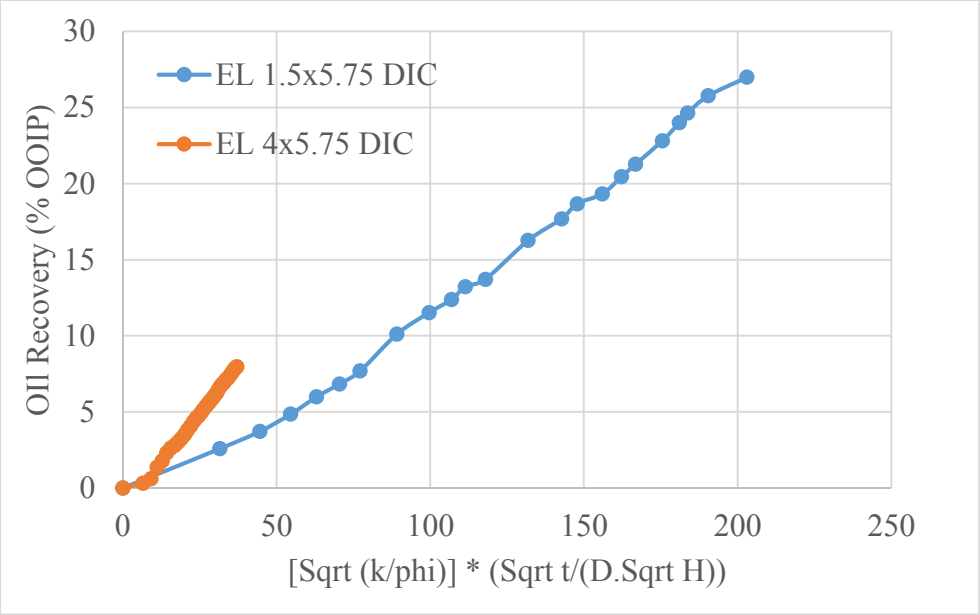

(c)

Figure 6-14 a, b & c: Scaling of Estaillades Limestone dynamic imbibition recovery curves with different scaling relationships

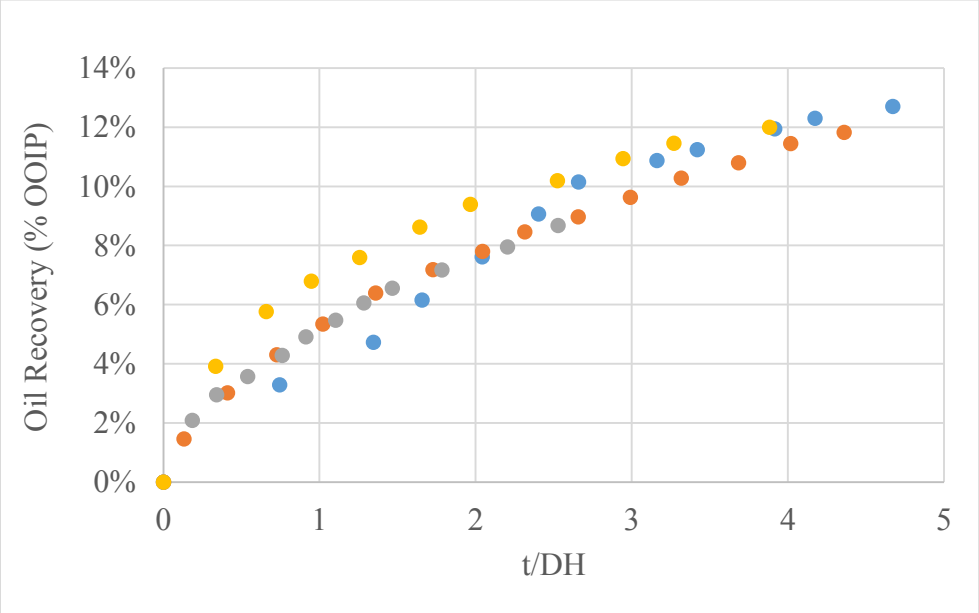

(a)

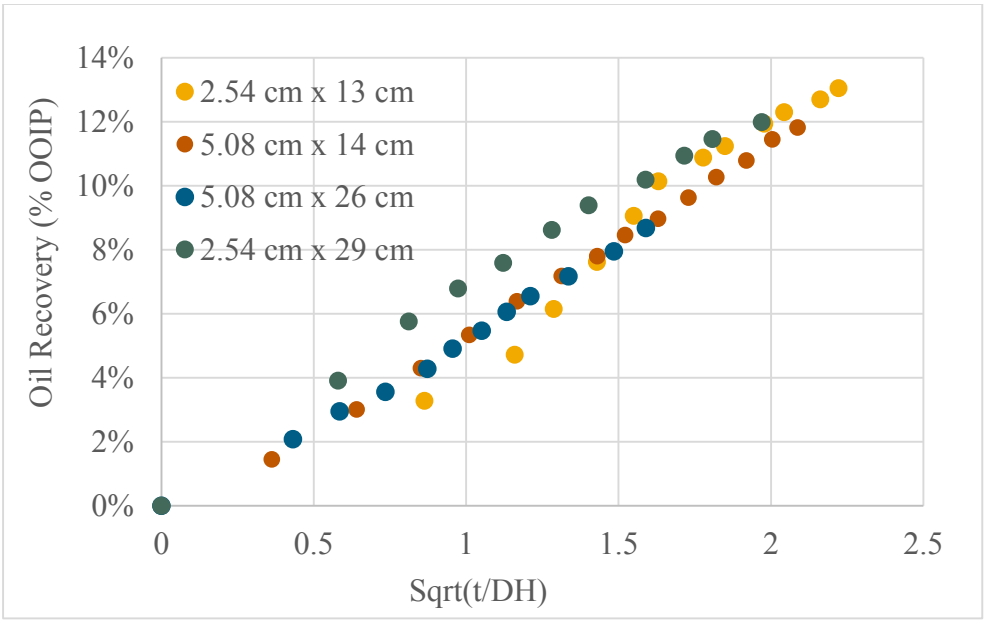

(b)

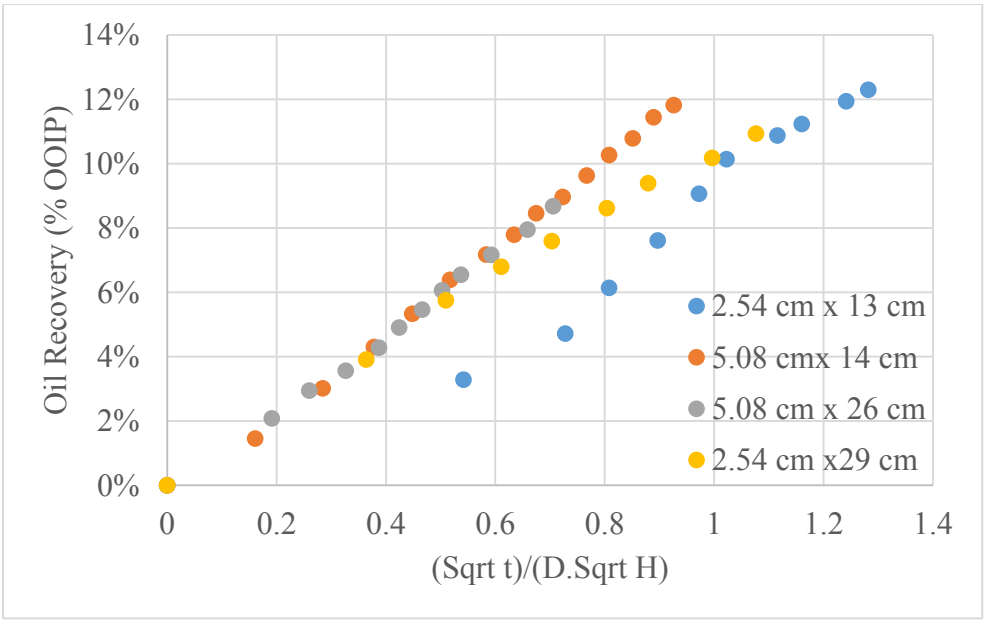

(c)

Figure 6-15 a, b & c: Scaling of dynamic imbibition recovery curves with different scaling relationships. Data from Mirzaei et al. (2013) for experiments performed with ultra-low IFT formulation.

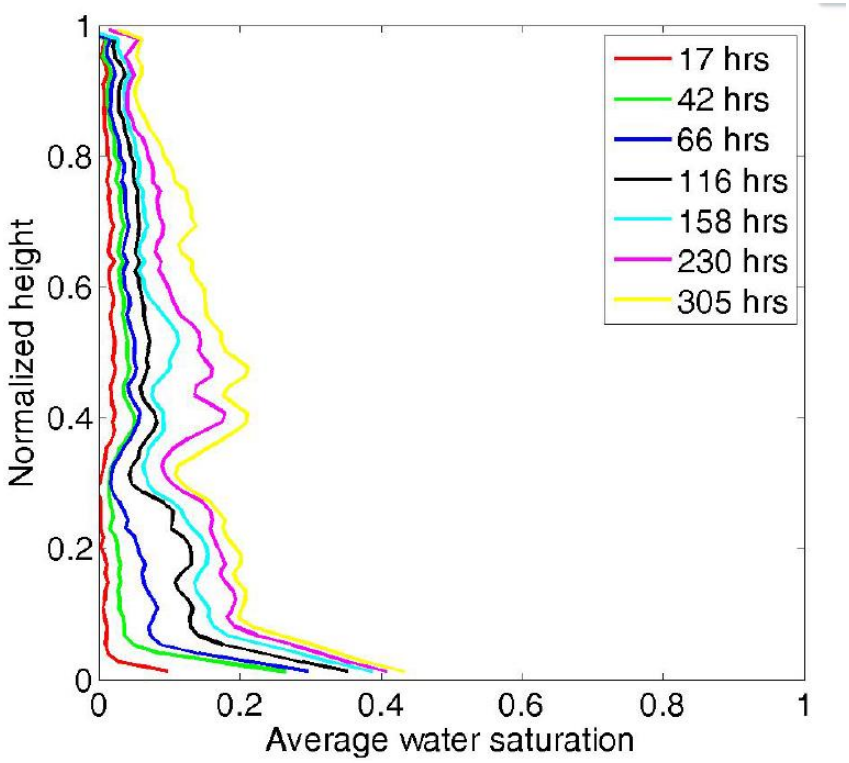

Figure 6-16: Average water saturation vs. height at different times for dynamic imbibition experiment labelled '1' from Mirzaei et al. (2013) obtained using CT scanner.

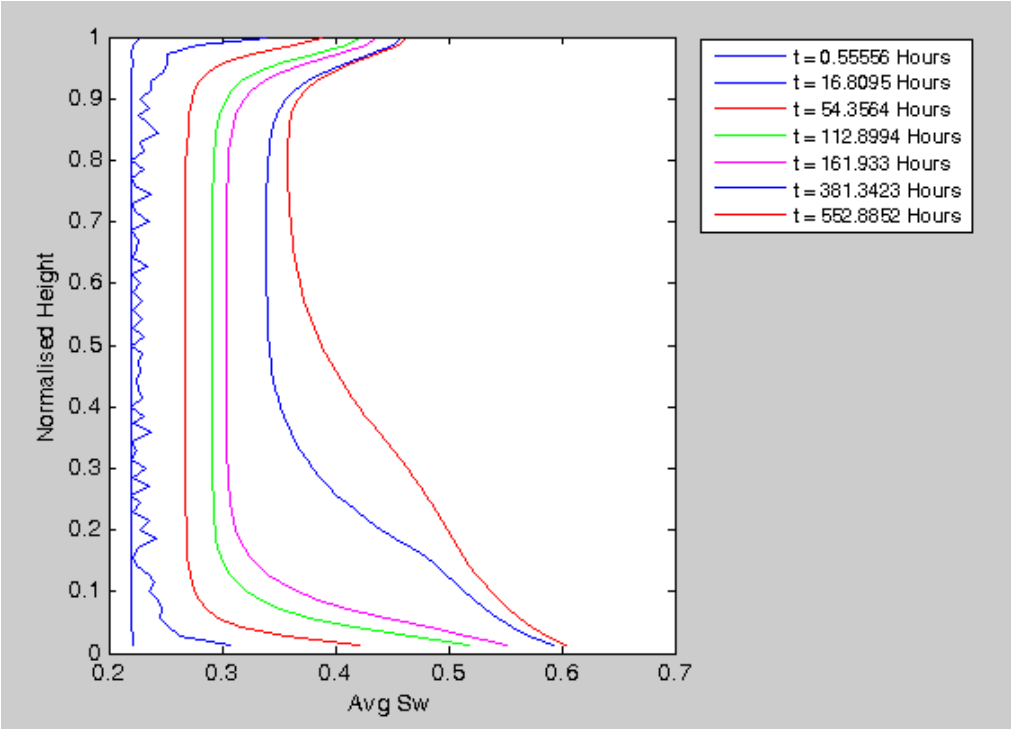

Figure 6-17: Average water saturation vs. height for static imbibition experiment performed on Estaillades Limestone (D=1.5 inch, H: 5.75 inch) from compositional mechanistic simulation.

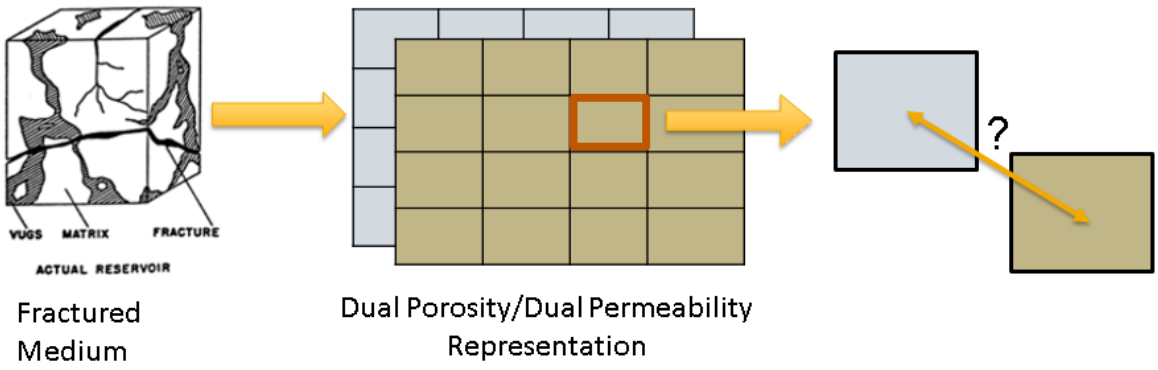

Figure 6-18: Schematic of matrix fracture interaction in a dual porosity/dual permeability representation of a fractured medium.

Chapter 7: Conclusions and Recommendations

In this work, surfactants are identified for different rock/oil/brine systems which can alter the wettability of an initial oil-wet/mixed-wet media to water-wet and significantly enhance recovery through spontaneous imbibition. Static and dynamic imbibition experiments as well as corefloods were performed using dilute (0.1 - 0.25 wt%) wettability altering surfactants. The imbibition experiments were performed at high and low inverse bond numbers resulting in capillary and gravity dominated flows, respectively. The recovery mechanisms for the two processes are analyzed by studying the velocity and saturation profiles. Scaling analysis is performed for gravity dominated flow and a new space-time scaling function is proposed. The scaling function is validated with different experimental studies. Conclusions are first presented for capillary dominated flow, followed by gravity dominated flow and finally for wettability altering corefloods. In the second part of this chapter recommendations are made for future work.

7.1 CONCLUSIONS

7.1.1 Capillary Dominated Flow

1. Three anionic surfactants were identified which altered the wettability of clay-rich sandstones. These surfactants belong to the class of ether sulphates. The number of ethoxy groups in the surfactant plays a major role in aqueous stability at higher salinities. It was observed that more the number of ethoxy groups in the surfactant, the higher was the aqueous stability.
2. Static imbibition experiments in low permeability (0.03 – 0.23 mD) sandstone reservoir cores result in high oil recovery (42-68% OOIP). Experiments were performed on cores which are 1 inch in diameter and 2 inch in height having initial water saturation in the range of 0.7 to 0.8.

3. Recovery mechanisms were analyzed using a three dimensional compositional numerical simulator. Simulation input parameters are validated by obtaining a match with the experimental data. The validated base case match was then used to study the velocity and saturation profiles. The profiles indicate counter current flows with oil velocity vectors pointing outwards. Similar visual observations were made during experiments which are captured through images. The saturation front moves radially inward with symmetric profiles at the top and bottom.
4. The imbibition recovery curves do not correlate with traditional scaling groups (Mattax and Kyte, 1962; Ma et al. 1997) for capillary driven flow in strongly water-wet media. It is observed that oil recovery varies linearly with square root of time.
5. The rate of oil recovery increases with increasing IFT: Experiments were performed on cores with almost same initial oil saturation using the same surfactant, but at different salinities. As a result of varying salinity the interfacial tension between oil/water is varied. The crude oil-brine IFT is 21.8 dyne/cm which is reduced to 1-10 dyne/cm by use of surfactants at different salinities. It was observed that the rate of recovery was higher for the higher IFT cases.

7.1.2 Gravity Dominated Flow

1. An anionic surfactant formulation was identified which can alter the wettability from oil-wet to water-wet on outcrop rocks Estaillades Limestone and Texas Cream Limestone.
2. Using the identified surfactant formulation static and dynamic imbibition experiments were performed on cores with same dimensions and boundary conditions. The only difference between the two experiments was that of flow of fluid surrounding the fracture, all other parameters were same. The only surface

open to interaction with the surfactant was the fracture surface; the lateral and top surfaces of the cylindrical core were sealed using epoxy. It was observed that dynamic imbibition process recovers oil faster than static imbibition.

3. Imbibition experiments were performed on cores with varying height and diameter. The cores have same permeability, porosity and initial oil saturation. All the surface areas of the core were open to flow. The results show that oil recovery decreases with increasing diameter and height. Also, oil recovery scaled linearly with square root of time.

4. Recovery mechanisms are analyzed using a FORTRAN based mechanistic simulator. Base case validation match is obtained with the experimental data which is used to study the velocity and saturation profiles. The oil phase velocity vectors indicate that majority of oil is recovered from the top which is supported by visual observations during experimentation. The saturation profiles are asymmetric at the top and bottom of the core with more water invasion at the bottom of the core because of higher gravitational potential at the bottom. The volume of core near its axis and towards the top is invaded last by the surfactant solution.

5. Analytical scaling groups for gravity dominated flow were tested considering the pressure drop only in the water phase, the pressure drop only in the oil phase and the pressure drop across both water and oil phases.

    a. Pressure drop in water phase: The model gives an accurate prediction with the change in diameter, but with an increase in height it predicts higher recovery while the experimental data shows decrease in oil recovery. As per the assumption that the aqueous phase enters only in x direction, an increase in diameter will result in more pressure loss in the aqueous phase and hence the validity of the assumption in this model holds better with an increase in

diameter. This is believed to be the reason for match obtained with the change in diameter.

b. Pressure drop in oil phase: The model gives good prediction of oil recovery with change in height but is insensitive to the change in diameter. As per the assumption that the oil is displaced only in z direction, an increase in height will result in more pressure loss in the oil phase and hence the validity of the assumption (pressure drop only in oil phase) in this model holds better with increase in height. This is believed to be the reason for match obtained with change in height of the core while the diameter remains the same.

c. Pressure drop in both phases: The model captures the decrease in recovery with diameter and height. Sensitivity to change in oil recovery with change in height is fairly accurate whereas the model over-predicts oil recovery with change in diameter. Model match with the experimental recovery curve is much better for the height compared to the diameter.

6. A new space-time scaling function t/DH is proposed for surfactant aided gravity dominated processes. Data with same boundary conditions, rock, fluids and varying dimensions can be correlated with the scaling function at early times with no fitting parameter involved. The scaling function is validated with the static and dynamic imbibition experimental data in this study as well as with data from Mirzaei et al. (2013) where dynamic imbibition experiments were performed on oil saturated cores using surfactant solutions which result in ultra-low oil-water IFT (gravity dominated process). A good correlation is obtained with the data from different studies indicating the effectiveness of the scaling function. The scaling is applicable to both static as well as dynamic imbibition cases.

7.1.3 Wettability Altering Corefloods

1. Corefloods were performed on cores from different reservoirs to study the effect of wettability altering surfactant flood on incremental oil recovery over waterflood. In this study, the injection scheme was altered to take the initial waterflood into account by injecting half pore volume brine and then a switch was made to the surfactant flood. This was done to mimic the current status of these reservoirs so that performance improvement after a switch to wettability altering surfactant slug injection can be gauged.
2. Incremental recoveries over waterflood of 16% and 11% were obtained for secondary surfactant flood and slug process respectively for carbonate reservoir 1. Similarly, incremental recoveries over waterflood of 11% and 7% were obtained for secondary surfactant flood and slug process respectively for carbonate reservoir 2. These cores are not fractured and displacement of oil by brine is due to viscous forces unlike the imbibition experiments where gravity and capillary forces are responsible for oil recovery. The incremental oil recovery due to surfactant injection is attributed to the favorable increase in the relative permeability values of oil as the wettability is changed from oil-wet to water-wet.
3. A key difference between the two reservoir systems is the surfactant slug pore volume. For reservoir 1 only 0.5 PV of surfactant slug leads to higher incremental recoveries compared to around 1 PV of surfactant slug injection for reservoir 2. Experiments indicate that surfactant performance at the reservoir conditions (temperature, salinity, heterogeneity) is a key variable in these processes. Despite the differences, for both the reservoirs oil recovery is more in the secondary surfactant injection mode compared to the slug process.

7.2 RECOMMENDATIONS

From the insights gained from this work the following recommendations are made for future work:

1. More experiments with varying rock dimensions should be conducted for the surfactant aided gravity dominated processes to further validate the applicability of the proposed new scaling function. For cylindrical cores, it is also crucial to study the imbibition behavior with high and low D/H (where D is diameter of core and H is height of the core) ratios or when one dimension is significantly small compared to other dimensions.
2. Imbibition experiments can be conducted under CT scanner to validate the simulation generated saturation profiles for capillary and gravity dominated flows. CT scanned experiments also provide valuable information about the permeability, porosity and saturation distribution in the core which is vital for accurate numerical simulations.
3. In this study, dynamic imbibition experiments were performed in a coreholder under confining pressure where surfactant solution was injected at a constant flow rate into the fracture at the bottom. For the experiments performed here the injection velocity was kept constant at 2.4 ft/day. It is of great value to determine whether the flow rate affects oil recovery. This will facilitate to infer whether residence time in the fracture has any impact on oil recovery. Also, the effect viscous pressure gradients due to flow of fluid in fractures can be investigated by varying the fracture width and flow rate. The fracture width can be varied by increasing the overburden pressure.
4. The numerical modeling of wettability alteration process is critically dependent on accurately capturing relative permeability and capillary pressure at different

surfactant induced wetting states. Experimental determination of these values will provide more robust simulation results.

5. At field scale the fractures are not exactly vertical but possess some inclination. Also, there are fractures intersecting each other which can have a significant impact on oil recovery. Investigating experimentally the effect of inclined fractures and intersecting fractures on imbibition recovery in these surfactant aided processes can provide valuable data for modeling purposes at larger scales.

References

Abbasi Asl, Y., Pope, G. A., & Delshad, M. 2010. Mechanistic Modeling of Chemical Transport in Naturally Fractured Oil Reservoirs. Paper SPE-129661-MS presented in SPE Improved Oil Recovery Symposium. Society of Petroleum Engineers. DOI: http://dx.doi.org/10.2118/129661-MS

Abdallah, W., et al., 2007. Fundamentals of Wettability, Schlumberger Oilfield Review.

Adibhatla, B., and Mohanty, K. 2008. Parametric Analysis of Surfactant-Aided Imbibition in Fractured Carbonates. *Journal of Colloid and Interface Science*, **317** (2), 513–22. doi:10.1016/j.jcis.2007.09.088

Adibhatla, B., & Mohanty, K. 2008. Oil Recovery from Fractured Carbonates by Surfactant-Aided Gravity Drainage: Laboratory Experiments and Mechanistic Simulations. Paper SPE-99773-PA, *SPE Reservoir Evaluation & Engineering,* **11** (1): 119-130.

Ahmadall, T., Gonzalez, M. V., Harwell, J. H., & Scamehorn, J. F. 1993. Reducing Surfactant Adsorption in Carbonate Reservoirs. Paper SPE-24105-PA, *SPE Reservoir Evaluation & Engineering*, **8** (02), 117-122.

Al-Hadhrami, H., and Blunt, M. 2001. Thermally Induced Wettability Alteration to Improve Oil Recovery in Fractured Reservoirs. Paper SPE-59289-MS, *SPE Reservoir Evaluation & Engineering,* **4** (3): 179-186.

Anderson, W. 1986a. Wettability Literature Survey-Part 1: Rock/Oil/Brine Interactions and the Effects of Core Handling on Wettability. Paper SPE 13932-PA, *Journal of Petroleum Technology*, **38** (10): 1125-1144.

Anderson, W. 1986b. Wettability Literature Survey-Part 2: Wettability Measurement. Paper 13933-PA, *Journal of Petroleum Technology*, **38** (11), 1-246.

Arshad, A., Al-Majed, A., Menouar, H., Muhammadain, A., and Mtawaa, B. 2009. Carbon Dioxide (CO2) Miscible Flooding in Tight Oil Reservoirs: A Case Study. Paper SPE 127616 presented at the Kuwait International Petroleum Conference and Exhibition, Kuwait City, 14-16 December.

Austad, T., and Standnes, D. C. 2003. Spontaneous Imbibition of Water into Oil-Wet Carbonates. *Journal of Petroleum Science and Engineering*, **39** (3): 363-376.

Barenblatt, G.E., Zheltov, I.P., and Kochina, I.N., 1960, Basic Concepts in the Theory of Seepage of Homogeneous Liquids in Fissured Rocks, *J. Appl. Math Mech*, Vol.**24**, No.5.

Buckley, J. S., Liu, Y., & Monsterleet, S. 1998. Mechanisms of Wetting Alteration by Crude Oils. Paper SPE 37230-PA, *SPE Journal*, **3** (01), 54-61.

Buckley, J. S. 2001. Effective Wettability of Minerals Exposed to Crude Oil. *Current Opinion in Colloid & Interface Science* **6** (3): 191-196.

Behbahani, H. S., Di Donato, G., & Blunt, M. J. (2006). Simulation of Counter-current Imbibition in Water-wet Fractured Reservoirs. *Journal of Petroleum Science and Engineering*, **50**(1), 21-39.

Chauveteau, G. and Sorbie K. S. 1991. Mobility Control by Polymers Critical Reports on Applied Chemistry. Basic Concepts in Enhanced Oil Recovery Processes. M. Baviere. New York, Elsevier Applied Science. 33: 43-87.

Chen, P. and K.K. Mohanty. 2013. Surfactant-Mediated Spontaneous Imbibition in Carbonate Rocks at Harsh Reservoir Conditions. SPE 153960-PA, *SPE Journal,* **18** (1): 124-133.

Chen, P. 2014. Enhanced Oil Recovery in Fractured Vuggy Carbonates. PhD Dissertation, The University of Texas at Austin.

Chilingar, G.V. and Yen, T.F. 1983. Some Notes on Wettability and Relative Permeabilities of Carbonate Reservoir Rocks, II. Energy Sources, 1 (7), 67-75.

Delshad, M., Najafabadi, N. F., Anderson, G., Pope, G. A., & Sepehrnoori, K. (2009). Modeling Wettability Alteration by Surfactants in Naturally Fractured Reservoirs. Paper SPE 100081-PA, *SPE Reservoir Evaluation & Engineering*, **12**(03), 361-370.

Delshad, M., Bhuyan, D., Pope, G.A., Lake, L.W. 1986. Effect of Capillary Number on the Residual Saturation of a Three-Phase Micellar Solution. Paper SPE 14911 presented at the SPE enhanced oil recovery symposium, Tulsa.

Di Donato, G., Huang, W., & Blunt, M. 2003. Streamline Based Dual Porosity Simulation of Fractured Reservoirs. Paper SPE 84036-MS presented in SPE Annual Technical Conference and Exhibition. Society of Petroleum Engineers.

Forrest, J., Birn, K., Brink, S., Comb, T.J., Cuthbert, B., Dunbar, R.B., Harju, J.A., Isaace, E., Jones, F., Khanna, P., Snarr, D.G., Sorensen, J.A., Wall, T.J., and Whitney, D., 2011. Working Document of the NPC North American Resource Development Study, Paper #1-6, Unconventional Oil, Tight Oil.

Farhadinia, M. A., & Delshad, M. 2010.Modeling and Assessment of Wettability Alteration Processes in Fractured Carbonates using Dual Porosity and Discrete Fracture Approaches. Paper SPE 129749-MS presented in SPE Improved Oil Recovery Symposium.

Gautam, P. S., & Mohanty, K. 2004. Matrix–Fracture Transfer Through Countercurrent Imbibition in Presence of Fracture Fluid Flow. *Transport in Porous Media*, **55**(3), 309-337.

Green D. W. & Willhite G. P. 1998. Enhanced Oil Recovery. Richardson, Texas: Society of Petroleum Engineers.

Gupta, R., and Mohanty, K. 2010. Temperature Effects on Surfactant-Aided Imbibition into Fractured Carbonates. Paper SPE 110204-PA, *SPE Journal*, **15** (3): 588-597.

Gupta, R., Adibhatla, B., and Mohanty, K. 2008. Parametric Study to Enhance Oil Recovery Rate from Fractured Oil-Wet Carbonate Reservoirs. Paper SPE 116485 presented at the SPE Annual Technical Conference and Exhibition, Denver, 21-24 September.

Gupta, R., Smith, G., Hu, L., Willingham, T., Lo Cascio, M., Shyeh, J., & Harris, C. 2011. Enhanced Waterflood for Carbonate Reservoirs-Impact of Injection Water Composition. Paper SPE 142668 presented at the SPE Middle East Oil and Gas Show and Conference, Manama, 25-28 September.

Gupta, A., & Civan, F. 1994. An Improved Model for Laboratory Measurement of Matrix to Fracture Transfer Function Parameters in Immiscible Displacement. Paper SPE-28929-MS presented in SPE Annual Technical Conference and Exhibition. Society of Petroleum Engineers.

Hagoort, J. 1980. Oil Recovery by Gravity Drainage. Paper SPE-7424-PA, *SPE Journal*, **20**, 139-150

Halvorsen, M. (2010). Wettability Alteration in Carbonates: The Effect of Water-Soluble Acids in Crude oil and Application of Enzyme for Wettability Alteration.

Hamon, G., Vidal, J. 1986. Scaling-up the Capillary Imbibition Process from Laboratory Experiments on Homogeneous and Heterogeneous Samples". Paper SPE 15852 presented at European Petroleum Conference, 20-22 October, London, United Kingdom.

Hirasaki, G., & Zhang, D. L. 2004. Surface Chemistry of Oil Recovery from Fractured Oil-wet Carbonate Formations. Paper SPE-88365-PA, *SPE Journal*, **9**(02), 151-162.

Jialu, W., Yuzhang, L., Maoqian, C., Li, L., & Jian, G. 2009. Experimental Study on Dynamic Imbibition Mechanism of Low Permeability Reservoirs. *Petroleum Exploration and Development*, **1**, 1-13.

John, A., Han, C., Delshad, M., Pope, G. A. and Sepehrnoori, K.: "A New Generation Chemical Flooding Simulator," SPE 89436, Proceedings of the SPE/DOE 14th Symposium on Improved Oil Recovery, Tulsa, OK,17–21 April, 2004.

Kazemi, H., Merrill, L.S., Porterfield, K.L., and Zeman, P.R., 1976, Numerical Simulation of Water-Oil Flow in Naturally Fractured Reservoirs, Paper SPE-5719-PA, *SPE Journal*, **16**(06).

Kathel, P., & Mohanty, K. K. 2013. Wettability Alteration in a Tight Oil Reservoir. *Energy & Fuels*, **27**(11), 6460-6468.

Killins, C. R., Nielsen, R. F., & Calhoun, J. C. 1953. Capillary Desaturation and Imbibition in Porous Rocks. Producers Monthly, 18(2), 30-39.

Kumar, K., Dao, E., & Mohanty, K. 2008. Atomic Force Microscopy Study of Wettability Alteration by Surfactants. Paper SPE-93009-PA, *SPE Journal,* **13** (2): 137-145.

Li, K., & Horne, R. N. 2002. A Scaling Method of Spontaneous Imbibition in Systems with Different Wettability. Presented at International Symposium of the Society of Core Analysts, California, USA.

Li, K., & Horne, R. N. 2006. Generalized Scaling Approach for Spontaneous Imbibition: An Analytical Model. Paper SPE 77544-PA, *SPE Reservoir Evaluation & Engineering*, **9**(03), 251-258.

Lake, L.W. 1989. Enhanced Oil Recovery. Prentice-Hall, Englewood Cliffs, NJ.

Ma, S., Morrow, N. R., & Zhang, X. 1997. Generalized Scaling of Spontaneous Imbibition Data for Strongly Water-Wet Systems. Paper SPE 77544-PA, *Journal of Petroleum Science and Engineering,* **18** (3): 165-178.

Morrow, N. R., Cram, P. J., & McCaffery, F. G. (1973). Displacement Studies in Dolomite with Wettability Control by Octanoic Acid. Paper SPE-3993-PA, *Society of Petroleum Engineers Journal*, **13**(04), 221-232.

Macaulay, R.C., Krafft, J.M., Hartemink, M., et al. 1995. Design of a Steam Pilot in a Fractured Carbonate Reservoir-Qarn Alam Field, Oman. Paper SPE-30300 presented at the International Heavy Oil Symposium, Calgary, Canada.

Madsen, L., and Lind, L. 1998. Adsorption of Carboxylic Acids on Reservoir Minerals from Organic and Aqueous Phase. Paper SPE-37292-PA, *SPE Reservoir Evaluation and Engineering*, **1** (1): 47-51.

Manrique, E., Thomas, C., Ravikiran, R., Izadi Kamouei, M., Lantz, M., Romero, J., and Alvarado, V. 2010. EOR: Current Status and Opportunities. Paper SPE 130113 presented at the SPE Improved Oil Recovery Symposium, Tulsa, April 24-28.

Mahani, H., Berg, S., Ilic, D., Bartels, W. B., & Joekar-Niasar, V. (2015). Kinetics of low-salinity-flooding effect. Paper SPE-165255-PA, SPE Journal, 20(01), 8-20.

Mattax, C. C., and Kyte, J. R. 1962. Imbibition Oil Recovery from Fractured, Water-Drive Reservoir. Paper SPE-187-PA, SPE Journal 2 (2): 177-184.

Mirzaei-Paiaman, A., Masihi, M., & Standnes, D. C. (2011). An Analytic Solution for the Frontal Flow Period in 1D Counter-current Spontaneous Imbibition into Fractured Porous Media including Gravity and Wettability Effects. *Transport in Porous Media*, **89**(1), 49-62.

Mirzaei Galeh-Kalaei, M., DiCarlo, D. A., & Pope, G. A. 2013. Visualization and Analysis of Surfactant Imbibition into Oil-Wel Fractured Cores. Paper SPE-166129-MS presented in SPE Annual Technical Conference and Exhibition. Society of Petroleum Engineers.

Mirzaei Galeh Mohammad. 2013. Imbibition of Anionic Surfactant Solution into the Oil-wet Matrix in Fractured Reservoirs. Ph.D. dissertation, The University of Texas at Austin.

Mohan, K., Gupta, R., & Mohanty, K. K. 2011. Wettability altering secondary oil recovery in carbonate rocks. *Energy & Fuels*, **25**(9), 3966-3973.

Nasiri, H. (2011). Enzymes for Enhanced Oil Recovery (EOR).

Nasralla, R., Bataweel, M., and Nasr-El-Din, H. 2013. Investigation of Wettability Alteration and Oil-Recovery Improvement by Low-Salinity Water in Sandstone Rock. Paper SPE 146322-PA, *Journal of Canadian Petroleum Technology,* **52** (2): 144-154.

Nelson, R. A. (2001). Geologic Analysis of Naturally Fractured Reservoirs. Gulf Professional Publishing, Boston, Massachusetts.

Noorishad, J., & Mehran, M. 1982. An Upstream Finite Element Method for Solution of Transient Transport Equation in Fractured Porous Media. *Water Resources Research*, **18**(3), 588-596.

Peters, E. J. 2009. Advanced Petrophysics. Greenleaf Book Group.

Peters, E. J., & Hardham, W. D. (1989, January). A Comparison of Unstable Miscible and Immiscible Displacements. Paper SPE 19640-MS presented in SPE Annual Technical Conference and Exhibition. Society of Petroleum Engineers.

Putra, E., Fidra, Y., & Schechter, D. S. 1999. Use of Experimental and Simulation Results for Estimating Critical and Optimum Water Injection Rates in Naturally Fractured Reservoirs. Paper SPE-56431-MS presented at SPE Annual Technical Conference and Exhibition.

Ren, B., Xu, Y., Niu, B., Ren, S., li, X., Guo, P., and Song, X. 2011. Laboratory Assessment and Field Pilot of Near Miscible CO2 Injection for IOR and Storage in a Tight Oil Reservoir of ShengLi Oilfield China. Paper SPE 144108 presented at the SPE Enhanced Oil Recovery Conference, Kuala Lumpur, 19-21 July

RezaeiDoust, A., Puntervold, T., Strand, S., and Austad, T. 2009. Smart Water as Wettability Modifier in Carbonate and Sandstone: A Discussion of Similarities/Differences in the Chemical Mechanisms. *Energy & Fuels* **23** (9): 4479-4485.

RezaeiDoust, A., Puntervold, T., and Austad, T. 2010. A Discussion of the Low-Salinity EOR Potential for a North Sea Sandstone Field. Paper SPE 134459 presented at the SPE Annual Technical Conference and Exhibition, Florence, 19-22 September.

Schechter, D. S., Zhou, D., and Orr, F. M. 1994. Low IFT Drainage and Imbibition. *Journal of Petroleum science and Engineering*, **11** (4): 283-300.

Schmid, K. S., and Geiger, S. 2012. Universal Scaling of Spontaneous Imbibition for Water-Wet Systems. *Water Resources Research,* **48** (3), doi: 10.1029/2011WR011566.

Seethepalli, A., Adibhatla, B., & Mohanty, K. 2004. Physicochemical Interactions During Surfactant Flooding of Fractured Carbonate Reservoirs. Paper SPE-89423-PA, *SPE Journal*, **9**(04), 411-418.

Sharma, G., & Mohanty, K. (2013). Wettability Alteration in High-Temperature and High-Salinity Carbonate Reservoirs. Paper SPE-147306-MS, *SPE Journal*, **18** (04), 646-655.

Shutang, G., Huabin, L., Zhenyu, Y., Pitts, M.J., Surkalo, H., and Wyatt K. 1996. Alkaline-Surfactant-Polymer Pilot Performance of the West Central Saertu, Daqing Oil Field. Paper SPE/DOE 35383 presented at the 1996 SPE/DOE tenth symposium on IOR, Tulsa, OK.

Song, C., and Yang, D. T. 2012. Optimization of CO2 Flooding Schemes for Unlocking Resources from Tight Oil Formations. Paper SPE 162549 presented at the SPE Canadian Unconventional Resources Conference, Calgary, 30 October-1 November.

Standnes, D. C., and Austad, T. 2000. Wettability Alteration in Chalk: 1. Preparation of Core Material and Oil Properties. *Journal of Petroleum Science and Engineering,* **28** (3): 111-121.

Standnes, D. C., and Austad, T. 2000. Wettability alteration in chalk: 2. Mechanism for Wettability Alteration from Oil-Wet to Water-Wet using Surfactants. *Journal of Petroleum Science and Engineering*, **28** (3): 123-143.

Standnes, D C, Nogaret L A D, Chen H-L, et al. 2002. An Evaluation of Spontaneous Imbibition of Water into Oil-wet Carbonate Reservoir Cores using a Nonionic and a Cationic Surfactant. *Energy & Fuels,* **16** (6): 1557-1564.

Stoll, M., Hofman, J., Ligthelm, D. J., Faber, M. J., & van den Hoek, P. (2008). Toward Field-Scale Wettability Modification—the Limitations of Diffusive Transport. Paper SPE-107095-PA, *SPE Reservoir Evaluation & Engineering*, **11**(03), 633-640.

Thomas, L. K., Dixon, T. N., and Pierson, R. G. (1983). Fractured Reservoir Simulation. Paper SPE-9305-PA, *SPE Journal.,* **23**(1), pp 42-54.

Treiber, L.E., Archer, D.L., and Owens, W.W. 1972. A Laboratory Evaluation of the Wettability of Fifty Oil-producing Reservoirs. Paper SPE-3526-PA, *Soc. Pet. Eng. J.,* **12** (6): 531-540.

Tweheyo, M. T., Zhang, P. and Austad, T. 2006. The Effect of Temperature and Potential Determining Ions Present in Seawater on Oil Recovery from Fractured Carbonate. Paper SPE 99438 presented at Proceedings of the Symposium on Improved Oil Recovery, Tulsa, 22-26 April.

UTCHEM Manual (Version 2013_8). The University of Texas at Austin, August 2013

Winsor, P.A. 1954. Solvent Properties of Amphiphilic Compounds. London: Butterworths Scientific Publications.

Wang, W., and Gupta, A. 1995. Investigation of the Effect of Temperature and Pressure on Wettability Using Modified Pendant Drop Method. Paper SPE 30544 presented at the SPE Annual Technical Conference and Exhibition, Dallas, 22-25 October.

Warren, J.E. and Root, P.J., 1963. The Behavior of Naturally Fractured Reservoirs. Paper SPE-426-PA *SPE Journal*, **3** (03), 245-255.

Xie X, Weiss W W, Tong Z, et al. 2005. Improved Oil Recovery from Carbonate Reservoirs by Chemical Stimulation. SPE 89424-P, *SPE Journal,* **10** (3): 276- 285.

Yang, F., Wang D., Wang G., et al. 2006. Study on High-Concentration Polymer Flooding To Further Enhance Oil Recovery. Paper SPE 101202 presented at the Annual Technical Conference and Exhibition, San Antonio, Texas, USA.

Zhou D., Jia L., Kamath J., and Kovscek A.R. 2002. Scaling of Counter-Current Imbibition Process in Low-Permeability Porous Media. *Journal of Petroleum Science and Engineering*, **33**: 61-74.

Zhou X., Morrow N.R. and Ma S. 2000. Interrelationship of Wettability, Initial Water Saturation, Aging Time and Oil Recovery by Spontaneous Imbibition and Waterflooding. Paper SPE-62507-PA, *SPE Journal*, **5**(2): 199-207.

Zhang, P., and Austad, T. 2006. Wettability and Oil Recovery from Carbonates: Effects of Temperature and Potential Determining Ions. *Colloids and Surfaces A: Physicochemical and Engineering Aspects* **279** (1): 179-187.

Zhang, J., Nguyen, Q. P., Flaaten, A., & Pope, G. A. 2009. Mechanisms of Enhanced Natural Imbibition with Novel Chemicals. Paper SPE-113453-MS, *SPE Reservoir Evaluation & Engineering*, **12** (06), 912-920.

Zhang, X., Morrow, N. R., & Ma, S. 1996. Experimental Verification of a Modified Scaling Group for Spontaneous Imbibition. Paper SPE-30762-PA, *SPE Reservoir Engineering*, **11** (04), 280-285.